Institut für Molekulare Mechanismen bei Krankheiten
der Vetsuisse-Fakultät Universität Zürich

Direktor: Prof. Dr. med. vet et phil. II Michael O. Hottiger

Musculoskeletal Research Unit (MSRU)
Leiterin: Prof. Dr. med. vet. Brigitte von Rechenberg, Dipl. ECVS

Arbeit unter wissenschaftlicher Betreuung von
Dr. Salim Darwiche, PhD, Musculoskeletal Research Unit (MSRU)

Effect of pulsed electromagnetic field therapy on bone repair and regeneration in two tibia osteotomy models in sheep

Inaugural-Dissertation

zur Erlangung der Doktorwürde der
Vetsuisse-Fakultät Universität Zürich

vorgelegt von
Anna Kaczmarek

Tierärztin
aus Lodz, Polen

genehmigt auf Antrag von
Prof. Dr. med. vet. Brigitte von Rechenberg, Referentin
Prof. Dr. Stephen Ferguson, Korreferent

2020

Institut für Molekulare Mechanismen bei Krankheiten
der Vetsuisse-Fakultät Universität Zürich

Direktor: Prof. Dr. med. vet et phil. II Michael O. Hottiger

Musculoskeletal Research Unit (MSRU)
Leiterin: Prof. Dr. med. vet. Brigitte von Rechenberg, Dipl. ECVS

Arbeit unter wissenschaftlicher Betreuung von
Dr. Salim Darwiche, PhD, Musculoskeletal Research Unit (MSRU)

Effect of pulsed electromagnetic field therapy on bone repair and regeneration in two tibia osteotomy models in sheep

Inaugural-Dissertation

zur Erlangung der Doktorwürde der
Vetsuisse-Fakultät Universität Zürich

vorgelegt von
Anna Kaczmarek

Tierärztin
aus Lodz, Polen

genehmigt auf Antrag von
Prof. Dr. med. vet. Brigitte von Rechenberg, Referentin
Prof. Dr. Stephen Ferguson, Korreferent

2020

Dedicated to the sheep of this study

Zusammenfassung

Die Marvel-Technologie wurde getestet, um die Frakturheilung unter Verwendung eines elektromagnetischen Feldes (PEMF- Pulsed Electromagnetic Field) zu verbessern und zu beschleunigen.

Eine standardisierte 3 mm-Tibia-Osteotomie wurde bei 14 Schafen (8 TI, 6 CI) durchgeführt, um eine Fraktur zu imitieren, die ein Modell mit einer nicht kritischer Frakturgröße darstellt. Eine Osteotomie von 17 mm wurde gemacht, um die Heilungsreaktion bei einem Defekt mit kritischer Größe zu testen. 12 von 15 Schafen bekamen ein autologes Knochentransplantatmaterial (6 TI, 6 CI). Alle TI-Schafe wurden über 9 (3mm Defekt) bzw. 12 (17mm Defekt) Wochen täglich mit PEMF behandelt. Die Heilungsreaktion wurde mit Röntgenaufnahmen, Mikro-CT, Biomechanik und Histologie bewertet.

Das 3-mm-Spaltmodell zeigte sowohl bei TI als auch bei CI eine gute Heilung. Ein Trend für höhere Werte in der Biomechanik (zweifache Zunahme, $p = 0{,}081$) und Kallusdichte ($p = 0{,}053$) wurde in TI beobachtet. Dies wurde durch den histologisch beobachteten dichten, gut integrierten und regelmäßig orientierten neuen Knochen bestätigt.

Im 17-mm-Defektmodell erreichten die TI-Tibiae 67% der Torsionssteifigkeit der gesunden Tibia, verglichen mit nur 30% der CI-Tibiae ($p = 0{,}034$). Das TI-Kallusvolumen ($p = 0{,}002$) und die Dichte ($p = 0{,}055$) waren auch dem CI überlegen. Darüber hinaus zeigte TI eine schnellere und besser ausgeprägte radiographische, makro- und mikroskopische Heilung.

Insgesamt beschleunigte und verbesserte die Marvel-Technologie den Knochenheilungsprozess und führte zu einer besseren neuen Knochenstruktur mit überlegenen biomechanischen Eigenschaften.

Summary

The Marvel technology was tested to enhance and accelerate fracture healing using Pulsed Electromagnetic Field (PEMF- Pulsed Electromagnetic Field).

A 3mm standardized tibia osteotomy was created in 14 sheep (8 Test Item (TI), 6 Control Item (CI)) to imitate a fracture, representing a non-critical size model. Further, a 17mm gap was done to test the healing response in an augmented critical size defect. 12 sheep were augmented with autologous bone graft material (6 TI, 6 CI) and 3 sheep were not augmented. All TI sheep received daily treatments (PEMF) over 9 (3mm gap) resp. 12 (17mm gap) weeks. The healing response was evaluated with radiographs, micro-CT, biomechanics and histology.

The 3mm gap model showed good healing in both TI and CI. A trend for higher biomechanical values (2-fold increase, p=0.081) and callus density (p=0.053) was seen in TI. This was corroborated by the histologically observed dense, well integrated and regularly oriented new bone.

In the 17mm graft model, the TI tibiae reached 67% of healthy tibia torsional stiffness compared to only 30% for CI tibiae (p=0.034). TI callus volume (p=0.002) and density (p=0.055) was also superior to CI. Moreover, TI exhibited a faster and more pronounced radiographic, macro- and microscopic healing.

Overall, the Marvel technology accelerated and enhanced the bone healing process, with no related abnormalities or complications. This resulted in better new bone structure, better callus morphology and superior biomechanical properties.

1 Introduction

1.1 Clinical problem

Bone fractures are one of the most commonly occurring injuries in both veterinary and human medicine. Despite all the improvements and advancements in fracture management, bone healing still remains clinically challenging. Complication rates in long bone and flat bone fractures are high with approximately 5 to 10 % of those fractures showing signs of impaired healing such as delayed union or in a worse case, becoming a non- union (Einhorn, 1995; Morshed, 2014). For the purpose of this thesis, focus will be set on long bone fractures.

1.2 Bone structure

Bone is an organ with a very complex composition. The most outer part, the periosteum, is a thin membrane that covers almost the whole bone, apart from the bone areas within the joint capsule or those that function as tendon or ligament attachment. This membrane consists of two layers: fibrous and osteogenic. The fibrous layer is the outer one and contains numerous blood vessels, nourishing the bone. The osteogenic layer is where the osteoblasts are located and is thus responsible for bone growth and regeneration.

The walls of a long bone are composed of cortical (compact) bone, which is the outer layer, and cancellous (spongy) bone- the inner part. The inner part of the diaphysis contains a medullary cavity containing the endosteal membrane and bone marrow.

There are four main types of cells within bone tissue: osteogenic progenitor cells, osteoblasts, osteocytes and osteoclasts. The osteogenic progenitor cells are undifferentiated and can mature into osteoblasts. Osteoblasts are the bone forming cells, which get embedded in the bone matrix and become osteocytes. Osteocytes are the primary mature bone cells, the role of which is to maintain mineral density of the matrix. They are the type of cells that is most likely to be found in healthy bone. Osteoclasts are responsible for bone resorption. Bone homeostasis relies on a delicate balance between bone formation and resorption (Biggane et al., 2016).

1.3 Fracture healing

Bone strength is naturally dependent on numerous factors, age and general health being amongst the most crucial ones. When a force applied against a bone is stronger than a bone itself, a fracture develops.

During the whole healing process, achieving a certain degree of fragment stabilization and micromotion in order to provide mechanically favourable healing conditions is of the utmost importance. To achieve this degree of stabilization, the following surgical methods have been established: internal fixation using implants like plates, screws, nails, rods, wires, pins or external fixation. The latter involves using unilateral and circular fixators, or the combination of both, namely hybrid fixators. Additional stabilization can be provided by applying a cast or a splint.

The functional healing of skeletal fractures is achieved upon the recovery of weight bearing (Saliev et al., 2019).

During normal fracture healing, a cascade of multiple processes is initiated. Bones heal in two ways: through direct or indirect healing.

Direct healing happens when bone fragments are tightly fixed together, therefore an anatomic reduction and perfectly stable conditions are a strict requirement. Healing occurs by direct involvement of osteoblasts and osteoclasts (Ghiasi et al., 2017; Marsell and Einhorn, 2011).

Indirect healing is certainly more common when it comes to long bone fractures. Its main difference compared to direct healing comes from unstable healing conditions. Such situations happen in inoperable fractures or in cases where some degree of motion exists. This occurs, for instance, with intramedullary nailing, external fixation, internal fixation of complicated comminuted fractures (Marsell and Einhorn, 2011). This type of healing is enhanced by micromotion and weight- bearing and includes four phases: inflammation, soft callus formation, hard callus formation, remodelling.

1.3.1 Phase I: Inflammation

The anabolic phase starts immediately after the bone structure has been disrupted. It is characterized by an increased local tissue volume and typically lasts up to seven days. The inflammation begins as the pro- inflammatory cytokines are released: TNF- Alpha, TGF- Beta, BMPs and Interleukins (IL-1beta, IL- 6, -17F, - 23), reaching a peak 24 hours after the trauma has occurred. These molecules are responsible for accelerating the inflammatory reaction and recruitment of the cells required for tissue regeneration, such as monocytes, macrophages, neutrophils, basophils, dendritic cells, mast cells, T-cells and B-cells (Turner et al., 2014).

At the same time, the hematoma, consisting of cells from both intramedullary and peripheral blood, is immediately formed and fills the fracture gap. Forming of the hematoma is a crucial part of the healing as it first acts as a temporary scaffold for the mesenchymal stem cells (MSCs) derived from the surrounding tissue and bone marrow. During the next days, granulation tissue formed by fibrin, collagen and reticulin slowly replaces the hematoma and bridges the fracture ends. Five to seven days after fracture, anabolic processes are accompanied by the catabolic ones.

1.3.2 Phase II: Soft callus formation

Around one week after the trauma, the formation of soft, cartilaginous callus is initiated (Einhorn and Gerstenfeld, 2015), reaching its peak at day seven to nine. The progenitor cells in the endosteum and periosteum play a vital role in this process as they differentiate into osteoblasts and initiate the callus formation from the periphery towards the fracture line. The mesenchymal progenitor cells located near the fracture gap differentiate into fibroblasts, producing fibrous tissue, or differentiate into chondrocytes, creating cartilage, which replaces the granulation tissue formed in the previous phase (Wang et al., 2017).

1.3.3 Phase III: Hard callus formation

The mechanisms leading to this transformation of the soft callus into the hard callus is called endochondral ossification. As the MSCs and progenitor cells differentiate into chondrocytes, the cartilage tissue is built. At that point, cartilage extracellular matrix mineralizes along with chondrocyte apoptosis. As a consequence, osteoblasts infiltrate the mineralized cartilage matrix and produce bone. This happens about 3 weeks after a fracture and typically lasts for three to four months until the soft callus is fully transformed into a hard callus (Einhorn and Gerstenfeld, 2015; Ghiasi et al., 2017).

1.3.4 Phase IV: Remodeling

The last phase starts when the cartilage is fully resorbed and replaced by hard callus. It is then gradually transformed into a lamellar bone structure, just like what was there before the trauma. Reestablishment of a central medullary cavity also takes place. This dynamic process is regulated by hematopoietic- derived osteoclasts and mesenchymal-derived osteoblasts (Einhorn and Gerstenfeld, 2015; Ghiasi et al., 2017; Marsell and Einhorn, 2011; Pivonka and Dunstan, 2012; Pivonka and Komarova, 2010).
It may take months or even years until this phase is fully completed. In healthy adults, a balance between the osteoclastic resorption and osteoblastic activity is always maintained. It is mediated by a variety of molecules like growth factors, hormones, cytokines or matrix proteins (Ledda et al., 2015).

1.4 Neovascularization

Concurrent to all of these processes, about 2-3 weeks after the fracture, neovascularization is established. The formation of new blood vessels, called angiogenesis, plays a vital role in the whole bone healing process. Better angiogenesis means a superior supply not only in cells that directly influence the healing (like MSCs, macrophages, neutrophils, monocytes, lymphocytes) but also in oxygen, nutrients and growth factors. It is therefore clear that impaired angiogenesis leads to insufficient supply of these components and may result in healing complications (Streit et al., 2016).

1.5 Impaired healing

There are conditions, when a desirable healing effect is not achieved as the fibrocartilage fails to bridge the gap and calcify, resulting in either a non-union or a delayed bony union. The pathogenesis of this process often involves factors like fracture displacement, substantial fracture gap size, inadequate immobilization, damage of the surrounding soft tissue or fracture site infection (Gossling et al., 1992). The age of the patient is crucial (older patients have an increased complication risk) as well as concomitant diseases and disorders (diabetes, liver diseases, osteoporosis, bone tumors), mineral or vitamin deficiencies (especially calcium, vitamin D, vitamin C) or certain medications (anticoagulants, steroids). Smoking and radiotherapy have a documented detrimental effect on bone regeneration as well. In addition, the speed and success of initial management are often decisive factors in how the healing proceeds.

When a fracture healing is prolonged, meaning it does not heal within the anticipated time frame but some clinical or radiological evidence of proceeding healing is apparent, a delayed union is diagnosed (Griffin et al., 2011; Griffin et al., 2008).

A non-union however, is established when a biological bone healing process fails completely. In this case, interventions beyond standard fracture fixation become necessary (Griffin et al., 2008).

According to their radiographic appearance, non- unions are classified as:

- hypertrophic, which develop abundant callus without achieving adequate stability. They are caused by a mechanical failure.
- atrophic, characterized by little to no callus formation and signs of bone resorption. They are caused by a biological failure (Griffin et al., 2011).

Delayed unions and non- unions are associated with substantial morbidity and pain, which significantly reduce the quality of life of patients and causes prolonged convalescence.

The economic impact is enormous as weeks or even months of inability of affected people to work generate extremely high costs, not only associated with amount of not working days but also with additional health care and treatments.

1.6 Critical sized defect and augmentation

Some fractures are too big to bridge alone and are therefore called critical sized defects. The pathogenesis includes severe trauma, developmental deformities, tumor resection or osteomyelitis. A critical size defect in bone, by definition, would not heal spontaneously or does not exhibit more than 10% regeneration. The size of such defect, in long bones, is defined to be larger than 2 to 2.5 times the diameter of the bone (Wang and Yeung, 2017).

In these cases, an additional material has to be introduced inside the defect to support the body in healing. Augmentation materials fulfil at least one of the following functions: osteogenic potential (e.g. contain cells), osteoinductivity (contain bone-inducing substances), osteoconductivity (scaffold for bone formation) and, in some cases, may also provide mechanical stability until bone is rebuilt (McAllister and Haghighat, 2007; Wang and Yeung, 2017).

Augmenting a defect is a standard and very common procedure, with over two million performed worldwide annually (Wang and Yeung, 2017).

There are several options when it comes to augmentation materials:

- autografts (harvested and transplanted within the same individual, derived most commonly from iliac crest bones), are considered the gold standard as they provide most complete and rapid integration
- allografts (harvested within the same species), the risk factors are: graft viability and integration, disease transmission, immunological response and possible rejection, as well as limited availability
- xenografts (harvested within another species), where the main cons are again rejection risk and availability
- alloplasts (synthetic materials like calcium sulfate and calcium phosphate compounds), which are not always reliable in their bone regeneration potential.

Autografts, despite the limited volume of available material, possible donor site complications, additional pain, increased operative time and blood loss are still the most effective method of bone augmentation.

1.7 Healing stimulation

Precisely because of all challenges and problems that need to be overcome during fracture healing management, different strategies of additional bone healing stimulation have been introduced and widely used for decades. They can be characterized as biological and biophysical.

1.7.1 Biological methods

- Local, using osteogenic materials like autologous bone marrow, autologous bone, peptide signalling molecules (FGF- 2 and PDGFs), morphogenetic factors (BMPs- bone morphogenetic proteins and Wnt proteins) and osteoconductive materials (calcium phosphate, calcium hydroxyapatite, calcium sulphates amongst others) (Einhorn and Gerstenfeld, 2015; Saliev et al., 2019). In particular, BMPs have been extensively investigated and BMP-2 and -7 were also approved by the FDA for some clinical uses. For example, BMP-7 can be used as a substitute of an autograft in a long bone non-union. It was shown to increase healing rates for fractures and wounds and decrease risk of infection. Although their application may cause some controversy, a rapid increase in their use was reported in the last decades (Garrison et al., 2010; Glass and Jain, 2013; Nakase and Yoshikawa, 2006).

- Systemic, which are being under investigation as a rather future possibility, for example, PTH (parathyroid hormone), humanized monoclonal anti- sclerostin, anti- Dickkopf- related protein 1 antibodies (art. 5, 13). PTH is a naturally occurring hormone, having a direct impact on mineral homeostasis of the body. Several studies proved that PTH treatment increased bone stiffness, mineral composition and density (Alkhiary et al., 2005).

1.7.2 Biophysical methods

- Low intensity pulsed ultrasound stimulation, which was shown to accelerate bone healing not only during a normal fracture repair process (Heckman et al., 1994) but also in the treatment of non-unions (Nolte et al., 2001; Randau et al., 2014). Acoustic pressure waves reach a bone, causing low-level micromechanical pressure. The healing mechanism is believed to be related to the piezoelectric properties of bone and production of mediators like prostaglandin E2. Low intensity pulsed ultrasound stimulation has been proven to increase formation of the callus, decrease healing time and enhance fracture healing.
- Pulsed Electromagnetic Field stimulation.

1.8 PEMF

Pulsed electromagnetic field stimulation (PEMF) is a non- invasive, local form of electric stimulation of different tissues. This method, due to its biosafety and therapeutic efficacy, was used for decades in fracture healing enhancement and acceleration. Furthermore, it is convenient and has no described side effects or feeling of discomfort.

One of the first reports describing positive effects of pulsed electromagnetic field stimulation on bone healing appeared already in 1972 by Kraus and Lechner (Kraus and Lechner, 1972) and in 1974 by Bassett et al. Since then, this stimulation method was widely applied in bone healing and to treat healing complications such as non-unions (Bassett et al., 1974). This was followed by an official approval of its clinical use by the FDA in 1979 (Trock, 2000).

1.9 Electromagnetism

Electromagnetic field is a combination of electrical and magnetic fields. A magnetic field is specified by the direction and the magnitude and is measured in Tesla. Its application for bone healing usually ranges from 0.01 to 2 mT and produces electrical fields within bone tissue ranging from 1 to 100 mV/cm (Chalidis et al., 2011; Marsell and Einhorn, 2011; Yuan et al., 2018).

Such induced voltages are supposed to be similar to those produced naturally during dynamic mechanical deformation of different tissues (Bassett, 1993; Bassett et al., 1964). This is related to the piezoelectric effect of hydroxyapatite in bone, which is manifested in its ability to convert mechanical energy to electrical current, therefore producing voltage (Trock, 2000). As a consequence, osteoblasts are stimulated, enhancing mineral deposition and increasing bone density. Also, direct electrical stimulation may lead in a similar pathway to bone regeneration enhancement (Balmer et al., 2018; Kubo, 2012; Noris-Suarez et al., 2007; Otter et al., 1998; Ryaby, 1998; Stroe et al., 2013).

Pulsing of EMF implies to the repetition of the electromagnetic pulses with a specific repetition rate. It is essential to remember that physiological effects are induced only in certain parametric “windows” and thresholds (Funk and Monsees, 2006). These windows are relating to the field amplitude, duration and frequency of exposure. The ideal parameters have not been established so far, but it was observed that a frequency range between 1-50 Hz was most effective for humans. The shorter the pulse, the stronger induced current is created (Biggane et al., 2016).

In fact, using parameters outside these windows may result not only in a lack of effects but possibly in negative consequences. It was shown, that fresh fractures in rats treated with High-intensity Electromagnetic Pulses, exhibited delayed callus formation and worse healing progress compared to the control group (Leisner et al., 2002).

Although the principle of treatments presented in most of the PEMF related studies stays the same, the PEMF characteristics greatly differ. Table 1.1 summarizes the designs and findings of 15 representative studies using various version of PEMF in vivo.

Bassett et al. described multiple discrepancies between studies with PEMF, for example, heterogeneous treatment regime, dissimilar pulse shape and duration, frequency characteristics, amplitude, spatial orientation and intensity among other factors (Bassett, 1993). These discrepancies and lack of standardization are still observed with recently published studies.

Midura et al. (Midura et al., 2005) and Fredericks et al. (Fredericks et al., 2000) showed a two-fold faster osteotomy healing in PEMF- stimulated rat or rabbit bones. Accelerated healing was also exhibited by human patients in multiple other studies (Capanna et al., 1994; Dhawan et al., 2004; Holmes, 1994; Mammi et al., 1993). Qualitative differences were documented by Cane et al. (Cane et al., 1993) and Borsalino et al. (Borsalino et al., 1988) in favor of treated groups compared to the controls in horses and humans respectively.

It is worth emphasizing that most of these studies exhibit very different treatment patterns and designs. The study conducted by Fredericks et al. used treated time as low as 30 minutes per day, whereas the majority of other studies were designed to use PEMF for multiple hours a day, sometimes as much as 12 hours (Sharrard, 1990). The treatments usually lasted several weeks, ranging from 1 week (Ding et al., 2011) to 12 weeks (Betti, 1999).

The study models were also extremely varied, counting, among others, fibular osteotomy in rats (Midura et al., 2005), metacarpal fracture in horses (Cane et al., 1993), hip osteoarthritis in humans (Borsalino et al., 1988), metatarsal non-union in humans (Streit et al., 2016) or lumbar fusion in humans (Mooney, 1990). As shown in the table 1.1 , device parameters also had wide ranges, with pulse frequencies starting at 1.5 Hz (Fredericks et al., 2000) and reaching 75 Hz in the majority of the studies (Borsalino et al., 1988; Capanna et al., 1994; Dallari et al., 2009). Some device parameters were not reported at all (Streit et al., 2016). Such variety and variability of treatment options makes it difficult to notice a standardized trend of data and build upon previously published findings. Moreover, the differences in these numerous parameters often result in diverse effects. In conclusion, there are only a few well-designed prospective studies available and it remains very difficult to draw clear findings and parameter windows from what is currently published (Shi et al., 2013).

Article	**Study Design**	**Treatment characteristics**	**Device parameters**	**Results** (treated group compared to the control)
Midura et al., 2005	Fibular osteotomy	15 rats 3h / day for 5 weeks	Physio Stim: 15 kHz, 5.56 ms, 2mT Osteo Stim: 1.5 Hz, 16ms	Physio Stim: **2x faster healing** Osteo Stim: not effective
Ding et al., 2011	Steroid-induced osteo-necrosis of the femoral neck	72 rats 4h a day for 1-8 weeks	15 Hz 4.5 ms 0-12 G	Osteonecrosis incidence with PEMF treatment: 29% Control with steroid: 75%, Control without steroid: 0%
Fredericks et al., 2000	Tibial osteotomy	108 rabbits Gr 1: 30 min/day Gr 2: 60 min/day	1.5 Hz 30 ms 0-1 Gauss	**2x faster healing with PEMF** in 60 min group 1.3x faster in 30 min treated group
Cane et al., 1993	Metacarpal and mid-diaph. fracture	6 horses (CI=TI) 30 days	75 Hz 1.3 ms 2.5-3 mT	Advanced healing in TI
Borsalino et al., 1988	Degen. Osteo-arthritis of the hip	32 people (TI=16 /CI=16) 8h/day 90 days	75 Hz, 1.3 ms 2.5 mV 18 Gauss	**Better healing** and denser callus in PEMF-treated group
Holmes et al., 1994	5th metatarsal non unions	9 people 8-10 h a day	15 Hz 4.5 ms 0-20 Gauss	All healed in 2-8 months
Streit et al., 2016	5th metatarsal non union	6 people 10h / day	Not described	TI healed in 8.9 weeks CI in 14.7 weeks
Betti et al., 1999	Femoral neck fracture	64 people (TI=30 /CI=34) 8h a day, 90 days	75 Hz 1.3 ms 2.5-3 mT	TI: 7% not healed CI: 17.6% not healed Necrosis in 28.5% TI and 47% CI
Shi et al., 2013	Long bone non- / delayed unions	58 people (TI=31 / CI=27) 8h a day	Not described	Union rates: TI: 77.4% CI: 48.1%
Capanna et al., 1994	Massive allografts after tumor resection	50 people (TI=15 / CI=18) Not described	75Hz 1.3 ms 3.0 mV	**TI: decreased healing time**
Dallari et al., 2009	Hip Revision Prosthesis	30 people (TI=15 /CI=15) >6h a day, 12weeks	75 Hz 1.3ms 2 mT	**TI higher bone density**, better osteotomy integration

Article (continuation)	**Study Design**	**Treatment characteristics**	**Device parameters**	**Results** (treated group compared to the control)
Dhawan et al., 2004	Primary hind foot arthrodesis in subtalar and talonav. joints	59 Subtalar joint (TI=22 / CI=37) 39 Talonav. (TI=19/CI=20) 10h a day, until fusion	EBI Medical 15 Hz 4.5 ms	**TI accelerated healing by several weeks** (faster fusion)
Mammi et al., 1991	Tibial osteotomy, deg. knee arthrosis	40 people (TI=20 / CI=20) 60 days	75 Hz 1.3 ms 3 mV	**advanced healing in 26.4% CI and 72.2% TI**
Mooney, 1989	Lumbar fusion	195 people (TI=98 / CI=97) min. 8h a day	1.5 Hz 1.8 Gauss	Healing rates: CI: 64.9 % TI: 82.7 %
Sharrard, 1990	Tibial shaft fracture, delayed union	45 people (TI=20 / CI=25) 12 h a day 12 weeks	15 Hz 20 pulses/ burst	TI: 5/20 union, 5/20 progress and 10/20 no change

Table 1.1: Representative review of PEMF studies, emphasizing discrepancies between study design as well as differences in PEMF device parameters, treatment regime and outcomes. Unless otherwise specified, all studies had a control group which was treated like the test group, except for PEMF application.

1.10 PEMF device

There are two main components building a PEMF therapeutic unit. The first one is a generator, which produces an alternating current at a specific frequency and amplitude. The second one is a coil, which receives the current and produces pulses of magnetic field that stimulate the tissues of the area where it is placed. As a consequence, a secondary electrical field is induced and produced in the bone (Bassett, 1993; Leisner et al., 2002).

1.11 PEMF effects on cellular mechanisms

There are several pathways through which PEMFs can affect cells and tissues. The calcium signalling is considered to be the main one as the intracellular calcium is a crucial factor in the translation of PEMF signal into biological responses.

The PEMF passes through the cell membrane. An electrical field is then induced in the cytosol and causes the release of intracellular calcium into the cytosol. Calmodulin is activated and bone cell viability is enhanced.
What is more, intracellular calcium increases nitric oxide levels, followed by an increase in cGMP and the activation of protein kinase G. This pathway promotes MSC and osteoblast differentiation and maturation and reduces pain through inflammatory cytokines such as IL1-Beta. It also influences angiogenesis by increasing the expression of FGF-2 and VEGF (Yuan et al., 2018).

A great range of subcellular and cellular responses to different PEMF forms have been documented. In general, this therapeutic method influences bone healing by promoting bone formation and suppressing bone resorption. This is achieved by influencing numerous processes and reactions that take part in osteo-, chondro- and angiogenesis. PEMF has an ability to stimulate cell migration and proliferation, cause changes in cell cycle and differentiation, growth factor expression and DNA replication (Saliev et al., 2019). Moreover, positive local influence on pain reduction is associated with this form of therapy (Ryang We et al., 2013).

Electromagnetic stimulation has many clinically relevant effects described in the literature:

- stimulate osteoblasts to secrete growth factors (e.g. BMP-2 and -4, TGF- beta), enhance expression of BMP-2, TGF- beta, osteoprotegerin, osteocalcin, stimulate osteoprogenitor cells, enhance the osteogenic effects of BMP-2 on mesenchymal cells (Aaron et al., 2004; Chalidis et al., 2011)
- increase DNA synthesis (Bassett, 1993; Brighton et al., 2001)
- increase levels of alkaline phosphatase, an early marker of osteogenesis (Saliev et al., 2019)
- increase osteoblastic calcium deposition (Bassett, 1989), enhance extracellular matrix protein synthesis and mineralization and cartilage matrix reconstruction (Aaron and Ciombor, 1993; Gossling et al., 1992)
- cause arteriolar vasodilation, accelerate intramedullary angiogenesis (Chalidis et al., 2011; Ikegami et al., 2015)
- limit inflammation by cytokine modulation, e.g. reduce IL-6 concentration (Benazzo et al., 2008)
- effect production of proteins regulating gene transcription

- affect membrane receptors (PTH, insulin, IGF-2, calcitonin receptors)
- activate the mTOR pathway in pre- osteoblasts and fibroblasts
- improve soft tissue repair (Chalidis et al., 2011)

As demonstrated, the range of different mechanisms and pathways through which PEMF influences processes within the bone is very broad and varied.

PEMF has been most commonly used as an additional treatment option for delayed unions and non-unions, successfully increasing the union rates. Also an early stage application has been reported to positively impact fresh fracture healing, substantially accelerating this process (Hannemann et al., 2011; Shi et al., 2013). It has also been used in treatment of joint or spine fusion, arthrodesis, congenital pseudarthrosis, osteotomy, osteoporosis, osteonecrosis, osteochondritis dissecans, osteogenesis imperfecta and osteoarthritis (Ding et al., 2011; Marks, 2000; Simonis et al., 2003; Trock et al., 1993; Vavken et al., 2009).
The effect of PEMF application on bone graft incorporation and improvement of biomaterial osteointegration (Dallari et al., 2009) has also been described.

1.12 Animal model

There are several possibilities when it comes to choosing a right animal model for fracture healing research. Nevertheless, there is no perfect one and each of them has its up- and downsides. Most commonly used are rabbits and rats as they are easy to maintain and to work with, however, the limitation is their small size (Gilsanz et al.,1988) and faster healing rates compared to humans. The other possibilities include: sheep, goats, pigs, guinea pigs, dogs and horses.
Sheep have similar bone metabolism as humans and are proven experimental animals for studies related to bone formation and defect healing (Martini et al., 2001).

Based on several studies conducted by MSRU using tibia defects (Bottlang et al., 2016; Plecko et al., 2013; Plecko et al., 2012; Richter et al., 2015), it has been demonstrated that standardization can be reliably achieved and sheep osteotomy models are appropriate for bone healing comparison purposes.

These studies had group sizes of either six or twelve and used female sheep of average age between 2-3 years and homogenous weight distribution (approximately 60-70 kg). Non- critical size defects ranging from 0 to 3 mm were created with either transverse or

45°angle tibia osteotomies. Sheep received full limb casts applied for the entire in-life phase. In some of these studies, animals were kept in suspension nets during first 3 weeks post operatively. Radiographic examinations were performed weekly in order to find the most optimal time point for sacrifice when differences between groups are largest. The sacrifice time point ranged from 6 to 12 weeks after surgery. It is worth mentioning that their main aim and focus were novel medical devices themselves (locking plates and screws), and not a healing enhancement therapy.

A sample size of six is relatively low but was successfully used in most of the mentioned studies and was proven to provide sufficient data when complication rates are very low. Calculating the optimal number of animals used for a trial is one of the most essential parts of designing a study. On one hand, too small sample size may not reflect the behavior of a population. On the other hand, too big sample sizes, while better statistically, leads to unnecessary experimental usage of animals. The sample sizes often used in these studies were sometimes only six, however, they were large enough for the detection of different effects between groups (Charan and Kantharia, 2013).

In these studies, some tendencies were observed, and although not statistically significant, they showed if the test item had positive healing potential.

For the purpose of this study, it has been decided that sheep is the most optimal animal model, as their size and weight are comparable to humans. Furthermore, the tibial bone shows great similarities with the one of humans when it comes to the macroscopic appearance and the bone mineral composition. The bone metabolism and remodelling properties and the pattern of bone ingrowth into the implants over time are also much alike. Sheep are a very reproducible and practical model: they are available, tolerate captivity well, are easy to house and handle. They also show good tolerance to surgery and resistance to infections and diseases. Although the bone microstructure differs from the one of humans and the sheep bone density is significantly higher, the inter-animal uniformity and already existing extensive database of biological information greatly compensate such limitations (Pearce et al., 2007).

1.13 Aim of the thesis

The aim of this thesis was to evaluate the impact of Marvel technology on bone healing in a standardized manner. This technology integrates electromagnetic therapy within a bone screw close to the fracture site, in order to enhance bone healing by locally amplifying the pulsed electromagnetic field stimulation.

Two sheep models using Marvel screws positioned across a tibia osteotomy were performed:

- 3 mm gap model: the tibia osteotomy was stabilized using internal fixation, leaving a 3 mm gap – a non-critical defect size.
- 17 mm graft model: a critical size defect of 17 mm was created in the tibia, which was stabilized also using internal fixation. The defect was augmented with autologous bone grafts (or left empty in a negative control group).

The effect of the Marvel technology was evaluated radiographically, biomechanically and histologically, by analysing fracture healing kinetics, torsional stiffness, callus volume and density, biocompatibility and microscopic bone healing.

2 Materials and Methods

2.1 Study Design

All animal experiments were conducted at the Musculoskeletal Research Unit (MSRU), Winterthurerstrasse 260, 8057 Zurich, Switzerland according to the Swiss laws of animal protection and welfare (Tierschutzverordnung, TVV 455.163 / Tierschutzgesetz, SchG 455).
The experiment was authorized by the cantonal ethical committee under the license no. ZH183/17.
For this study, two transverse tibia osteotomy models in sheep were used:

1. A 3 mm interfragmentary Gap Model
2. A 17 mm interfragmentary Graft Model

The 3 mm gap model experiment contained a Test Item (TI) group and a Control Item (CI) group. The 17 mm graft model experiment contained a Test Item (TI) group, a Positive Control Item (CI) group and a Negative Control Item (NCI) group (see Table 2.1).

14 adult, female, Swiss alpine sheep with an age range between 24-30 months (Ø 28.7 months) and an average bodyweight of 62.70-76.60 kg (Ø 66.98 kg, at delivery) served as experimental animals for the 3mm gap model. While for the 17mm graft model 15 (12 with autograft, 3 without) adult, female, Swiss alpine sheep with an age range between 24-34 months (Ø 31.2 months) and an average bodyweight of 58.60-86.65 kg (Ø 72.85 kg, at delivery) were used.

To standardize the gap sizes, two custom made cutting guides were used. The bone fragments were fixed using standardized internal fixation either with a 12 hole (3mm gap) or a 13 hole (17mm gap) broad Locking Compression Plate (LCP) and 3.5mm Locking Screws. The two holes next to the gap were left empty (hole 7, 8) to place the two Marvel screws perpendicularly to the plate by use of a specially developed Marvel drill guide. After placement of the cortical screws from cranially to caudally, Marvel transducers with corresponding wire connectors were attached to both screw heads. The surgical procedure was the same (same implant placement) for all animals in the 3 mm gap model and all animals in the 17 mm graft model, regardless of the group (TI, CI or NCI). Indeed, in all animals, two Marvel screws were implanted on either side of the defect and connected to the implanted Marvel transducer.

Experiment	**Group**	**Marvel transducer implanted**	**Marvel outer coil applied**	**PEMF treatment administered**	**Autolo-gous bone graft applied**
3 mm gap model	Test Item (TI)	Yes	Yes	Yes	No
	Control Item (CI)	Yes	Yes	No	No
17 mm graft model	Test Item (TI)	Yes	Yes	Yes	Yes
	Control item (CI)	Yes	Yes	No	Yes
	Negative Control (NCI)	Yes	Yes	No	No

Table 2.1: Treatment Group Description.

After surgery, the operated limbs of all animals were casted and the animals of the 17 mm gap were additionally kept in suspension during the first 4 weeks after surgery.

Operated sheep limbs in the TI group were treated with Pulsed Electromagnetic Field Stimulation (PEMF) treatments after surgery (twice daily, 90 mins each, starting 4 days post-OP until sacrifice). The CI and NCI group animals received no PEMF treatment, but the outer coil was applied nonetheless for the same amount of time (twice daily, 90 mins each, starting 4 days post-OP until sacrifice). This was done to make sure that the sheep in all groups (TI, CI and NCI) use their limbs the same way and carry the same load throughout the in-life phase.

Therefore, in the 3mm gap model, the TI consisted of the Marvel screws connected to the implanted transducer as well as the outer coil connected to the power amplifier, which delivered the PEMF treatment. The CI in the 3mm gap model consisted of all of the above-listed components, except for the connection to the power amplifier (no PEMF treatment). For the 17mm graft model, in addition to the list of components above, both TI and CI included the autograft material, while the NCI did not (Table 2.1).

Cast changes and radiographs in three projections (anteroposterior (0°), two angled planes: caudal (265°) and cranial (275°)) were performed weekly beginning in week 3 post-operatively until sacrifice. After 9 weeks of follow up, all sheep of the 3 mm gap model were sacrificed, while all animals of the 17 mm gap model were sacrificed after 12 weeks. After sacrifice, fracture healing was evaluated radiologically (radiographs and Micro-CT), biomechanically and histologically.

Both tibiae of each animal were harvested, cleansed from surrounding tissue, labelled, macroscopically examined for hardware failures, screw loosening, tissue reaction, and callus formation. Local draining lymph nodes (lnn. poplitei) were harvested and macroscopically evaluated. Photographs were taken of representative implant-related macroscopic findings and stored digitally. For transport, both tibiae of each sheep were wrapped in wet gauzes soaked with saline solution and placed in plastic bags, labeled with the sheep number and limb side (left or right).

The operated and non-operated tibiae were immediately transported to Scanco Medical AG for Xtreme CT II scanning. Afterwards they were transported to the Institute for Biomechanics ETHZ, Prof. Ferguson, for biomechanical testing.

After biomechanical testing, the remaining part of the treated tibiae were prepared for histological processing. Ground section were cut, and microradiographs were taken before mounting and staining. Histomorphometrical, histological, and fluorescence analyses were performed. Afterwards, thin sections were cut, stained and histologically evaluated. An overview of analyses and their purposes is presented in the Table 2.2.

Analysis	Purpose	Time points
Radiographs	Radiographs of the operated tibia were taken at different angles to allow better visualization of the callus formation at the cis- and trans-cortex. Radiologic healing was semi-quantitatively evaluated focusing on callus formation, callus and defect density over time. The callus area was quantitatively measured using Osirix	3mm gap model: Post OP and weeks 3,4,5,6,7,8 and 9
		17mm graft model: Post OP and weeks 3,6,9 ,12
Fluorescence	Determination of Calcium deposition, indicative of new bone formation at the fracture gap area and surrounding at different time points by means of fluorescence marker injection	3 w. post OP: calcein green 6 w. post OP: xylenol orange 48h before sacrifice: oxytetracycline
Macroscopic evaluation	Local draining lymph nodes were collected evaluated. callus formation, mechanical stability and inflammation was documented.	At sacrifice
Micro-CT	Evaluation of callus volume and density as well as callus distribution	Immediately after sacrifice
Biomechanics	Non-destructive torsional loading for evaluating torsional stiffness (Nm/deg)	Immediately after sacrifice
Histology	Evaluation performed qualitatively (for type of bone healing, predominant cell types, vessel formation) and quantitatively (histomorphometrical analysis for percentage of new bone)	After biomechanical testing

Table 2.2: Overview of analyses and their purposes.

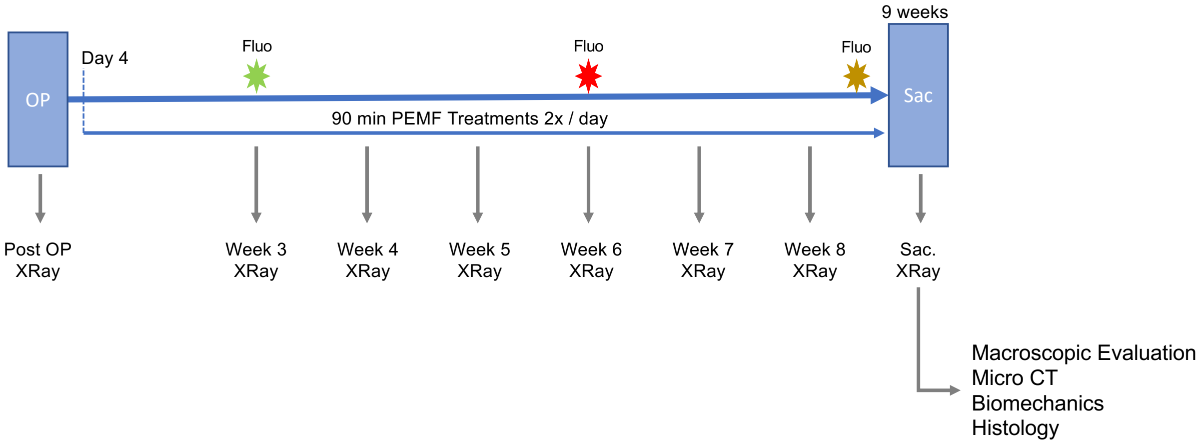

Figure 2.1: Timeline and evaluation methods for 3mm gap model.

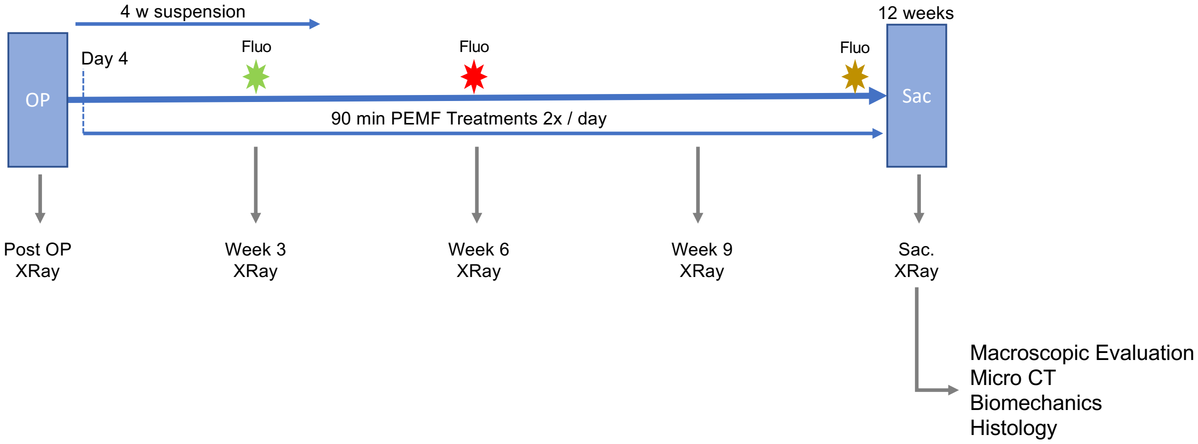

Figure 2.2: Timeline and evaluation methods for 17mm graft model.

Experiment	Treatment Group	Number of Sheep	Operated Limb (L:R)
3 mm gap model	Test Item (TI)	8	4 : 4
	Control Item (CI)	6	3 : 3
17 mm graft model	Test Item (TI)	6	3 : 3
	Control Item (CI)	6	3 : 3
	Negative Control (NCI)	3	2 : 1

Table 2.3: Animals per group.

Experiment	Treatment Group	Average age in months	Average weight in kg
3 mm gap model	Test Item (TI)	30.5 ± 2.9	67.4 ± 2.8
	Control Item (CI)	32.0 ± 1.1	66.4 ± 4.5
17 mm graft model	Test Item (TI)	36.0 ± 1.1	71.8 ± 9.5
	Control Item (CI)	36.0 ± 1.1	73.3 ± 7.5
	Negative Control (NCI)	27	74.0 ± 2.3

Table 2.4: Group characteristics.

Both the 3 mm model and 17 mm model provide an ideal, standardized situation to evaluate bone healing under physiological biomechanical loading. Indeed, standardized operating procedure allows the reliable creation of reproducible defects and the secure placement of a fixation plate. In addition, sheep have the ideal size for implanting device such as the Marvel implants, because devices of the same size would be destined for human use.

2.2 Animal Test System

2.2.1 Randomization and Allocation

Animals were randomly selected by hand and allocated to treatment groups. The operated hind limb was alternated from one sheep to the next to ensure an equal distribution within the groups.

Animal husbandry conformed to the Swiss requirements. Community tap water from the city of Zurich was available ad libitum. Hay and mineral supplements were provided ad libitum. The animals were fasted at least 24 hours before anesthesia but were allowed access to water ad libitum.

There was daylight cycle and environmental conditions were continuously monitored for temperature and humidity. Occasionally rise of temperature and humidity occurred, usually following room cleaning or other reasons and are considered not to have any influence on this type of study.

During acclimatization, sheep were housed in group pens (“Strickhof”: YUS-D-11).

After surgery, sheep were moved to smaller, single boxes (“Minipig 1”: YMP-E-4 or

“Minipig 2": YMP-E-5), where they could still maintain eye and nose contact to other sheep. Housing pens always provided at least 2 m^2 per animal.

The first three control animals (86.04, 86.05, 86.06) were kept together in a bigger box (“Minipig 1”: YMP-E-4) from the tenth day post-surgery. They were in group as there were no cables attached to the coils during the treatment time, however, to ensure no bias between the groups, these control animals were also put in small individual boxes after about three and a half weeks. In this way, all sheep had the same movement possibility.

2.3 Experimental procedure

2.3.1 Anesthesia

Standardized anesthesia was performed and anesthesia health checks were performed as a general check of cardiovascular and respiratory function prior to sedation as well as prior to induction of anesthesia.

After 16 to 24 hours of fasting and 30 minutes before induction of anesthesia, the animals were premedicated with buprenorphine (0.01 mg/kg BW im, Temgesic®, Reckitt Benckiser AG, Wallisellen, Schweiz) and either xylazine (0.1 mg/kg BW im, Xylazin Streuli ad us. vet., Streuli Pharma AG, Uznach, Schweiz, animals 86.01-86.07) or medetomidine (0.005-0.01 mg/kg BW im, Medetor®, Virbac AG, Opfikon, Schweiz, animals 86.08-86.29). A catheter was placed into one jugular vein and prophylactic antibiotics (penicillin 30’000 IU/kg BW iv, Penicillin natrium Streuli ad us vet, Streuli Pharma AG, Uznach, Schweiz; gentamicin 4 mg/kg BW iv, Vetagent® ad us. vet., MSTD Animal Health GmbH, Luzern, Schweiz), as well as a pre-emptive analgesic drug, carprofen (4 mg/kg BW iv, Rimadyl®, Zoetis Schweiz GmbH, Zürich) were given intravenously. A booster for tetanus (3’000 IU/sheep sc, Tetanus Serum Intervet, MSTD Animal Health GmbH, Luzern) was administered subcutaneously.

Anesthesia was induced with midazolam (0.1 mg/kg BW iv, Midazolam Sintetica, Sintetica AG, Mendrisio, Schweiz), ketamine (3-5 mg/kg BW iv, Ketanarkon® 100 ad us. vet., Streuli Pharma AG, Uznach, Schweiz) and propofol (0.4-0.6 mg/kg BW iv, or more if needed, Propofol 1% MCT Fresenius, Fresenius Kabi AG, Oberdorf, Schweiz), the latter administered to effect. After laryngeal desensitization with lidocaine spray, the trachea was intubated and correct placement was confirmed by expired carbon dioxide monitoring ($F_{et}CO_2$).

Anesthesia was maintained with a balanced anesthetic protocol, employing the administration of isoflurane (1%–3%, Attane™, Isoflurane ad us. vet., Provet AG, Lyssach, Schweiz) in oxygen via an adult F-circuit, a variable rate infusion of propofol (1 mg/kg/h) and ketamine (1.2 mg/kg/h). The cornea was protected with ophthalmic ointment. Intraoperatively, Ringer's lactate solution was administered at a rate of 5-10 mL/kg/h.

Monitoring parameters included: electrocardiogram (ECG), heart rate, pulse rate and invasively or non-invasively measured blood pressures (systolic, mean and diastolic arterial) via an arterial catheter in an auricular artery. Furthermore, inspired and expired concentrations of carbon dioxide, oxygen and isoflurane, as well as esophageal temperature and saturation of arterial blood (SpO_2) was monitored. All parameters were constantly measured and recorded in 10-minute intervals.

2.3.2 Surgical procedure

Unless otherwise noted, all mentioned surgical instrumentation and implants were from DePuy Synthes®.

Figure 2.3: Surgical set.

2.3.2.1 Presurgical preparation and surgical access (both models):

The anesthetized sheep were placed in lateral recumbency with the upper hind limb in flexion and retracted craniodorsally fixed to the surgery table. The lower hind limb was exposed on its medial side up to above the stifle joint. The limb was firmly supported through an inflatable table-mat routinely used during surgeries.

The entire operated limb was clipped prior to surgery and the surgical site scrubbed and cleansed according to surgical routine with the limb in suspension. The animals were draped according to routine, where the limb was draped separately, such that it could be moved during surgery without jeopardizing sterility.

An approximate 16-18 cm incision was performed at the medial aspect of the tibia shaft extending from the tarsus to the metaphysis of the proximal tibia. Bleeding was controlled with electrocautery. The soft tissue and fascia were incised and dissected down to the bone. At the proximal end of the tibia, the muscles at the caudal aspect was slightly incised at their insertion to the bone and retracted caudally, exposing the full tibia shaft.

2.3.2.2 Procedure for 3mm Gap Model:

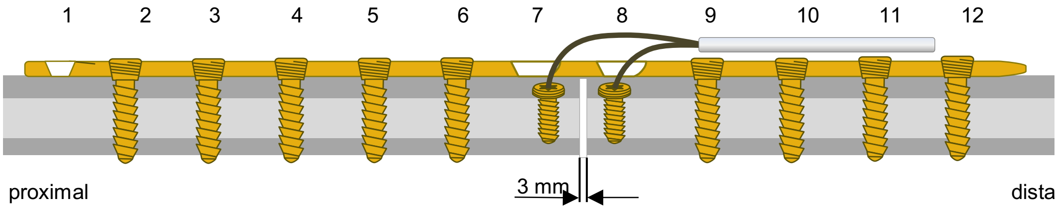

Figure 2.4: Procedure for 3mm gap model.

A 12-hole, broad, straight veterinary 3.5 mm locking compression plate (VP4045.12, length 159 mm, stainless steel) was adapted to the medial aspect of the tibia shaft with the most distal hole about 1 cm above the tibiotarsal joint. The plate was slightly contoured to fit the tibial shaft. A special developed cutting guide, with 4 rubber rings in place (2 proximal, 2 distal), was temporarily fixed to the bone using 2.0 drill guides and k-wires (2.0*150mm; 292.200.01) at both ends.

Using 2.0mm LCP drill guides and a 2.0mm LCP drill (310.534), the cutting guide was temporarily fixed to the intact tibia with four monocortical Ø2.7/3.5mm screws (L20 mm, steel, 202.920), two proximal and two distal, starting with screw position 9&6, thereafter 10&5).

An oscillating saw (saw blade 519.150) was used to perform the osteotomy through the guiding slot under constant irrigation with 0.9% saline solution. After removal of the cutting guide, the fragments were repositioned and fixed with the 12-hole LCP, utilizing the 3-mm distance holder to ensure a standardized parallel gap.

The already drilled holes were fixed again using the monocortical screws, starting with screw position 9 and 6 followed by 10 and 5. Afterwards screw positions 4, 11, 3 were drilled bicortically using a 2.8 drill guide with a 2.8 mm drill bit (310.284) and 3.5-mm bicortical screws (213.028 - 213.036) in measured lengths were implanted. The k-wires were removed and holes 12 and 2 were drilled and screws implanted. Afterwards the monocortical screws were removed step by step in an alternating fashion and replaced by bicortically placed 3.5mm screws in measured lengths, leaving screw holes 1, 7 and 8 empty.

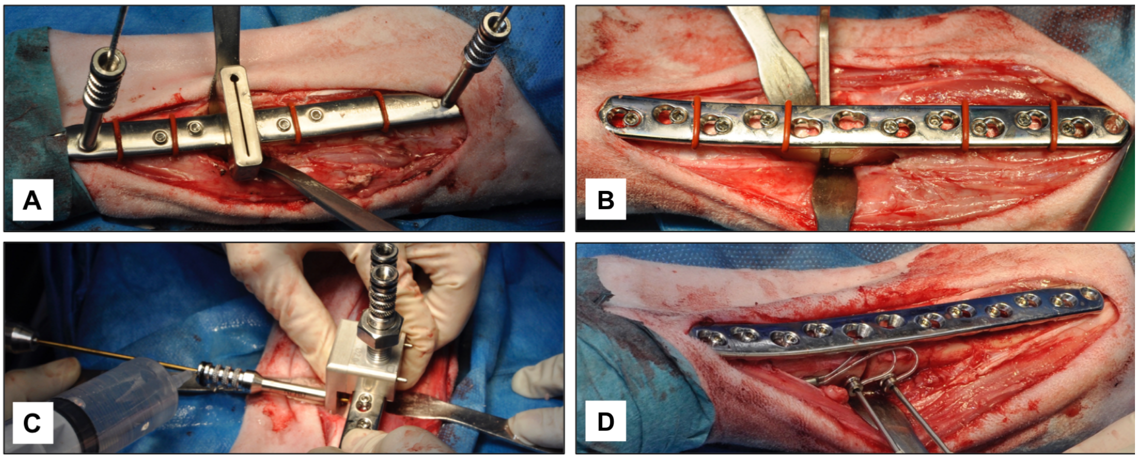

Figure 2.5 (A, B, C, D): Most important surgical steps for the 3mm gap model: Cutting guide fixed with 2 k-wires and 4 monocortical screws (A), Plate fixed with bicortical screws, 7.+8. left empty (B), Drilling guide for Marvel screws fixed on plate (C), Marvel technology implantation and resistance measurement (D).

2.3.2.3 Procedure for 17mm Gap Model:

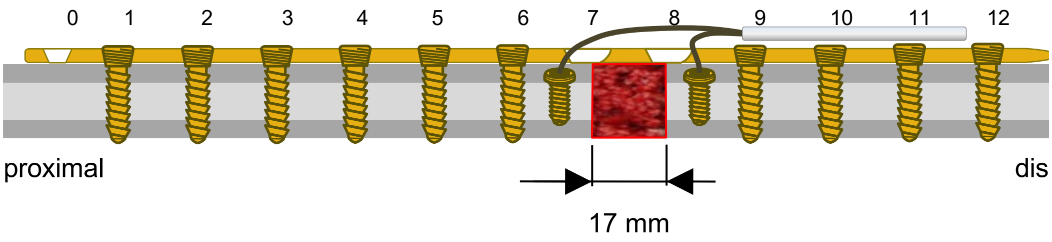

Figure 2.6: Procedure for 17mm graft model.

A 13-hole broad, straight veterinary 3.5 mm locking compression plate (VP4045.13, Vet LCP 3.5, straight, broad, 13 holes, length 172 mm, stainless steel) was adapted to the medial aspect of the tibia shaft with the most distal hole about 1 cm above the tibiotarsal joint. The plate was slightly contoured to fit the tibial shaft. A special developed cutting guide, with 4 rubber rings in place (2 proximal, 2 distal), was temporarily fixed to the bone with Kirschner wires (2.0*150mm; 292.200.01) at both ends.

Using 2.0mm LCP drill guides and a 2.0mm LCP drill (310.534), the cutting guide was temporarily fixed to the intact tibia with four monocortical Ø2.7/3.5mm screws (L20 mm, steel, 202.920) two proximal and two distal, starting with screw position 9 and 6, thereafter 10 and 5).

An oscillating saw (saw blade 519.150) was used to perform the osteotomy through the guiding slots under constant irrigation with 0.9% saline solution. After removal of the cutting guide, the fragments were repositioned and fixed with the 13-hole LCP, utilizing the 17-mm distance holder to ensure a standardized parallel gap.

The already drilled holes were fixed again using the monocortical screws starting with screw position 9 and 6 followed by 10 and 5. Afterwards screw positions 4, 11, 3 were drilled bicortically using a 2.8 drill guide with a 2.8 mm drill bit (310.284) and 3.5-mm screws (213.028 - 213.036) in measured lengths were implanted. The k-wires were removed and holes 12, 2 and 1 were drilled and screws implanted.

Afterwards the monocortical screws were removed step by step in an alternating fashion and replaced by bicortically placed 3.5mm screws in measured lengths.

All screws were tightened again using a torque limiter of 1.5 Nm (511.773) in the first 6/12 animal (86.01 - 86.06). In all other animals, the screws were tightened with a normal screw driver (314.030) until they were firmly locked as detected by the surgeon. Screw holes 1, 7 and 8 were left empty.

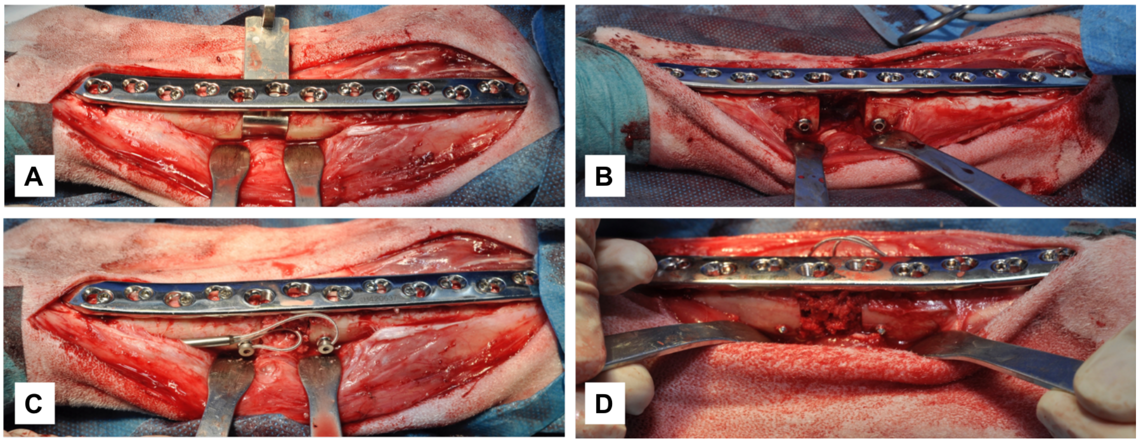

Figure 2.7 (A, B, C, D): Most important surgical steps for the 17mm Graft Model: LCP fixed with bicortical screws with 17mm spacer placed in the gap (A), Marvel screws in place (B), Transducer in place, caps attached, autograft filling the defect, cranial view (C), Autograft inside the gap, caudal view (D).

2.3.2.4 Marvel technology placement and closure (both models):

After fixation of the plate and retightening of the LCP screws, the rubber rings were cut and removed. The Marvel drill guide base was placed to the two remaining LCP holes (Nr.7+8) in the middle of the VET plate to assure a perpendicular drilling of the drill holes.

To drill the cortex holes for the Marvel screws, a Ø2.5mm drill guide was attached to the drill guide base and the two holes (proximally and distally of the gap) were drilled bi-cortically using a 2.5 drill bit and the thread was cut using a taping device. 3.5 mm cortex screws (204.020 or 204.022) were inserted in the designated holes.

The two wire caps of the Universal Transducer SI-ES (Magnetodyn® Technology) were attached to both hexagonal cortical screw heads (Marvel screws). The wire was looped to allow for movement of the wire during the healing period. The transducer was positioned under muscle tissue distally. In sheep 86.13 to 86.29, re-worked transducer caps were used in order to avoid cap loosening. Specifically, the transducer cap cone was widened by 0.2 mm then the cone void was filled with non-elastic epoxy resin and the taper was additionally grid blasted.

The resistance of the transducer was measured using an ohmmeter to verify that the handling and implantation procedure did not damage the transducer. A value of 90±15 Ohms was indicative of a functioning transducer.

Routine closure of muscle, fascia, subcutaneous tissue and skin was performed.

Radiographs in 3 different planes (anteroposterior (0°) and two angled planes: cranial (275°) and caudal (265°)) were taken immediately after surgery with the animals still under anesthesia. A full cast was applied to the operated limb. The animals were recovered from anesthesia and observed for bloating, respiratory problems and any signs of discomfort or pain until they could eat, drink and stand normally.

2.3.3 Casting and suspension

All operated limbs received a cast for the duration of the in-life period, with cast changes performed at each radiographic time point (see Figure 2.1 and Figure 2.2).

The first full limb cast was applied after the surgery, still in general anesthesia, when a radiographic examination confirmed optimal placement of the implants and the Marvel technology components. Subsequent cast changes were performed after each radiographic examination, without a use of any sedation.

Animals of the 17 mm graft model were, in addition, kept in suspension during the first 4 weeks after surgery, to decrease the risk of postoperative tibia fracture or implant breakage. Casting the hindlimbs alone minimizes this risk substantially, however, some uncontrolled movements still occur, especially when the sheep tries to get up. The suspension excludes this risk almost completely as animals are able to support themselves inside it, without exerting high forces on the postoperative limbs. In case of skin irritation caused by the suspension nets, they would be additionally padded or repositioned.

Animals with the 3 mm gap did not receive the suspension nets, as it had been proven in the previously conducted experimental trials (Bottlang et al. 2010; Plecko et al. 2012; Plecko et al. 2013; Bottlang et al. 2016), that this precaution method was not necessary for the non- critical size defects as the gap would likely heal before the plate bends.

Both casts and suspension systems were checked at least twice daily, to ensure optimal comfort of the animals. Neither suspension systems nor casts were interfering with the placement of the belts for the Marvel coils or the administration of the PEMF treatment.

Figure 2.8: Casted sheep in the suspension system.

2.3.4 Postoperative routine analgesia

Buprenorphine (0.01 mg/kg BW, im, Temgesic®, Reckitt Benckiser AG, Wallisellen, Schweiz) was applied as pre-emptive analgesia and additional sedative 30-45 minutes before induction of anesthesia and every 4-6 hours after recovery on the day of surgery and as deemed necessary for up to three days after surgery depending on pain assessment.

Carprofen (4 mg/kg BW, SID, iv, Rimadyl®, Zoetis Schweiz GmbH, Zürich) was given as pre-emptive analgesia prior to induction of anesthesia and for five days after surgery depending on pain assessment.

Paracetamol (10mg/kg BW, iv, BID, Paracetamol Fresenius, Fresenius Kabi AG) was given to the animals of the 17 mm graft Model postoperatively as deemed necessary, BID-TID every 8 – 12 h for 3-4 days.

2.3.5 Prophylactic antibiotic therapy

Prophylactic antibiotic therapy was administered for five days starting on the day of surgery: penicillin (30’000 IU/kg BW, BID, iv, Penicillin natrium Streuli ad us vet, Streuli Pharma AG, Uznach, Schweiz)) and gentamycin (4mg/kg/BW, SID, iv, Vetagent® ad us. vet., MSTD Animal Health GmbH, Luzern, Schweiz).

A booster for tetanus (3’000 IU/sheep sc, Tetanus Serum Intervet, MSTD Animal Health GmbH, Luzern) was administered subcutaneously on the day of surgery.

2.4 In-life observations

All in-life observations and examinations of the animals were performed by veterinarians, veterinary engineers or special trained animal caretakers under supervision following standardized operating procedure. Medical records were kept for each animal, and the observations listed below recorded.

A first general health check was performed by a veterinarian on the day of arrival to the MSRU. Also during the acclimatization period all animals were observed several times a day for any signs of abnormalities. A blood sample for hematological and chemical examination was taken from every sheep and checked by a veterinarian. Only healthy sheep were included in the study. The animals were weighed once prior to surgery during the acclimatization period for the exact medication dosage calculation.

General health check of cardiovascular and respiratory function was performed prior to sedation and prior to induction of general anesthesia. All sheep received a study specific ear tag and a subcutaneous transponder for identification purposes during the general anesthesia.

During the postoperative observation period all animals were checked at least twice daily. Any signs of pain, lameness, discomfort or loss of appetite were documented in the medical records.

After the surgery was completed, the animals were transported to their single boxes and examined at least three times in the first two hours after surgery, until normal behavior and clinical parameters were restored. Hay was provided at least twice daily, with the exception of the day of cast change, when the animals were fasted for at least 12 hours to prevent bloating and the day prior to surgery, when the animals had to be fasted for 24 hours. Water was provided ad libitum.

Environmental conditions were continuously monitored using a data logger for temperature and humidity (temperature range 10-35°C, relative humidity range 10-95%). There was daylight cycle.

2.5 Pulsed electromagnetic field therapy

All sheep in the study were fitted with the Marvel outer coil (Figure 2.9 and Figure 2.10) for 90 mins, twice per day, for the duration of the in-life period, starting at day 4 after surgery. Custom straps were designed to allow ease of handling, ensuring sheep would be minimally disturbed without compromising the animal's ambulation. The straps were also designed to distribute the weight of the coil on the lower back of the sheep. The outer coil was custom shaped to fit a casted sheep hindlimb. Sheep in the test groups of both the 3 mm gap model and the 17 mm graft model had their outer coils connected to the PEMF generators. These generators were designed to create a 5 mT alternating magnetic field inside the outer coil (flux density of 3-5 mT and a frequency of 12-20 Hz). This magnetic field creates up to 700mV electrical potential within the internal transducer thereby delivering an electromagnetic therapy between the two implanted Marvel screws, which act as electrodes across the tibia defect.

The first treatment always started in the morning, around 8 AM, ended therefore at 9.30 AM. The afternoon treatment would typically start around 2 PM and end at 3.30 PM. The average time between both treatments was 5 hours 18 minutes. There were, however, situations with both shorter and longer breaks between the morning and afternoon treatments, especially on days when radiographs and cast changes were planned.

There were some situations when treatment was interrupted, for instance, because of excessive movement of the animal inside the box or by stepping on the cable connecting the coil to the generator. In such cases, the cause of the interruption was resolved if possible (e.g. shortening or extending the length of the cable, checking if the machine works properly) and the treatment was resumed.

Figure 2.9: Pictures of sheep fitted with the Marvel outer coil.

Figure 2.10: Closer picture of the Marvel outer coil and straps attached to it during the pre- surgical coil fitting.

2.6 Radiographic follow-up

Radiographs were taken immediately after surgery with the animals still under anesthesia in three different planes: anteroposterior: 0°, two angled planes: 275° (anterior, cranial) and 265° (posterior, caudal). All radiographs were performed at 50 kV and 2.0 mAs.

The anteroposterior projection was used for the exact gap area evaluation, as the position of the plate, screws and the Marvel technology components allow for a clear undisturbed view of the defect. It also shows the callus formation at both cis and the trans cortices.

The angled projections were used for the evaluation of the healing progression on the cranial and caudal tibia cortices. Additionally, these projections would make it possible to detect any caps loosening or detachments.

Starting three weeks post-surgery, radiographs were taken in the same planes as postoperatively during cast changes:

- 3 mm Gap Model:
  During In-life phase: 3, 4, 5, 6, 7, and 8 weeks
  Post mortem: 9 weeks
- 17 mm Graft Model:
  During In-life phase: 3, 6, 9 weeks
  Post mortem: 12 weeks

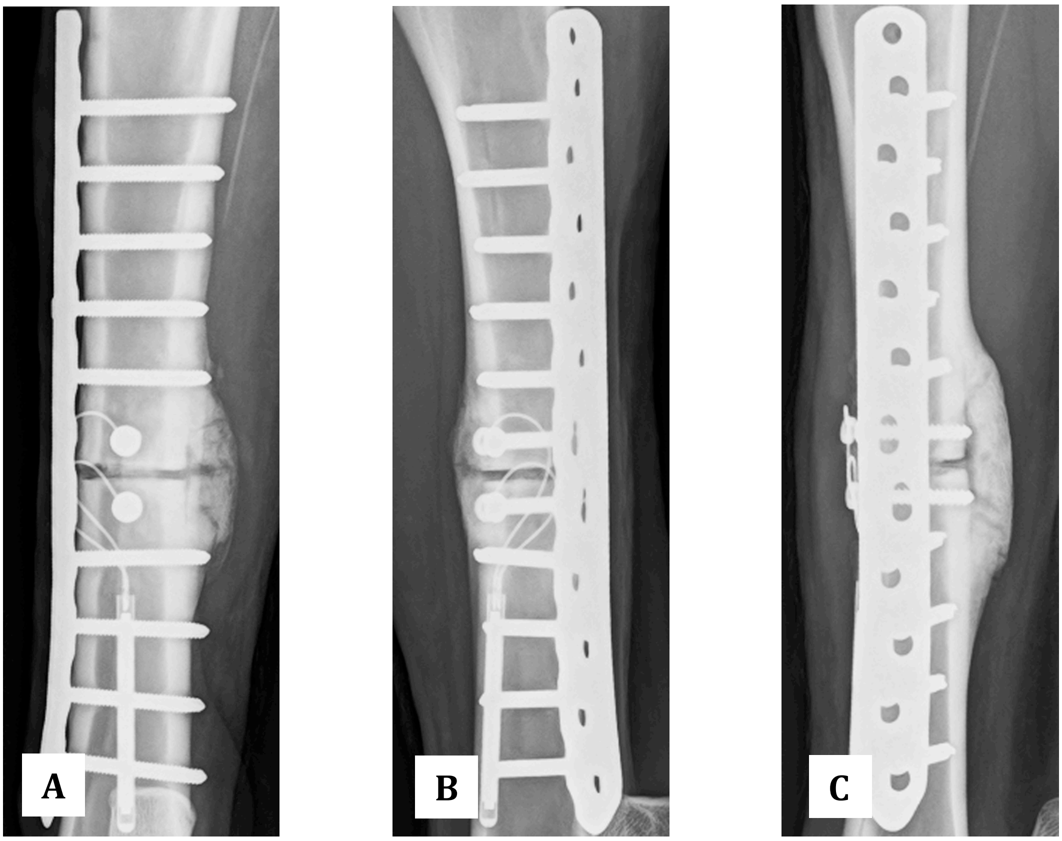

Figure 2.11 (A, B, C): Example of the three radiographic projections: anteroposterior: 0° (A), oblique 275° (anterior, cranial) (B) and oblique 265° (posterior, caudal) (C) of sheep 86.28 at week 6 post OP.

2.7 Fluorescent marker injections

Fluorescent dyes were injected at different time points post-surgery. The dyes were given in order to document new bone formation at different time points. They first irreversibly bind to the calcium in blood and then are incorporated in the bone, thereby documenting new bone deposition and remodeling at various stages of healing. This deposition happens normally within 48 hours of dye injection, therefore, the dyes were given 2 to 3 days before the planned calcium deposition timepoint. Three different dyes were used at three timepoints as follows:

3 weeks post-surgery:	Calcein green; 5 mg/kg BW, sc
6 weeks post-surgery:	Xylenol orange; 90mg/kg BW, sc
48-72h prior to sacrifice:	Oxytetracycline; 20 mg/kg BW, sc

The oxytetracycline injection was therefore performed at 9 weeks for the 3mm gap model and at 12 weeks for the 17mm graft model.

Solutions of calcein green (0.5%) and xylenol orange (9%) were freshly prepared in the laboratory while commercially available oxytetracycline (Engemycin 10%, MSD Animal Health GmbH, Luzern) was used as delivered. The weight from before the surgery was used for the dosage approximation. Shortly before the application, the dyes were put at room temperature to prevent an unpleasant sensation in the animals. The dyes were injected subcutaneously in four different application regions so that no higher volume than 20 ml was deposited in one region.

2.8 Sacrifice, tissue harvest and processing

Animals were slaughtered according to the Swiss law of animal welfare. A captive bolt gun was used for the stunning procedure, providing instant unconsciousness and causing the animal to collapse. After stunning was verified by negative response of eye reflexes, main blood vessels of the neck were cut, causing exsanguination of the animal.

Tissue harvest after sacrifice:

After sacrifice, both limbs were harvested and immediately labelled. Radiographs of the operated limbs were taken in three projections: anteroposterior at 0° and two angled planes at 265° and 275°.

Local draining lymph nodes (lnn. poplitei) were harvested, photographed and macroscopically examined. Changes in lymph nodes were recorded using the following parameters: size, color, consistency, and any other observations, as appropriate. The lymph nodes were then fixed and stored in a 4% buffered formalin solution. Further processing and histological evaluation were not performed for this study.

Both tibiae of each animal were cleaned from surrounding tissue and labeled with the sheep number and limb side (left or right). A macroscopic examination (see 3.12.1) of the implantation sites and surrounding tissue was conducted. Digital pictures were taken of the operated tibiae in all planes. Non-operated tibiae from the negative control group (86.25 R, 86.26 L, 86.27 R) were not harvested. The resistance of the implanted transducer was measured at the caps using an ohmmeter.

Afterwards screws and plate were removed and stored in plastic bags labelled with the study number and animal number. Thereafter, digital pictures were taken in all planes without implants. Representative implant-related macroscopic findings were photographed. Both tibiae of each sheep were wrapped in saline soaked gauze and placed in plastic bags for transport, labeled with the sheep number and limb side (left or right).

All harvested tibiae (operated and non-operated) were immediately transported (same conditions see above) to Scanco Medical AG for μ-CT scanning. After μ-CT scanning, tibiae were transported (same conditions see above) to the Institute for Biomechanics ETHZ for immediately biomechanical testing. Operated tibiae from the negative control group (86.25 L, 86.26 R, 86.27 L) did not undergo biomechanical testing and were transported directly to the MSRU after μ-CT scanning for histological processing. After biomechanical testing, non-operated tibiae were discarded and operated tibiae were transported (same conditions see above) to the MSRU for histological processing.

2.9 Micro-CT scanning

All operated and non-operated tibiae from the TI and CI groups of both models were sent to Scanco Medical AG for Micro-CT scanning (52 tibiae in total). Only the operated tibiae from the NCI group of the 17mm graft model were scanned (3 tibiae in total), as the non-operated contralateral tibiae were not harvested in these animals. The scans were performed using an XtremeCT II scanner, operating with an X-ray tube with 60.7 μm resolution and 68 kVp voltage. The region of interest for scanning was defined and a distance of at least 150 mm was scanned.

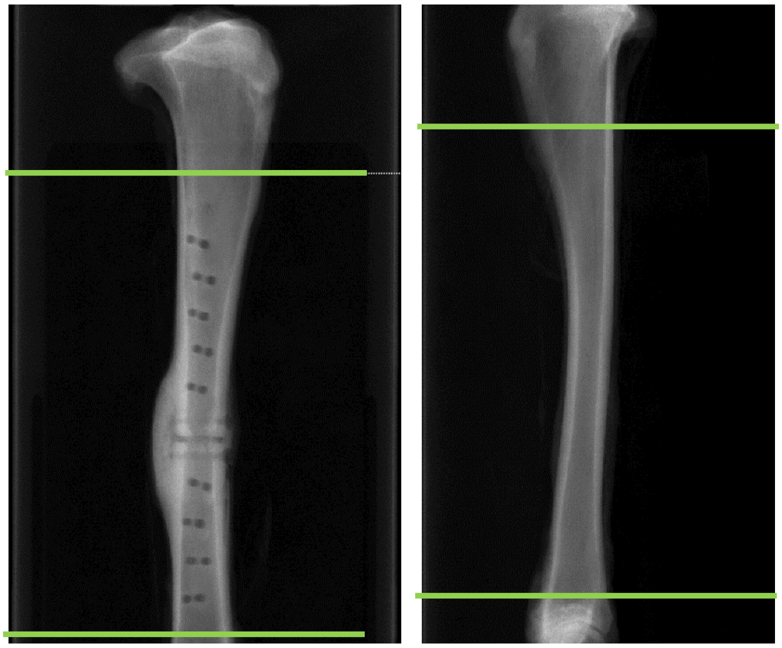

Figure 2.12: Scanned region of interest are indicated between the two green horizontal lines in the operated (left panel) and non-operated (right panel) tibia.

2.10 Biomechanical testing

In total, 26 pairs of sheep tibiae (operated and non-operated) were biomechanically tested at the Institute of Biomechanics of ETHZ. All mechanical torque tests were performed using an Instron® E10000 electrodynamic testing machine, following a standardized test protocol.

Biomechanical testing was always proceeded by careful preparations of the samples. To prevent slipping of the bone, several steps were undertaken. First of all, periosteum and all remaining soft tissue were removed from the potted area. Secondly, four screws were inserted perpendicular to the major bone axis in the distal epiphyses, providing further stabilization. Wet gauze was placed around the fracture area to ensure proper tissue preservation.

The proximal epiphysis was potted first, while the bone was aligned having both ends centered on the mechanical rotation axis. Alignment was maintained with a rigid metal bar joining the proximal and distal pot. Potting depth was adjusted to ensure a minimal distance of 10 mm between the Beracryl and the nearest screw hole from the fracture plate. The spacing between the proximal and distal Beracryl surface after embedding was noted and ranged between 140 mm and 160 mm, depending on the tibia length, but ideally as similar as possible for each individual.

Experiment	Group	OP Limb Distance between the pots in mm:	Contralateral limb Distance between the pots in mm:
3 mm gap model	Test Item (TI)	153.0 ± 10.8	153.0 ± 10.1
	Control Item (CI)	144.5 ± 11.1	145.1 ± 6.1
17 mm graft model	Test Item (TI)	146.7 ± 8.9	148.2 ± 10.4
	Control item (CI)	154.8 ± 11.1	154.2 ± 10.6

Table 2.5: Distance between the pots of both limbs in all groups.

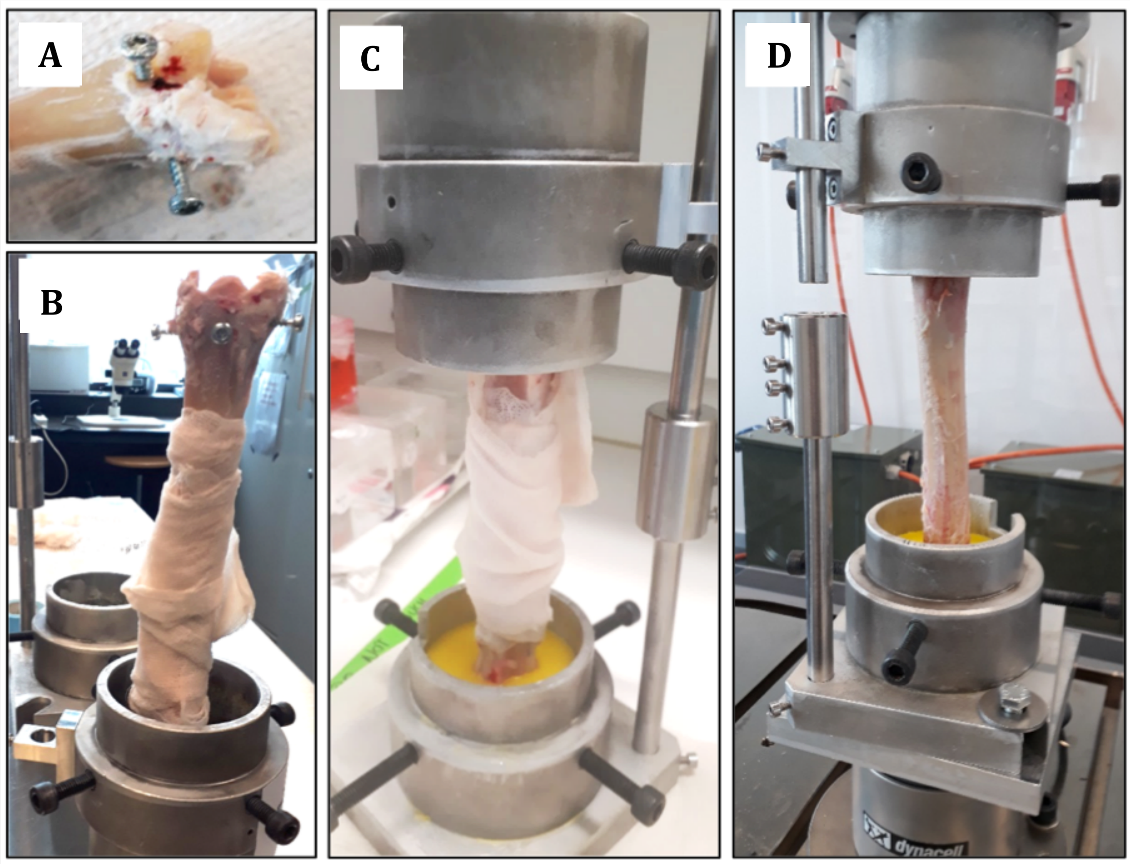

Figure 2.13 (A, B, C, D): Tibia preparation for embedding, inserting four screws perpendicular to the major bone axis in the distal epiphysis (A) and aligning the proximal epiphysis in the first pot (B). Beracryl embedding with alignment of both joints centered in the mechanical rotation axis (C). Embedded tibia installed on the Instron® E10000 (D).

Non-destructive torque testing was performed according the following protocol:

1. Manually load sample with a 5 N axial load
2. Hold 5 N (axial) for the entire test
3. Rotate the proximal part in the internal rotation direction at 5 degree/min

4. Stop the internal rotation when torque reaches 10 Nm
5. External rotation back to initial sample position at 5 degree/s to allow sample removal

Rotation (in degrees) and torque (in Nm) were recorded during the torque test at a sampling rate of 20 Hz. The test was run in angle control until the end detection of 10 Nm was reached. The test was manually stopped for samples not reaching 10 Nm after 12 degrees of internal rotation.

2.11 Histology Processing

In all operated tibiae, the proximal and distal ends were cut and discarded and the remaining part of the operated tibiae were separately placed in plastic molds, labelled and fixed in 40% ethanol for at least 1 week, followed by a series of ethanol dehydration (50 to 100%):

- 3x2 days in 50% ethanol
- 2x2 days in 70% ethanol
- 2x2 days in 80% ethanol
- 2x2 days in 90% ethanol
- 2x2 days in 96% ethanol
- 4x2 days in 100 % ethanol
- 2x3 days in xylol as an intermedium to MMA (Methylmethacrylate).

After complete dehydration, all samples were degreased in xylene and subsequently infiltrated in liquid methylmethacrylate (MMA). Polymerization was carried out in plastic molds closed with a lid that were kept at 4°C for at least 2 weeks, thereafter in a water bath at room temperature until polymerization occurs. Finally, the plastic molds were placed in an uncovered incubator (37°C) to complete hardening of the samples. The whole process took at least 4 weeks until the tibia blocks were fully polymerized and ready to cut.

The polymerized bone blocks were cut lengthwise (longitudinally) to the screw axis in the midline of the bone sample using an Exact® 310 saw. These non-decalcified samples were used for histomorphometrical and fluorescence analysis. Therefore, about 1000 μm ground sections were cut.

Microradiographs of all performed ground sections were taken prior to mounting the slices on Acropal slides and surface staining.

Toluidine blue was used as a surface staining of the ground sections and the bone healing response was qualitatively and semi-quantitatively assessed as described in the analysis sections (2.12.5 Histomorphometry and 2.12.7.2 Assessment of bone activity, tissue character and healing response in the gap areaHistomorphometry).

After preparation of ground sections, the remaining samples were taken for preparation of thin sections (5μm) which were cut with a precision rotary microtome (Leica RM2155). The exact area of interest was manually chosen so that it included the defect area and both Marvel screws. The 3mm model gap was small enough to present the whole area of interest on a single slice. The 17 mm gap model had to be divided in two areas: proximal Marvel screw plus the defect and distal Marvel screw plus the defect. Thin sections were stained with toluidine blue, van Kossa/ McNeal and HE staining according to routine and used for histology evaluation on cellular level and the evaluation was focused on the cellular reactions of the tissue (see 2.12.7 Histological Evaluation).

2.12 Analysis

2.12.1 Macroscopic Evaluation at sacrifice

Macroscopic evaluation of the whole tibia, implantation sites and surrounding tissue was conducted and pictures of the region of interest were taken.

The macroscopic evaluation included such parameters like plate appearance and screw displacement, presence of callus/ossification around the implants, fibrosis around the screw hole or metallosis. Regarding the Marvel technology, following parameters were checked: screw integration, placement of transducer and caps, appearance of the surrounding tissue. Resistance of the implanted transducer was measured and noted.

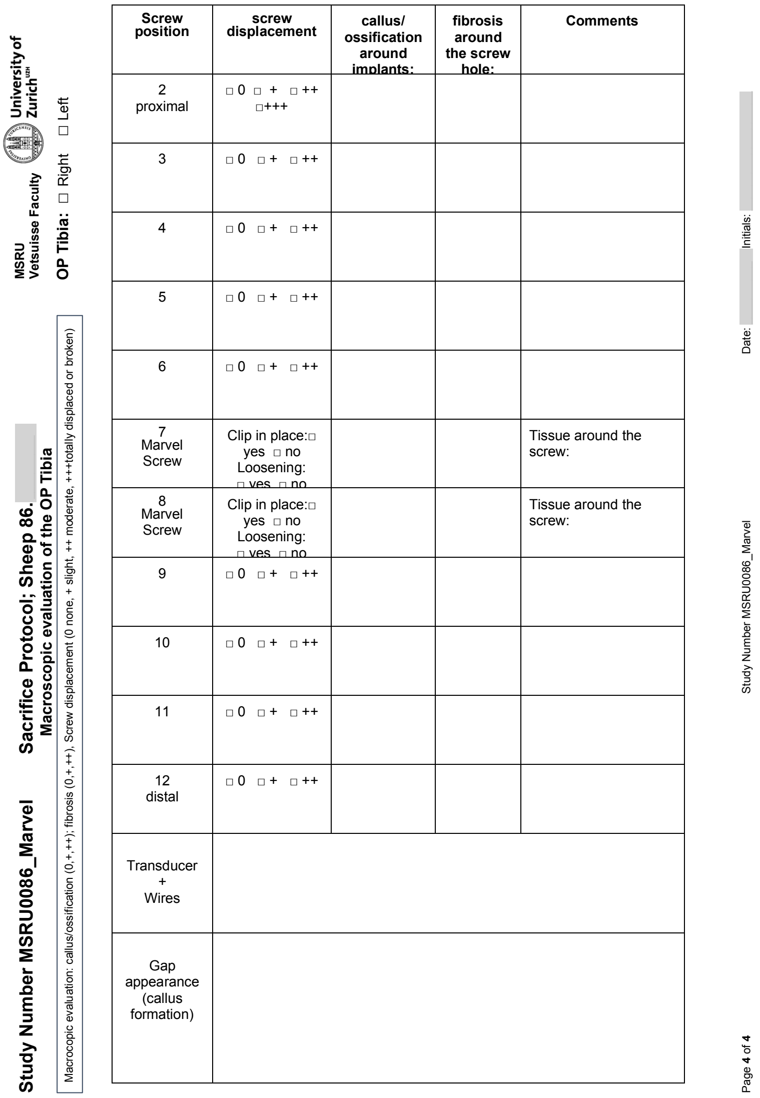

Study Number MSRU0086_Marvel **Sacrifice Protocol; Sheep 86.**

Macroscopic evaluation of the OP Tibia

MSRU
Vetsuisse Faculty

University of Zurich

OP Tibia: ☐ Right ☐ Left

Macroscopic evaluation: callus/ossification (0,+,++); fibrosis (0,+,++), Screw displacement (0 none, + slight, ++ moderate, +++totally displaced or broken)

Screw position	screw displacement	callus/ ossification around implants:	fibrosis around the screw hole:	Comments
2 proximal	☐ 0 ☐ + ☐ ++ ☐+++			
3	☐ 0 ☐ + ☐ ++			
4	☐ 0 ☐ + ☐ ++			
5	☐ 0 ☐ + ☐ ++			
6	☐ 0 ☐ + ☐ ++			
7 Marvel Screw	Clip in place:☐ yes ☐ no Loosening: ☐ yes ☐ no			Tissue around the screw:
8 Marvel Screw	Clip in place:☐ yes ☐ no Loosening: ☐ yes ☐ no			Tissue around the screw:
9	☐ 0 ☐ + ☐ ++			
10	☐ 0 ☐ + ☐ ++			
11	☐ 0 ☐ + ☐ ++			
12 distal	☐ 0 ☐ + ☐ ++			
Transducer + Wires				
Gap appearance (callus formation)				

Page 4 of 4 Study Number MSRU0086_Marvel Date: Initials:

Figure 2.14: Macroscopic evaluation sheet.

2.12.2 Micro-CT analysis

The global morphometry analysis of Micro-CT scans from both operated and non-operated limbs was performed at the Mechanical Engineering and Mechanics Department at Lehigh University.

In order to create 3D surface models a “slice-by-slice” tissue segmentation was done. This method is highly reliable and used to separate the new callus tissue (including mature, highly mineralized callus) from the existing cortical bone. Regions of new tissue were manually selected within each slice, proceeding by a recombination of these slices into a 3D region.

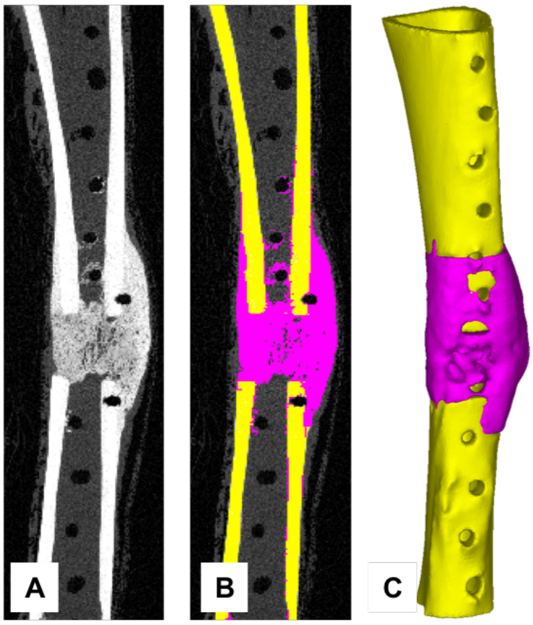

Figure 2.15 (A, B, C): CT morphometry transverse sections: original scan (A), selected new bone and old bone after slice by slice tissue segmentation (B), 3D reconstruction (C).

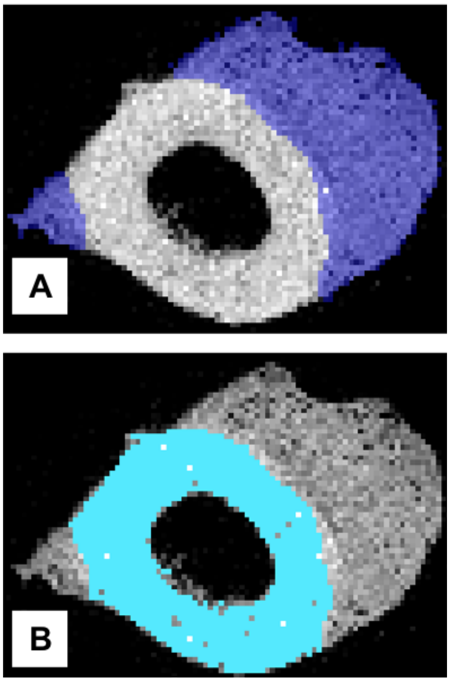

Figure 2.16 (A, B): Micro-CT morphometry cross sections segmentation: new bone (A), old bone (B).

2.12.3 Biomechanical analysis

The slope of the linear part of the loading curve (above 6 Nm for most samples) was calculated to determine the torsional stiffness (in Nm). This was done for both operated and non- operated limbs, where the healthy bones served as references. All loading curves were checked at the Institute of Biomechanics of ETHZ, to ensure the correct selection of the linear part of the curve.

The normalized stiffness results were reported as % of contralateral tibia stiffness. The comparison of the mechanical performance of the TI and CI specimens was performed.

2.12.4 Radiographic Evaluation

2.12.4.1 Semiquantitative Scoring of radiographs

Interpretation of radiographs was performed by two independent, board certified reviewers (Prof. Brigitte von Rechenberg, Dipl. ECVS and Prof. Mark Flückiger, Dipl. ECVR). Semiquantitative scores were given following a scoring system specifically adapted for this study (Table 2.6). Two additional parameters were evaluated (Table 2.7) but not included in the total score.

Cortical Callus Formation (0°, anteroposterior plane)	
0	no callus noted
1	callus not reaching into the defect
2	callus bridging the defect < 50%
3	callus bridging the defect >50% but <100 %
4	callus bridging the defect completely
Cis-Cortex Callus Formation (0°, anteroposterior plane)	
0	no callus noted
1	callus not reaching into the defect
2	callus reaching into the defect, fracture line in callus visible
3	callus reaching into the defect, fracture line in callus less visible
4	callus reaching into the defect, fracture line in callus not visible
Trans-Cortex Callus Formation (0°, anteroposterior plane)	
0	no callus noted
1	callus not reaching into the defect
2	callus reaching into the defect, fracture line in callus visible
3	callus reaching into the defect, fracture line in callus less visible
4	callus reaching into the defect, fracture line in callus not visible

RUST Score (0°, anteroposterior plane)		
1	a) fracture with fracture line and no callus formation	
2	b) fracture with callus formation and a fracture line	
3	c) fracture with bridging callus, but the fracture line is still visible across both cortices	
4	d) complete bridging of the callus with no evidence of fracture line	

Callus Opacity (0°, anteroposterior plane)	
0	soft tissue opacity
1	< 50% of normal
2	> 50-100% of normal
3	> 100% (superimposition)
Defect Opacity (0°, anteroposterior plane)	
0	soft tissue opacity
1	< 50% of normal
2	> 50-100% of normal
3	> 100% (superimposition)
Cranial Cortical Gap (275° angled plane)	
0	no callus noted
1	callus not reaching into the defect
2	callus reaching into the defect, fracture line in gap visible
3	callus reaching into the defect, fracture line in gap less visible
4	callus reaching into the defect, fracture line in gap not visible
Caudal Cortical Gap (265° angled plane)	
0	no callus noted
1	callus not reaching into the defect
2	callus reaching into the defect, fracture line in gap visible
3	callus reaching into the defect, fracture line in gap less visible
4	callus reaching into the defect, fracture line in gap not visible
➔ Total score 0-30	

Table 2.6: Score system for semiquantitative radiologic evaluation including total score of all evaluated parameters.

Blurred cortex	
0	no
1	yes
Callus at tip of Marvel screw	
0	no
1	yes at one screw tip
2	yes at two screw tips

Table 2.7: Additionally evaluated radiological parameters.

2.12.5 Histomorphometry

Microradiographs of all ground sections were taken in order to corroborate the structure of calcified tissues in the toluidine blue stained samples.

Then, quantitative histomorphometric evaluation was conducted using computer-based histomorphometric measurements.

First, ground sections were captured using a microscope (Leica Z6 APOA, Leica DFC 420C, Glattbrugg, Switzerland) in a standardized magnification (0.5x7.11) as digital images in TIF-format. Thereafter, the images were prepared for measurements. The tissues of interest were manually color-highlighted interactively using a standardized pixel-detecting tool of Adobe Photoshop 12 (Adobe Systems, San Jose, CA).

2.12.5.1 Total section evaluation (3 mm gap model)

Old bone, new bone and non-bone (non-bone containing tissue like fibrous tissue, fat, bone marrow tissue) in the complete (standardized captured) image were color-highlighted. The region of interest (ROI) was the gap area including both Marvel screws up to the 6th and 9th screw in the plate. Following colors were used:

- old bone: light blue (R: 0; G: 210; B: 255; #00d2ff),
- new bone: dark green (R: 34; G: 79; B: 7; #224f07)
- non-bone: pink (R: 242; G: 40; B: 211; #f228d3)
- background: beige (R: 198; G: 156; B: 96; #c69c60).

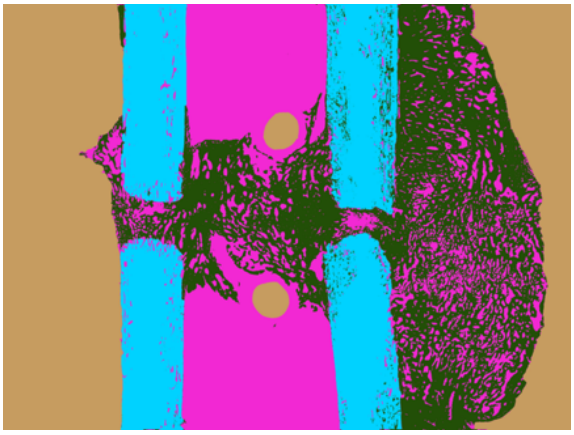

Figure 2.17: Animal 86.08, example for total ground section evaluation of the 3 mm gap model. Old bone (light blue), new bone (dark green), and non-bone tissue (pink), back-ground (beige), the round dots in beige display the Marvel screw areas.

2.12.5.2 Total section evaluation (17 mm gap model)

Old bone, callus (containing autograft material within the gap area and newly formed bone), non-bone (non-bone containing tissue like fibrous tissue, fat, bone marrow tissue) and cartilaginous tissue in the complete (standardized captured) image were color-highlighted. The callus consisted of newly formed bone and implanted autograft material, because the embedded autograft (old bone) and the newly formed bone could not be distinguished. The region of interest (ROI) was the gap area including both Marvel screws up to the 6th and 9th screw in the plate. Following colors were used:

- old bone: light blue (R: 0; G: 210; B: 255; #00d2ff),
- callus: dark green (R: 34; G: 79; B: 7; #224f07)
- non-bone: pink (R: 242; G: 40; B: 211; #f228d3)
- cartilaginous tissue: yellow (R: 255, G: 255, B: 0; #ffff00)
- background: beige (R: 198; G: 156; B: 96; #c69c60).

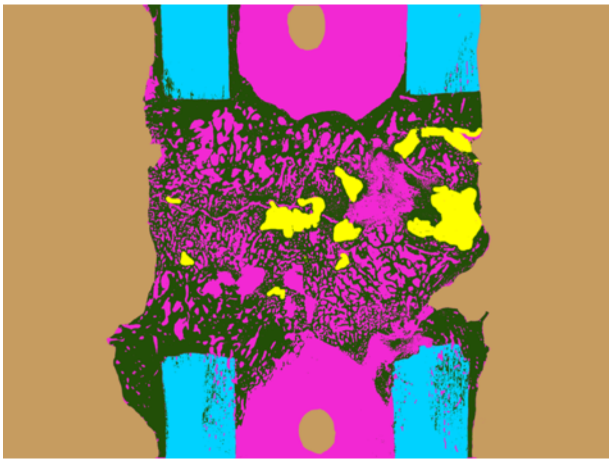

Figure 2.18: Animal 86.13, example for total ground section evaluation of the 17 mm graft model. Old bone (light blue), callus (dark green), cartilaginous tissue (yellow) and non-bone tissue (pink), back-ground (beige), the round dots in beige display the Marvel screw areas.

2.12.5.3 Sectoral evaluation of callus formation (3 mm and 17 mm gap)

Callus formation (new bone formation) at the cis cortex, endosteal and at the trans cortex were color-highlighted. For the 17 mm graft model, the callus consisted of newly formed bone and implanted autograft material, because it could not be distinguished between the embedded autograft (old bone) and the newly formed bone. The following colors were used:

- callus cis cortex: pink (R: 242; G: 40; B: 211; #f228d3)
- endosteal callus: light blue (R: 0; G: 210; B: 255; #00d2ff),
- callus trans cortex: dark green (R: 34; G: 79; B: 7; #224f07)
- rest tissue: beige (R: 198; G: 156; B: 96; #c69c60).

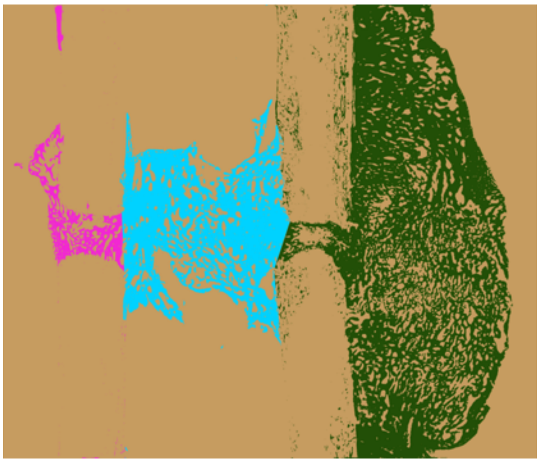

Figure 2.19: Animal 86.08, example for sectoral ground section evaluation of callus at cis cortex (pink), endosteal callus (light blue) and callus at trans cortex (dark green), and rest (beige) in the 3 mm gap model.

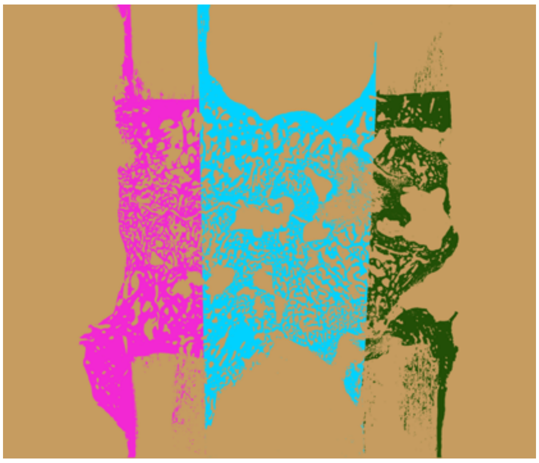

Figure 2.20: Animal 86.13, example for sectoral ground section evaluation of callus at cis cortex (pink), endosteal callus (light blue) and callus at trans cortex (dark green), and rest (beige) in the 17mm graft model.

Afterwards, the colored images were analyzed using a specialized image analysis software program (Fiji, ImageJ, version 2.0,0-rc-46/1.50g, build 179d1b4146, date 2016-03-04, open source image processing software, copyright 2010-2018) and the colored fractions were automatically detected and measured in number of pixels.

The background was excluded from the calculation. All remaining pixels within the area of interest were set as 100% and the percentage of new bone formation located at the cis and trans cortex as well as endosteal callus were calculated.

2.12.6 Fluorescence

Fluorescent sections were descriptively evaluated for differences of dye integration between groups at three different time points (calcein green at 3 weeks, xylenol orange at 6 weeks and oxytetracycline (Engemycin 10%, MSD Animal Health GmbH, Luzern) prior to sacrifice, either at 9 weeks (3mm model) or 12 weeks (17mm model). Digital images of the region of interest (defect area) were recorded. Therefore, 8x8 single images were taken in a 1.25 magnification and merged together using a special microscope, camera and specific merging software (Leica LAS-X standard software Leica Microscopes, “Stitching function”; Leica DM 6000B, Leica DFC 350 FX, Leica Microsystems CMS GmbH, Mannheim, Germany).

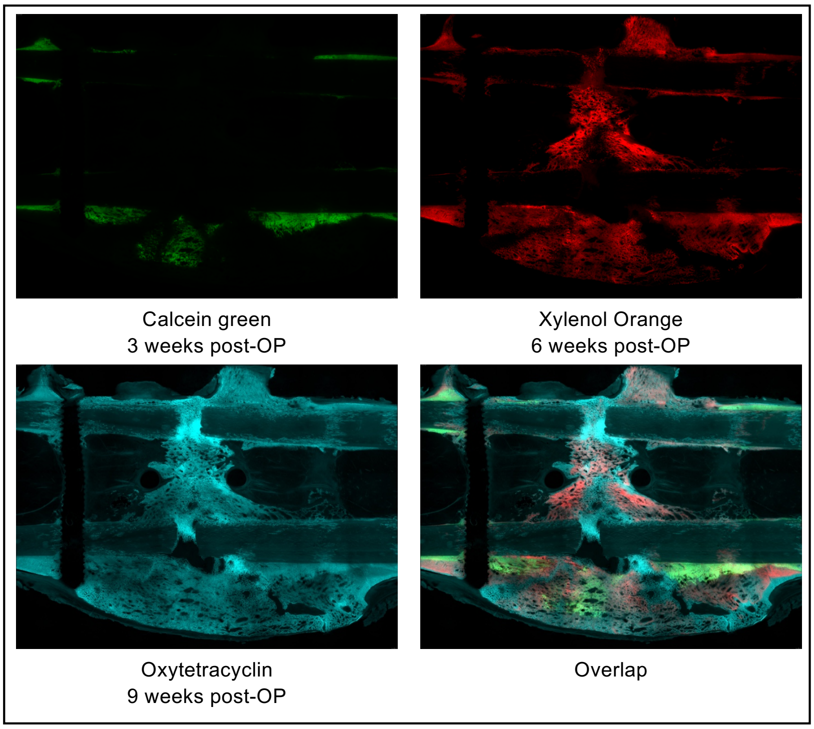

Figure 2.21: Representative sample (86.12, TI) for fluorescence evaluation of the 3 mm gap model, calcein green (top left), xylenol orange (top right), oxytetracycline (bottom left), merged image (bottom right).

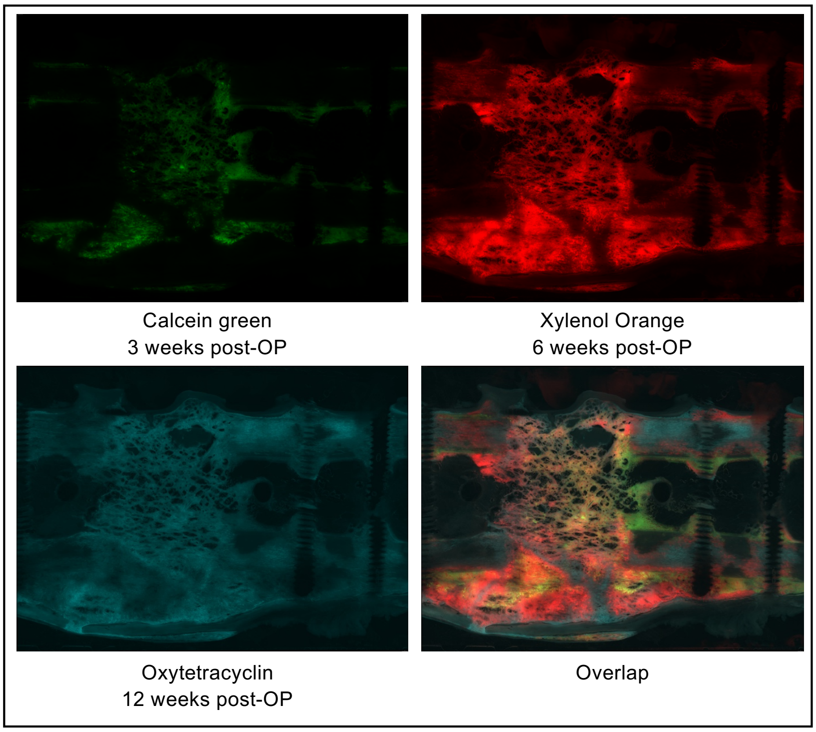

Figure 2.22: Representative sample (86.18, TI) for fluorescence evaluation of the 17 mm graft model, calcein green (top left), xylenol orange (top right), oxytetracycline (bottom left), merged image (bottom right).

2.12.7 Histological Evaluation

2.12.7.1 Assessment of local tissue effects in the Marvel screws area

Semiquantitative evaluation of biocompatibility parameters (inflammation and tissue response), and additional observations (traumatic necrosis, foreign debris) were performed according to ISO 10993-Part 6 Annex E (Third edition 01.12.2016) using a light microscope (microscope Leica DMR system). The evaluation was performed by two independent observers.

Biocompatibility scoring contained both inflammation and tissue response and was separately performed in the implant surrounding area (screw hole) at the cis and the trans cortex.

Inflammation was characterized by such cellular components as polymorphonuclear cells, eosinophils, lymphocytes, plasma cells, macrophages, giant cells, necrosis and osteolysis.

Tissue response was described by remodeling reaction including neovascularization, fibrous capsule formation/fibrosis and fatty infiltration (at the cis and trans cortex area only).

Due to the greater importance of inflammatory cell infiltrates and necrosis, these parameters were multiplied by a factor two to provide a weighted value as compared to tissue remodeling parameters, which describe more a secondary effect and healing response. The values were summarized, and then an average score for Test group and Control group calculated.

The average score for the control treatment was subtracted from the Test group average to determine a comparative reactivity grade based on following scale:

- minimal or no reaction	(0.0 to 2,9)
- slight reaction	(3.0 to 8,9)
- moderate reaction	(9.0 -15.0)
- severe reaction	≥15.1

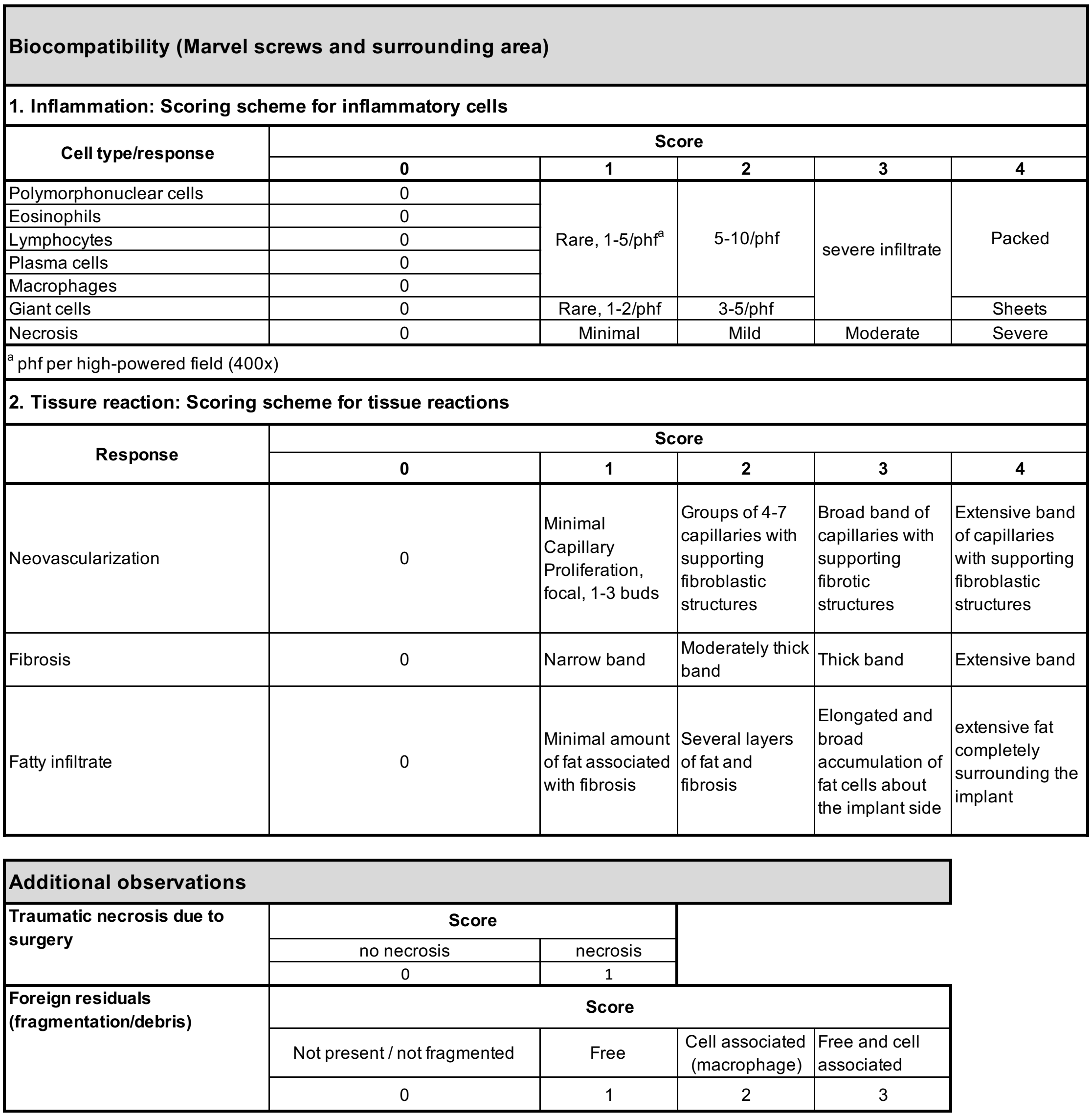

Biocompatibility (Marvel screws and surrounding area)

1. Inflammation: Scoring scheme for inflammatory cells

Cell type/response	Score				
	0	1	2	3	4
Polymorphonuclear cells	0	Rare, 1-5/phf[a]	5-10/phf	severe infiltrate	Packed
Eosinophils	0				
Lymphocytes	0				
Plasma cells	0				
Macrophages	0				
Giant cells	0	Rare, 1-2/phf	3-5/phf		Sheets
Necrosis	0	Minimal	Mild	Moderate	Severe

[a] phf per high-powered field (400x)

2. Tissure reaction: Scoring scheme for tissue reactions

Response	Score				
	0	1	2	3	4
Neovascularization	0	Minimal Capillary Proliferation, focal, 1-3 buds	Groups of 4-7 capillaries with supporting fibroblastic structures	Broad band of capillaries with supporting fibrotic structures	Extensive band of capillaries with supporting fibroblastic structures
Fibrosis	0	Narrow band	Moderately thick band	Thick band	Extensive band
Fatty infiltrate	0	Minimal amount of fat associated with fibrosis	Several layers of fat and fibrosis	Elongated and broad accumulation of fat cells about the implant side	extensive fat completely surrounding the implant

Additional observations

Traumatic necrosis due to surgery	Score	
	no necrosis	necrosis
	0	1

Foreign residuals (fragmentation/debris)	Score			
	Not present / not fragmented	Free	Cell associated (macrophage)	Free and cell associated
	0	1	2	3

Figure 2.23: Scoring scheme for Biocompatibility containing Inflammation, tissue response and additional observations.

2.12.7.2 Assessment of bone activity, tissue character and healing response in the gap area

Bone activity parameters (bone resorption and formation), tissue character (endochondral ossification, maturity of callus) and healing response (defect unity) were evaluated using ground and thin sections in three different areas:

- fracture ends and defect at trans-cortex
- fracture ends and defect at cis-cortex
- endosteal defect area.

Scoring scheme is shown in Table 2.8.

Bone activity					
Bone Resorption	**Score**				
	0	**1**	**2**	**3**	**4**
	no	1-25%	26-50%	51-75%	76-100%
Bone formation	**Score**				
	0	**1**	**2**	**3**	**4**
	no, granulation tissue only	1-25%	26-50%	51-75%	76-100%

Tissue character					
Endochondral ossification	**Score**				
	0	**1**	**2**	**3**	**4**
	no	1-25%	26-50%	51-75%	76-100%
Maturity of callus/new bone	**Score**				
	0	**1**	**2**	**3**	**4**
	non union (fibrous tissue)	mainly mesenchymal tissue with some cartilage (endochondral ossification)	mainly cartilage and some new bone	more bone than catrilage	dense/mature bone

Healing response					
Defect unity	**Score**				
	0	**1**	**2**	**3**	**4**
Defect united in %	0	not united, <25%	26-50% united	51-75% united	76-100% united

Table 2.8: Scoring scheme for bone activity parameters, tissue character and healing response evaluated using ground and thin sections

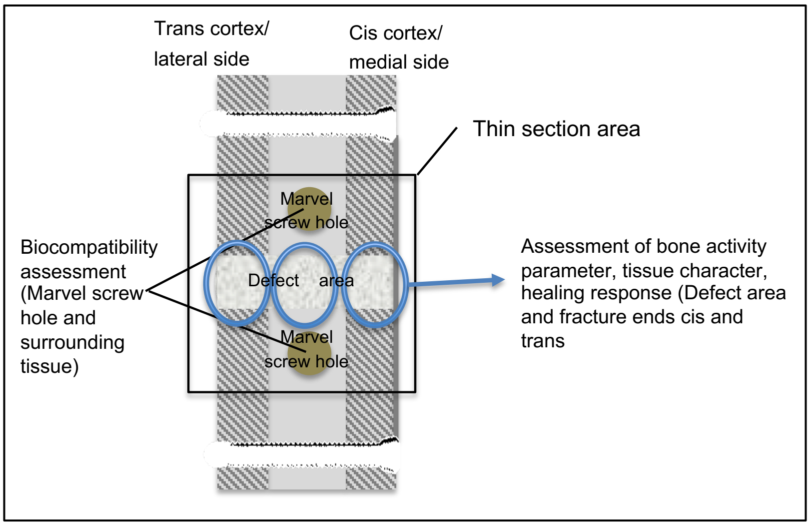

Figure 2.24: Thin section evaluation including biocompatibility assessment, bone activity parameter, tissue character and healing response.

2.13 Statistical Analysis

Descriptive statistics were computed for the TI, CI and NCI groups in both the 3mm gap model and the 17mm graft model. Statistical analysis of data was performed to compare TI versus CI in both the 3mm gap model and the 17mm graft model using unpaired two-tailed T-tests. Differences were considered statistically significant when the p-value was below 0.05. Statistical analyses and plots were performed with the SPSS software (version 23).

3 Results

3.1 3 mm Gap Model

3.1.1 Excluded Animals

12/14 sheep completed the study as planned. Two animals (86.01, 86.02) had to be excluded and were replaced by reserve animals (86.28, 86.29).

Animal 86.01 (TI) had to be excluded from the group analysis due to implant failure of the internal fixation. A complete collapse of the fracture gap laterally at the trans cortex was already detected 3 weeks post-surgery during radiographic examination. The two most distal screws (hole 11 and 12) were broken and the screw in hole 9 (closest to the distal end of the defect) was displaced and bent. The sheep showed a very nervous and uncooperative behavior, which was likely the primary cause of the fixation failure.

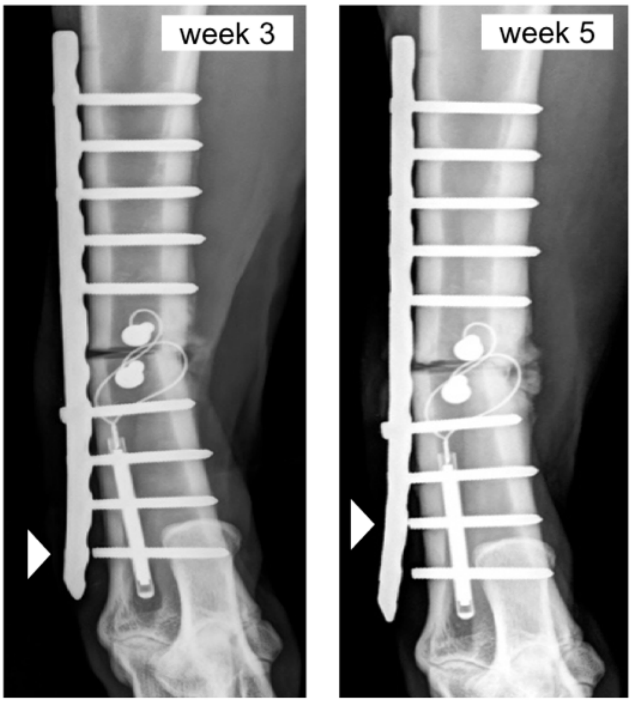

Figure 3.1: Animal 86.01: anteroposterior projections of the left tibia taken 3- and 5-weeks post-surgery. Collapse of fracture gap due to implant failure (breakage of screw 12, indicated by the white arrow) and dislocation of screw 9 are visible already after 3 weeks, proceeding with breakage of screw 11 at the 5-week time point (indicated by the white arrow).

In **animal 86.02 (TI)** the macroscopic evaluation at sacrifice revealed a moderately detached transducer cap at the proximal Marvel screw with fibrous tissue between cap and screw head. As it was not detected with radiographic follow up, the exact time point of cap detachment could not be determined. Therefore, the PEMF treatment may not have been systematically administered throughout the in-life phase. This observation prompted the decision to exclude this animal.

3.1.2 Anesthesia, surgery and post-operative recovery period

As part of pre- surgical preparations, 2 to 3 days prior to surgery blood samples for hematology and chemistry examinations were taken and carefully examined. Any parameters suggesting possible infections (e.g. elevated white blood cell count), muscle disorders (elevated creatine kinase level), metabolic problems (kidney values: creatinine, blood urea; electrolyte levels: sodium, potassium, chloride, bicarbonate) or anemia (e.g. low red blood cell count) were taken into particular consideration. Only healthy animals were enrolled in the study.

In total, 12 animals included in the group analysis (86.03-12, 86.28-29) underwent surgery with a 3 mm gap. The overall anesthesia time was between 123-334 min (Ø 200min) and 223 minutes for the TI compared to 187 minutes for the CI. This parameter was not expected to influence the outcome of the study. The surgical procedure itself lasted between 61-125 min (Ø 92 min).

In all 12 animals, the tibia osteotomies including internal fixation, as well as the placement of the Marvel screws could be performed without any complications. This was possible thanks to the advanced equipment, specially designed screw and cutting guides and experienced surgeons.

For each sheep, the number of the used Universal Transducer SI-ES as well as the measured resistance (Ohm) was noted. The resistance values were within the functional range for both TI (between 90-102 Ohm) and CI (between 90-93 Ohm). The detailed measurements for each sheep are attached in Appendix 1.

In 8/12 animals, no complications occurred during Marvel technology placement and recovery from anesthesia. The Universal Transducer SI-ES could be easily subcutaneously placed at the distal part of the tibia and caps tapped onto the screw heads using a hammer. Nevertheless, in 3/12 animals, the Universal Transducer SI-ES had to be replaced during or immediately after surgery. In one animal (86.03, TI), it was replaced because a too high resistance value (140 Ohm) was measured. In a second sheep

(86.09, TI), the cap could not be fixed at the screw head and therefore the transducer was immediately replaced during surgery. In a third sheep (86.10, TI), the postoperative radiograph revealed a detached cap at the distal screw. This sheep underwent a second surgery during the same anesthesia and the cap was fixed at the screw head again. Due to this second surgical intervention, the anesthesia time of this sheep was prolonged to 334 min. Neither complications during anesthesia nor postoperative complications occurred. No further cap loosening occurred in these replaced or reattached caps. Due to the complications related to the cap attachment at the hexagonal screw head, the caps were re-worked, so that in the last two sheep of the 3mm model (86.28, 86.29), transducers with re-worked caps were implanted. No further complication concerning cap loosening was observed with these re-worked caps.

In 1/12 sheep (86.07), an anesthesia complication occurred. This animal developed a respiratory arrest immediately after extubation. Due to difficult reintubation with various intubation attempts an injury with strong bleeding and massive swelling of the larynx occurred. In addition, a pulmonary edema was diagnosed, which was immediately treated with furosemide twice (first dose: 4mg/kg BW, second dose after 10 minutes: 2 mg/kg BW). Phenylephrine was applied onto the larynx and into the nose to subdue the swelling. The sheep was mechanically ventilated and stabilized over half an hour. After the second extubation, oxygen was applied via an intranasal catheter. After one hour, the sheep recovered and was transported to the stable, no further complications occurred during the recovery period of this sheep.

3.1.3 Detached transducer caps after surgery and re-design

In total 9/24 transducer caps became detached, either already during surgery (N=2), or between 3-7 weeks (N=7). In Table 3.1 all detached caps of the 3mm gap model are noted.

Group	Animal	Proximal cap detached	Distal cap detached
excluded	86.02	slightly detached, fibrous tissue between cap and screw head, detected at sacrifice, not visible during radiographic examination	-
CI	86.04	-	detached but still in place, radiologically detected at 4 weeks post OP
CI	86.07	radiologically detected at 7w post OP	radiologically detected at 4w post OP
CI	86.08	radiologically detected at 5w post OP	radiologically detected at 3w post OP
CI	86.09	transducer replaced during surgery because cap did not hold	-
TI	86.10	-	postoperative radiograph revealed detachment, therefore 2. Surgery during the same anesthesia
TI	86.12	radiologically detected at 5w post OP, 2. Surgery reattachment of the cap	-
Number of detached caps:		**5 in total (3 in CI, 2 in TI)**	**4 in total (3 in CI, 1 in TI)**

Table 3.1: Detached caps in the 3 mm gap model.

In two TI animals (86.03, 86.10), the caps detached already during surgery and were immediately reattached still under the same general anesthesia. 5 caps of 3 CI animals (86.04, 86.07, 86.08) became detached between 3-7 weeks post-surgery. These detachments were all detected during the weekly radiographic examination. No reattachment was performed because they belonged to the non-treated CI group.

In one animal of the TI group (86.12), cap loosening at the proximal screw was observed 5 weeks after surgery during the weekly radiographic examination. This sheep underwent a second surgery and the cap successfully was reattached. Therefore, a 5 cm long incision was made cranially of the plate in the area of the proximal Marvel screw. Antibiotics and analgesics were given intravenously for three days. No further complications evolved from this event. The re-worked caps were implanted in animals 86.28, 86.29 and no further detachments occurred.

3.1.4 In-life clinical observations

None of the 12 animals included in the group analysis revealed serious or persistent clinical abnormalities influencing the overall outcome of the study.

The casts were successfully changed during every radiographic examination and were carried until the sacrifice.

Four animals (TI: 86.11, 86.28, CI: 86.04, 86.07) developed pressure sores, mostly at the knee region. Special care was taken that the cast edges were always sufficiently padded and that the cast ended above the patella. Pressure sores were treated with betadine solution and honey cream and healed well within a few weeks. Three animals (TI: 86.03, CI: 86.05, 86.09) lied down more than usual without any further clinical signs.

All animals tolerated both the casts and coils and therapy could be applied without complications.

3.1.5 Macroscopic findings at sacrifice

In all 12 animals, the sacrifice procedure after 9 weeks was performed according to routine. A careful macroscopic examination was successfully conducted. All samples, including lymph nodes and both tibiae were harvested as planned.

Overall, the anatomical dissection performed right after sacrifice showed that in both TI and CI groups, the tissue adjacent to the implants did not show any alteration of the normal structure. No hematoma, edema, encapsulation or other additional gross findings were recorded. The universal transducer and its cables stayed in place. No encapsulation or granuloma were found around the implanted Marvel technology (universal transducer, cables, caps). The status of the detached caps detected radiographically during the in-life period (Table 3.1) was confirmed macroscopically at sacrifice. No further cap detachment was detected.

Resistance of the transducer was successfully measured in order to confirm its connection to the caps. In TI, the resistance values ranged from 88 to 300 Ohm, whereas in CI, from 86 to 110 Ohm or were not functional. Meticulous exploration of the gap area and verification of fragment stability showed a macroscopically stable callus in 6/6 TI and 5/6 CI tibiae. In 1/6 CI sample (86.07), the fracture ends were movable and the gap unstable.

In addition, no macroscopic abnormalities were found in all harvested lymph nodes.

98/108 locking head screws (TI=49, CI=49) were found locked and correctly placed in the plate. 10/108 screws were found between slightly and severely displaced in 1/6 animals of the TI group (86.03: N=2) and in 4/6 animals of the CI group (84.04: N=3, 86.05: N=1, 86.06: N=1, 86.08: N=3). Out of these, two screws of two CI animals were broken at the neck (86.04, 86.05). No macroscopic abnormalities seemed to be directly related to these broken screws. Nevertheless, in animal 86.04, the body of the broken screw could not be removed and remained in the bone, causing some artefacts for μ-CT scanning.

Metallosis at the screw head - plate junction was found in all sheep of both groups (TI=6, CI=6) dominantly at the distal screw holes 9 - 12.

All 24 Marvel screws were firmly integrated in the bone, no macroscopic loosening was observed and no metallosis was found.

3.1.6 Micro-CT morphometry and structural analyses

The global morphometric analysis using the "slice by slice" tissue segmentation was performed successfully and accurately depicted callus and cortical bone. Also the highly mineralized callus could be successfully distinguished from the old bone. Looking at the results of the global morphometry, box plots representing all 12 animals (6 TI and 6 CI) are shown in Figure 3.2.

Although differences in callus volume and mature callus volume were not detected between CI and TI, a clear tendency for higher callus density in TI was observed (p=0.053), with a mean difference of 88.44 mg HA/cm^3.

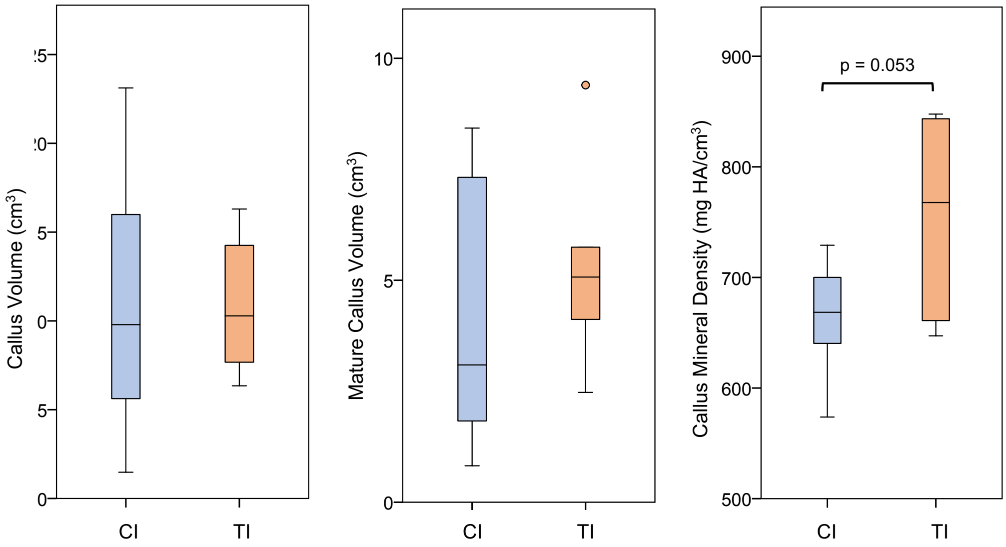

Figure 3.2: Callus volume in cm^3, mature callus volume in cm^3, callus mineral density in mg HA/cm^3 comparing CI and TI (n = 6).

3.1.7 Biomechanics

Biomechanical testing gave a comprehensive assessment of the fracture healing response. All results are reported as mean ± SD.

The gauge length was 148 ± 6 mm for non-operated tibiae and 146 ± 14 mm for operated tibiae. Non-operated tibiae from the 3 mm gap model (12 in total) exhibited an overall torsional stiffness of 6.77 ± 1.76 Nm/deg. The non-operated tibiae in the CI group had a torsional stiffness of 6.04 ± 1.51 Nm/deg while the non-operated tibiae in the TI group had a torsional stiffness of 7.51 ± 1.81 Nm/deg. This difference was not statistically significant (p=0.158).

The operated tibiae in the CI group had a torsional stiffness of 3.25 ± 2.41 Nm/deg while the operated tibiae in the TI group had a torsional stiffness of 6.13 ± 2.73 Nm/deg. This difference was also not statistically significant (p=0.081), likely due to the high variability between samples (74% and 44% relative standard deviation in CI and TI respectively). Stiffness values for individual animals are shown in Appendix 7: Biomechanics.

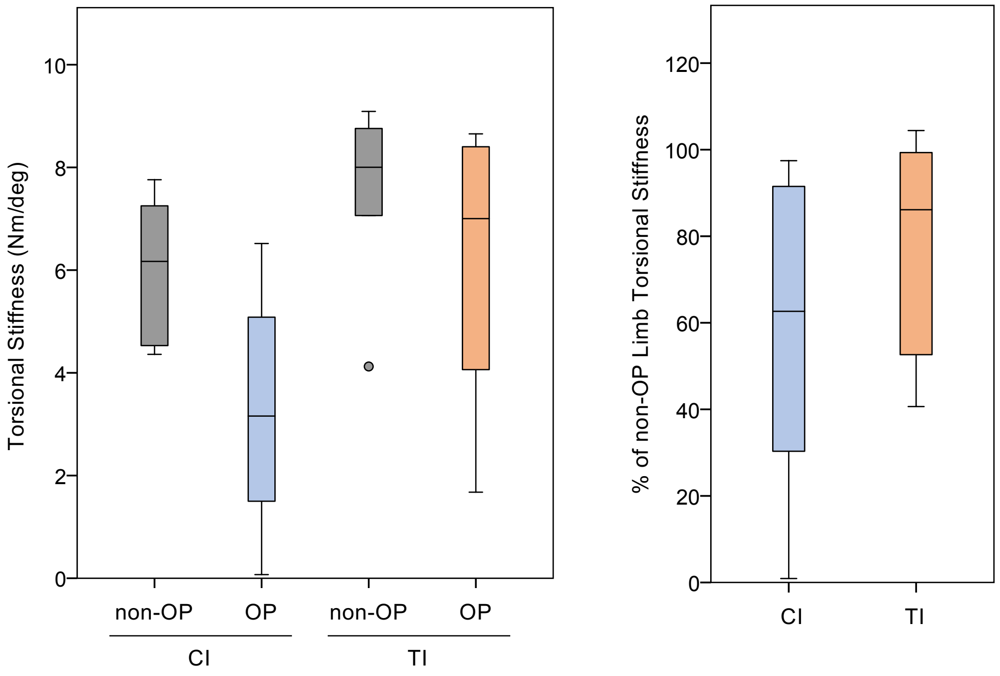

Figure 3.3: Torsional stiffness in Nm/deg of operated and non-operated tibiae and percent (%) torsional stiffness of operated tibiae compared to contralateral non-operated tibiae in CI and TI (n = 6).

Normalizing the operated tibia stiffness to the contralateral non-operated tibia stiffness, the TI group tibiae reached 78 ± 26 % of the contralateral non-operated tibiae stiffness. The CI group tibiae reached 57 ± 40 % of the contralateral non-operated tibiae stiffness.

The difference between CI and TI was also not statistically significant (p = 0.322). Normalized stiffness values for individual animals are shown in Appendix 7: Biomechanics. The operated tibia from sheep 86.07 (CI) had a very low torsional stiffness (0.07 Nm), indicating a delayed union.

3.1.8 Radiographic evaluation

3.1.8.1 Semiquantitative Scoring of radiographs

It was possible to evaluate all radiographs of the 3mm gap model. The analysis was performed by two independent, board certified reviewers (Prof. Brigitte von Rechenberg and Prof. Mark Flückiger). Radiographs were randomly presented unknown for group and time point. Overall, the congruency of scores was very high and of those differing the mean value between both scores were taken.

Radiographs were taken of all animals immediately after surgery and as proposed when changes of casts were performed at 3, 4, 5, 6, 7 and 8 weeks. Radiographs at 9 weeks were taken after sacrifice but still with the same conditions as if they would have been done in-life. Identical settings were used (50 kV, 2.0 mAs).
Performing radiographs at 3 angled projections (0°, 265° and 275°) was highly reliable and allowed good assessment of each sides of the callus. The anteroposterior (0°) projection was used not only for the detailed gap area evaluation but also for the healing at the cis and trans cortices as the position of the plate, screws and the Marvel technology components allowed for a clear undisturbed view of the defect.
The 265° and 275° angled projections were used for the evaluation of the healing progression on the caudal and cranial tibia cortices respectively. Additionally, these projections made it possible to detect any caps loosening or detachments.
Callus formation at the cranial cortex could be visualized in radiographs taken at the 275° angle whereas new bone formation at the caudal cortex was clearly visible in radiographs taken at the 265° angle.
Overall, callus formation was enhanced in the TI compared to the CI group. Callus formation was visible as early as 3 weeks in both groups, although mainly at the trans cortex stemming from the periosteum. In the TI group, the callus formation was more advanced, smaller in size and focused at the gap compared to the CI group, where three animals (86.04, 86.06 and 86.08) showed callus formation at the gap resembling slightly an irritation callus. In all three of these animals, a slight collapse at the trans-cortex was

noticed. In the TI group, all animals showed callus formation at the gap and periosteum. Differences of callus formation between groups started at 4 weeks and were more pronounced at 5 weeks. In 5/6 sheep (86.10, 86.11, 86.12, 86.28 and 86.29), a bridging callus was noticed at this time point in the TI group, whereas in CI only in 3/6 animals (86.04, 86.06, 86.08). At 6, 7 and 8 weeks, differences were even more pronounced. At the time of sacrifice, 5/6 sheep of TI showed a bridging callus (sheep 86.10, 86.11, 86.12, 86.28 and 86.29) compared to 3/6 in CI (sheep 86.04, 86.06, 86.08). The quality of the callus (smoothness, size and opacity) was superior in the TI group.

Individual scores corroborated these results. Differences over time starting at 5 weeks, although not statistically significant, showed a clear tendency for higher values of TI.

<u>The mean total score</u> (overall callus) was higher in the TI group throughout the entire time period from 3 to 9 weeks. The total score consisted of the addition of all individual semiquantitative scores. It included the scores of cortical callus formation, Rust score, cis and trans cortex at 0° angle, cranial at 275° angle and caudal score at 265° angle and callus opacity.

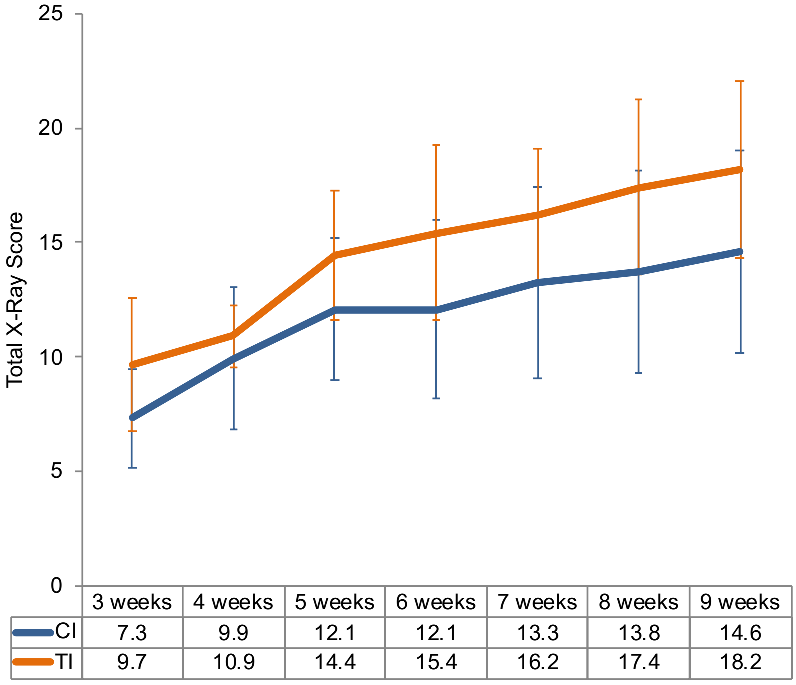

	3 weeks	4 weeks	5 weeks	6 weeks	7 weeks	8 weeks	9 weeks
CI	7.3	9.9	12.1	12.1	13.3	13.8	14.6
TI	9.7	10.9	14.4	15.4	16.2	17.4	18.2

Figure 3.4: Mean ± SD total radiographic score (0 – 30) plotted for TI and CI (n=6) at 3, 4, 5, 6, 7, 8 and 9 weeks post-operatively. The means are also listed in the table.

<u>Cortical callus formation</u> demonstrated similar results as the total scores. It was highest between 5 and 7 weeks. After 7 weeks differences became smaller due to the fact that in the TI group the callus had already bridged.

The RUST Score was also higher in the TI group mainly between 5 and 9 weeks. At 4 weeks, scores of the TI group were even slightly lower compared to the CI group.

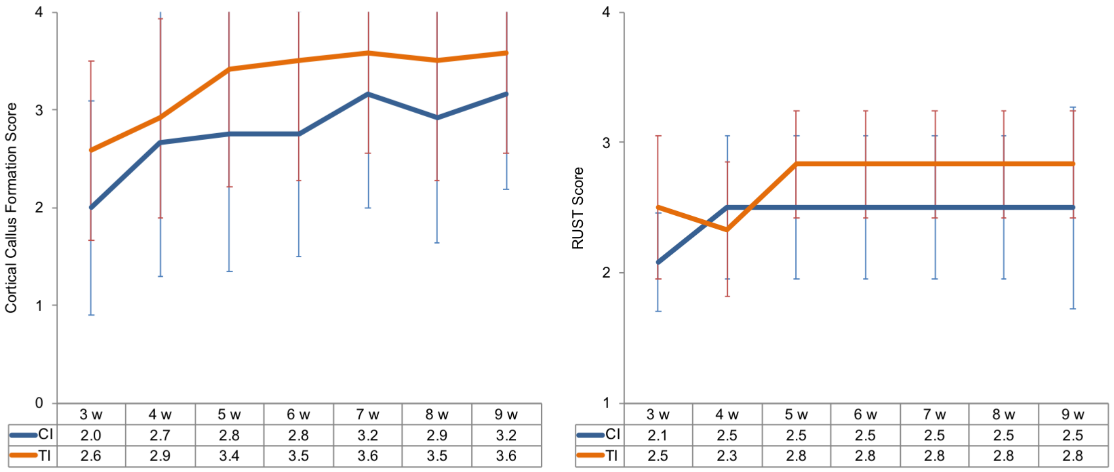

	3 w	4 w	5 w	6 w	7 w	8 w	9 w
CI	2.0	2.7	2.8	2.8	3.2	2.9	3.2
TI	2.6	2.9	3.4	3.5	3.6	3.5	3.6

	3 w	4 w	5 w	6 w	7 w	8 w	9 w
CI	2.1	2.5	2.5	2.5	2.5	2.5	2.5
TI	2.5	2.3	2.8	2.8	2.8	2.8	2.8

Figure 3.5: Mean ± SD of cortical callus formation score (0 – 4) and RUST score (1 – 4) for TI and CI (n=6) at 3, 4, 5, 6, 7, 8 and 9 weeks post-operatively. The means are also listed in the tables.

The cis cortex showed also higher scores starting at 5 and extending to 9 weeks. At earlier time points (3 and 4 weeks) almost no differences were noticed. The mean highest score was at 9 weeks with 2.7 out of a maximum of 4.

The trans cortex showed higher scores throughout the entire period from 3 to 9 weeks. The mean highest score was at 9 weeks with 2.6 out of a maximum of 4.

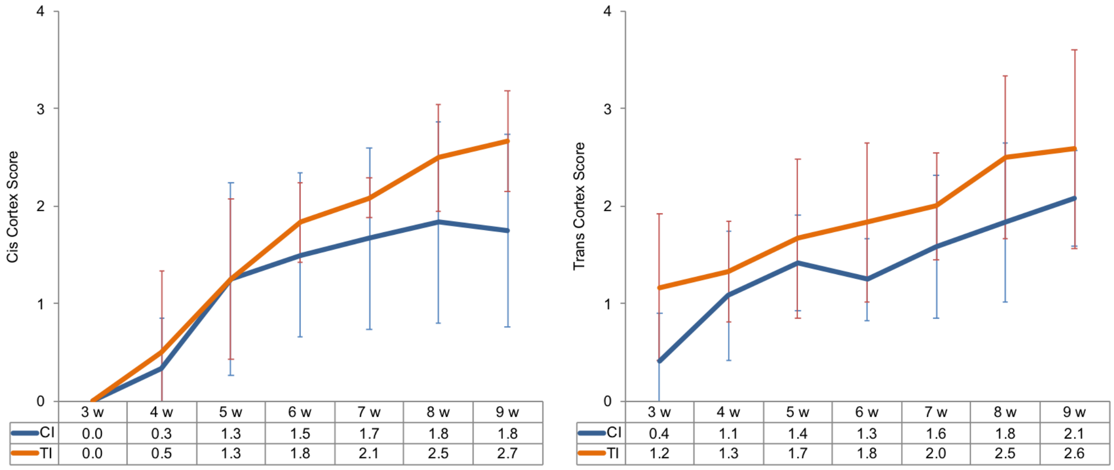

	3 w	4 w	5 w	6 w	7 w	8 w	9 w
CI	0.0	0.3	1.3	1.5	1.7	1.8	1.8
TI	0.0	0.5	1.3	1.8	2.1	2.5	2.7

	3 w	4 w	5 w	6 w	7 w	8 w	9 w
CI	0.4	1.1	1.4	1.3	1.6	1.8	2.1
TI	1.2	1.3	1.7	1.8	2.0	2.5	2.6

Figure 3.6: Mean ± SD of cis cortex score (0 – 4) and trans cortex score (0 – 4) for TI and CI (n=6) at 3, 4, 5, 6, 7, 8 and 9 weeks post-operatively. The means are also listed in the tables.

The cranial cortex evaluation focus was on healing at the cis cortex. Scores over time in this area were almost identical as in the trans cortex, except in the early time points of 3 and 4 weeks, where scores were slightly lower.

The caudal cortical gap revealed scores of the trans cortex. Similar to the RUST Score, the TI group showed a slightly lower score than the CI group, but at all other time points TI scores were higher.

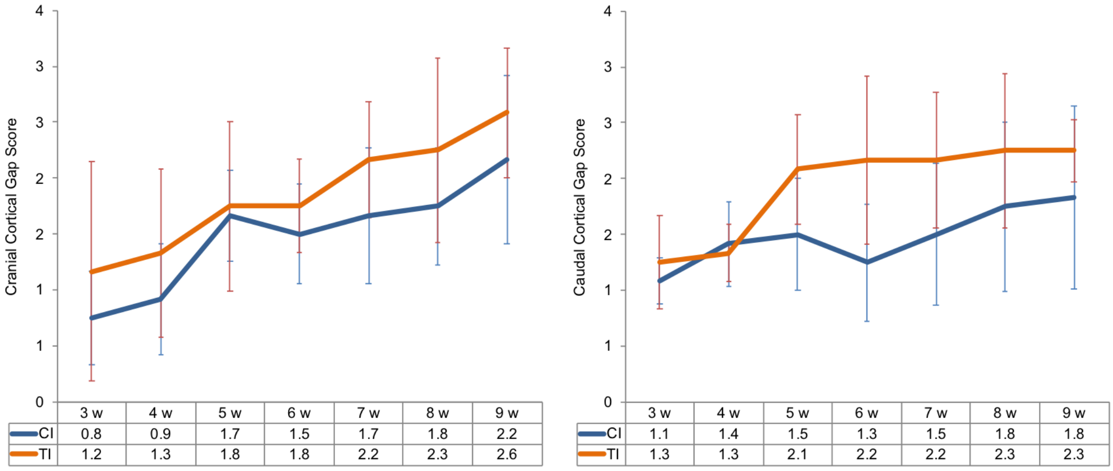

	3 w	4 w	5 w	6 w	7 w	8 w	9 w
CI	0.8	0.9	1.7	1.5	1.7	1.8	2.2
TI	1.2	1.3	1.8	1.8	2.2	2.3	2.6

	3 w	4 w	5 w	6 w	7 w	8 w	9 w
CI	1.1	1.4	1.5	1.3	1.5	1.8	1.8
TI	1.3	1.3	2.1	2.2	2.2	2.3	2.3

Figure 3.7: Mean ± SD of cranial cortical gap score (1 – 4) and caudal cortical gap score (1 – 4) for TI and CI (n=6) at 3, 4, 5, 6, 7, 8 and 9 weeks post-operatively. The means are also listed in the tables.

Callus opacity was higher in the TI group compared to the CI throughout the entire period. Only at 3 weeks, scores were equal in both groups. However, it has to be noticed that scores were always below 2 indicating that opacity was always less than 50% of the original cortical bone.

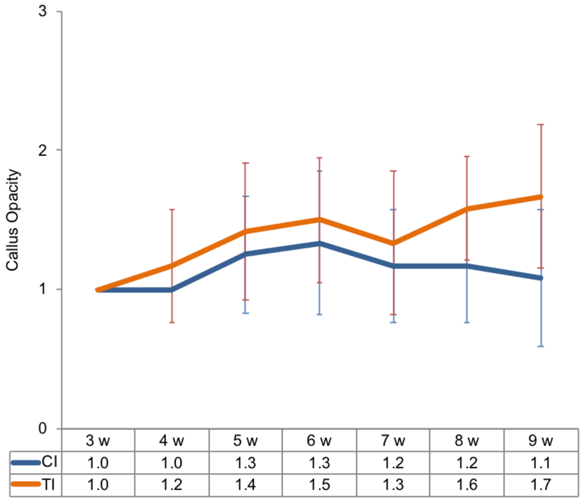

	3 w	4 w	5 w	6 w	7 w	8 w	9 w
CI	1.0	1.0	1.3	1.3	1.2	1.2	1.1
TI	1.0	1.2	1.4	1.5	1.3	1.6	1.7

Figure 3.8: Mean ± SD of callus opacity score (1 – 3) for TI and CI (n=6) at 3, 4, 5, 6, 7, 8 and 9 weeks post-operatively. The means are also listed in the table.

<u>Screw tip callus formation</u> described the periosteal reaction at the tip of the Marvel screws that always penetrated the trans cortex until the first thread. Although it did not contribute any stability to the overall callus, it was expected to indicate a reaction of the osteogenic periosteum through the pulsed electromagnetic stimulation. Callus formation at both Marvel screws was observed in all TI sheep from week 4 onwards, whereas this was only observed in 4/6 CI sheep from 4 weeks onwards and 1/5 CI sheep from 7 weeks onwards. One CI sheep only developed callus formation at one Marvel screw tips. Since this valuable did not contribute to the stability of the gap healing it was not included in the summary of the total score.

<u>Cortex blurring</u> described the stage of bone resorption and new bone formation, which radiographically is indicated through blurring of the fragment edges. Since cortex blurring does not contribute to the overall stability of gap healing, the parameter was not included in the total score calculations. However, more cortex blurring is a sign of higher callus maturity. Differences between the groups were obvious between 5 and 9 weeks, where 5/6 TI sheep clearly showed cortex blurring already at 5 weeks while 5/6 CI sheep only at 7 weeks.

3.1.9 Histomorphometry

Twelve toluidine blue stained histological ground sections were histomorphometrically evaluated with success. Microradiographs of the ground sections were used to corroborate the structure of calcified tissue in the toluidine stained samples.

The evaluation was performed using total section and sectoral analysis. For each sample, percentages of old bone, new bone, as well as non-bone structures (non-bone containing tissue) were successfully measured for the total section. Sectoral evaluation made it possible to distinguish new bone formation at the endosteal, cis and trans area in all samples.

Overall, histomorphometrical measurements revealed comparable and good healing of the gap area for both TI and CI.

3.1.9.1 Total section evaluation

Overall, no significant differences were found between TI and CI for any of the values of the total section analysis. Nevertheless, slightly higher values were found for old and new bone in TI, while values for non-bone tissue were slightly lower in TI than CI.

Mean results and their standard deviations for histomorphometrical evaluation of the total section are shown in Figure 3.9 and Table 3.2.

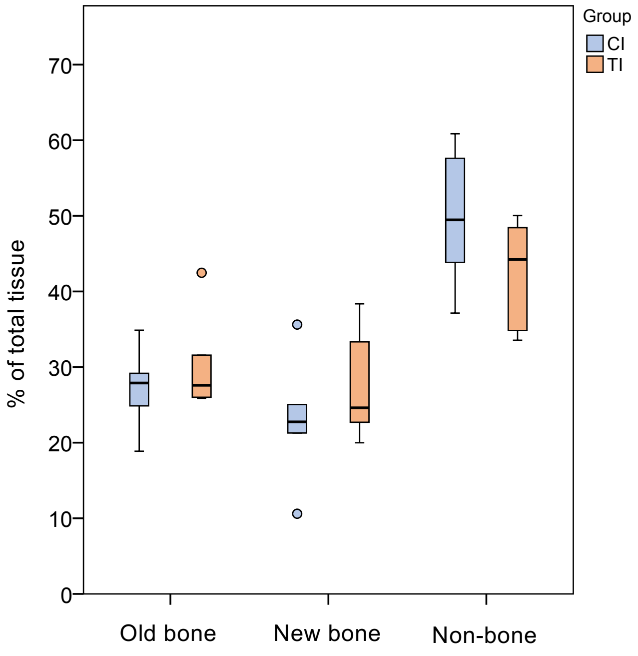

Figure 3.9: Histomorphometric measurements 9 weeks post-surgery of % old bone, % new bone, and % non-bone structures for TI (n=6) and CI (n=6). Results represent the percentage of the total area measured.

Group	Total Section Analysis		
	Old Bone [%]	Callus [%]	Non-bone [%]
CI	27.26	23.01	49.73
TI	30.19	27.27	42.55

Table 3.2: Histomorphometric measurement means 9 weeks post-surgery of % old bone, % new bone, and % non-bone structures for TI (n=6) and CI (n=6). Results represent the percentage of the total area measured.

3.1.9.2 Sectoral evaluation

Overall, no statistically significant differences were found between TI and CI for any of the values of the sectoral analysis. Slightly higher values were found for callus formation at the cis- and at the trans cortex in TI and higher values endosteally in CI.

Mean results and their standard deviations for the sectoral histomorphometrical evaluation are shown in Figure 3.10 and Table 3.3.

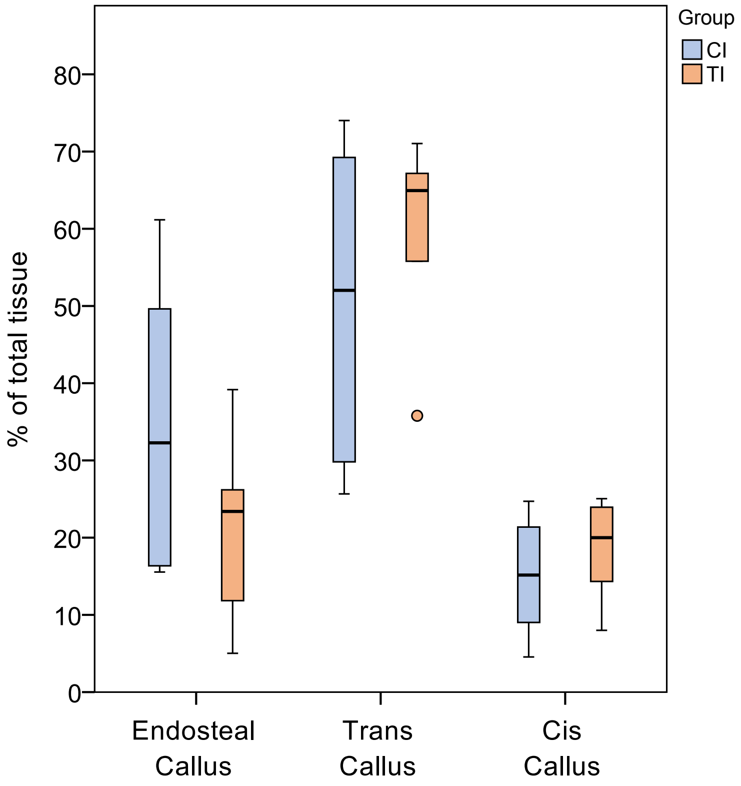

Figure 3.10: Sectoral histomorphometric measurements 9 weeks post-surgery of % endosteal callus, % trans callus and % cis callus for TI (n=6) and CI (n=6). Results represent percentage of the total area measured.

Group	Sectoral Analysis		
	Cis Callus [%]	Endosteal Callus [%]	Trans Callus [%]
CI	15.00	34.54	50.46
TI	18.55	21.50	59.95

Table 3.3: Sectoral histomorphometric measurement means 9 weeks post-surgery of % endosteal callus, % trans callus and % cis callus for TI (n=6) and CI (n=6). Results represent percentage of the total area measured).

3.1.10 Fluorescence

It was possible to evaluate 12 unstained histological fluorescence sections of two groups, TI (N=6) and CI (N=6). Fluorescence markers were injected at 3 weeks (calcein green), 6 weeks (xylenol orange), and 9 weeks post-surgery (oxytetracycline, 48 hours prior to sacrifice).

Fluorescence dyes were well visible in all specimens. Calcium deposition at the various time points could easily be followed with the different colors in all samples but one (86.07). In this sample calcein green was hardly visible at 3-week time point. At 6- and 9-weeks slight deposition mainly in the bone marrow cavity was seen (delayed union, Figure 3.11).

At 3 weeks calcein green deposition was only detected in small amounts, mostly at the transcortical periosteal callus in both TI and CI (Figure 3.12 and Figure 3.13).

At 6 weeks xylenol orange was visible in moderate quantities in both TI and CI. It could also be detected within the bone marrow and the gap at both cortices. Slightly pronounced visibility was recorded for TI versus CI at both cortices (Figure 3.12 and Figure 3.13).

At 9 weeks oxytetracycline indicated good calcium deposition and therefore an ongoing remodeling process in the cis and trans cortex of the TI group and to a lesser degree within the bone marrow. In the CI group, this relationship was inverted (more deposition within the bone marrow than at the cortices)(Figure 3.12 and Figure 3.13).

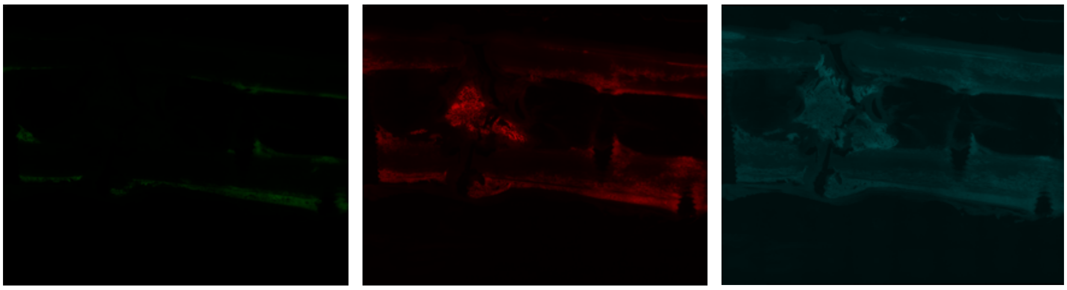

Calcein green at 3 weeks Xylenol orange at 6 weeks Oxytetracycline at 9 weeks

Figure 3.11: Fluorescence images of 86.07 CI, at 3 weeks only hardly visible calcium deposition, at 6 and 9 weeks slight deposition, but mainly in the bone marrow cavity and not in the gap area (delayed union)

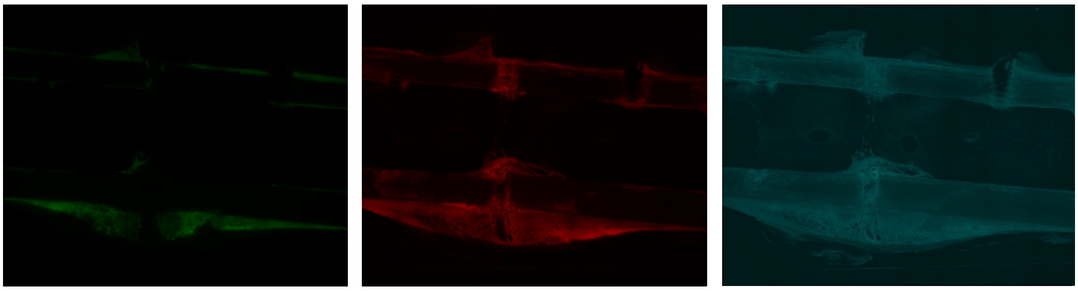

Calcein green at 3 weeks Xylenol orange at 6 weeks Oxytetracycline at 9 weeks

Figure 3.12: Representative fluorescence images for TI (86.11), only slight calcium deposition at 3 weeks, pronounced deposition especially at the fracture ends at 6 and 9 weeks

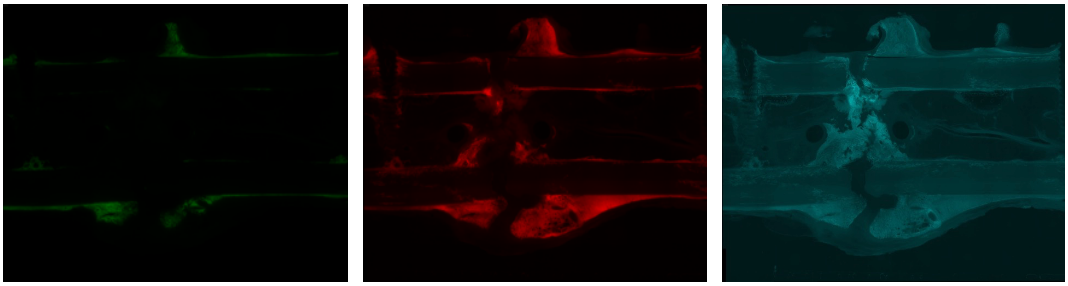

Calcein green at 3 weeks Xylenol orange at 6 weeks Oxytetracycline at 9 weeks

Figure 3.13: Representative fluorescence images for CI (86.09), only slight calcium deposition at 3 weeks, more pronounced at 6 and 9 weeks mostly in the bone marrow cavity

3.1.11 Histological evaluation

Assessment of biocompatibility parameters (inflammation and tissue response) and additional observations (traumatic necrosis and foreign debris) of TI and CI at the Marvel screws surrounding tissue of each tibia sample were performed without any problems. Bone activity (resorption and formation), tissue character (cartilage formation, callus maturity) and healing response (defect unity) were scored at the facture ends of cis and trans cortices as well as in the whole gap area.

A total of 36 Hematoxylin-Eosin (N=12), toluidine blue (N=12) and von Kossa stained (N=12) histological sections of two groups (TI:6 and CI:6) were evaluated according to ISO-Norm 10993-6:2016(E). The evaluation was performed by two independent observers.

3.1.11.1 Semiquantitative analysis of local tissue effects

Neither test nor control item demonstrated any abnormal tissue reactions. In both groups, a physiological number of immune cells within the bone marrow cavity surrounding the Marvel screws was observed. Individual results are listed in Table 3.4.

Overall, no polymorphonuclear cells, eosinophils, lymphocytes, plasma cells, necrosis, osteolysis, fatty infiltrates or foreign debris were noted in the area of the Marvel screws in any of the TI or CI samples.

Mild to moderate fibrosis in combination with neovascularization was found in 1/6 samples of TI (mild in 86.11) and in 3/6 samples of the CI (mild in 86.08, 86.09 and moderate in 86.07).

In 86.07, this was accompanied by a moderate number of macrophages and giant cells.

	Evaluation zone: Marvel screws and surrounding												
	Test group:	PEMF-treated											
	Control group:	non-treated											
	Animal ID	**Test group**						**Control group**					
		86.03	86.10	86.11	86.12	86.28	86.29	86.04	86.05	86.06	86.07	86.08	86.09
Biocompatibility	**1. Inflammation**												
	Polymorphonuclear	0	0	0	0	0	0	0	0	0	0	0	0
	Eosinophils	0	0	0	0	0	0	0	0	0	0	0	0
	Lymphocytes	0	0	0	0	0	0	0	0	0	0	0	0
	Plasma cells	0	0	0	0	0	0	0	0	0	0	0	0
	Macrophages	0	0	0	0	0	0	0	0	0	2	0	0
	Giant cells	0	0	0	0	0	0	0	0	0	2	0	0
	Necrosis/ osteolysis	0	0	0	0	0	0	0	0	0	0	0	0
	SUB-TOTAL	0	0	0	0	0	0	0	0	0	4	0	0
	SUB-TOTAL (x2)	0	0	0	0	0	0	0	0	0	8	0	0
	2. Tissue response												
	Neovascularisation	0	0	1	0	0	0	0	0	0	2	1	1
	Fibrosis/fibrous membrane	0	0	1	0	0	0	0	0	0	2	1	1
	Fatty infiltrate	0	0	0	0	0	0	0	0	0	0	0	0
	F.2 SUB-TOTAL	0	0	2	0	0	0	0	0	0	4	2	2
	TOTAL (1.+2.)	0	0	2	0	0	0	0	0	0	12	2	2
	GROUP TOTAL	2						16					
	Average (Ø)	0.33						2.67					
	Ø TI - Ø CI *	-2.34 = 0											
additional observations	Traumatic necrosis	0	0	0	0	0	0	0	0	0	0	0	0
	Foreign debris	0	0	0	0	0	0	0	0	0	0	0	0

* Used to determine irritant ranking shown below as the conclusion. A negative difference is recorded as zero.

Conclusion: Under the conditions of this study, the Test group was considered to demonstrate the following:
_X_ minimal or no reaction (0.0 up to 2.9);
___ slight reaction (3.0 upt to 8.9);
___ moderate reaction (9.0 upt to 15.0);
___ severe reaction (>15.1)
to the tissue as compared to the non-treaed Control group.

Table 3.4: Results of biocompatibility evaluation at the Marvel screws and surrounding tissue of each tibia sample (light grey labelled animals TI group) for the 3 mm gap model.

3.1.11.2 Semiquantitative analysis of bone activity, tissue character and healing response in the gap area

For both TI and CI groups, bone activity parameters showed high scores for bone formation (Score 3-4: between 51-100% new bone formation) at the fracture ends and in the gap area. Slightly higher bone activity scores were achieved by the TI. For all TI samples and 5/6 CI samples, bone resorption was only observed within a normal range (score 0-1, 0-25%), typical for a bone remodeling process. One control item animal (86.07) showed moderately elevated scores for bone resorption with a score value of 2 for cis cortex (resorption reaching 26-50%) and 3 for the trans cortex (51-75%).

Tissue character was described based on the maturity of the callus and presence of endochondral ossification within the fracture gap and at the fracture ends. The mean total score for callus maturity was higher in TI (3.50) comparing to CI (2.72). In the TI, newly formed bone at the fracture ends (both cis and trans) was already highly organized and integrated. This was characterized by dense and regularly oriented structure in the longitudinal axis. Furthermore, in comparison to CI a more pronounced degree of vascularization and a thicker osteoid seam with highly activated osteoblasts (Figure 3.14 M) was evident. Endochondral ossification was higher in CI (score=0.89), indicating a less advanced healing process compared to TI (score=0.22). The overall healing response was characterized by a defect unity score, which showed higher values for gap closure in the TI with a mean total score of 3.56 compared to CI with 2.78.

Individual scoring results for semiquantitative analysis of bone activity, tissue character and healing response in the gap area of TI and CI are illustrated in Table 3.5.

Representative images of the histological samples can be found in Figure 3.14 A-N.

Group	Animal ID	Bone activity						Tissue character						Healing response (thick section)		
		Bone resorption			Bone formation			Endochondral ossification			Maturity of callus/new bone			Defect unity		
		Cis	defect	trans	cis	defect	trans	cis	defect	trans	cis	defect	trans	cis	defect	trans
Test Item	86.03	0	1	1	3	3	2	1	0	0	3	2	1	2	3	1
	86.10	0	0	0	4	4	4	0	0	0	4	4	4	4	4	4
	86.11	0	0	0	4	4	4	0	0	0	4	4	4	4	4	4
	86.12	0	1	1	4	3	3	1	1	1	3	3	3	4	4	3
	86.28	0	1	0	4	4	3	0	0	0	4	4	4	4	4	3
	86.29	0	0	0	4	4	4	0	0	0	4	4	4	4	4	4
	Mean	**0**	**0.50**	**0.33**	**3.83**	**3.67**	**3.33**	**0.33**	**0.17**	**0.17**	**3.67**	**3.50**	**3.33**	**3.67**	**3.83**	**3.17**
	Mean total gap	**0.28**			**3.61**			**0.22**			**3.50**			**3.56**		
Control Item	86.04	0	0	0	4	4	4	1	0	1	3	4	4	3	4	4
	86.05	0	0	1	4	4	3	1	2	2	4	3	2	4	4	1
	86.06	0	0	0	4	4	4	0	0	0	4	4	4	4	4	4
	86.07	2	0	3	1	3	0	0	2	0	0	3	0	1	2	1
	86.08	0	0	1	4	4	2	1	1	0	4	4	2	4	4	2
	86.09	1	0	1	2	3	0	1	4	0	2	2	0	1	3	0
	Mean	**0.50**	**0**	**1.00**	**3.17**	**3.67**	**2.17**	**0.67**	**1.50**	**0.50**	**2.83**	**3.33**	**2.00**	**2.83**	**3.50**	**2.00**
	Mean total gap	**0.50**			**3**			**0.89**			**2.72**			**2.78**		

Table 3.5: Results for semiquantitative analysis of bone activity, tissue character and healing response in the gap area (range: 0-4) for TI and CI.

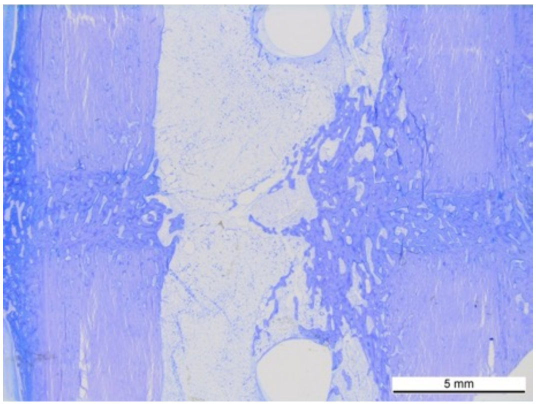

A: Animal 86.11, TI, overview gap, well organized callus at both cortices, no callus around the marvel screws in the bone marrow cavity, toluidine blue, mag. 1x7.11

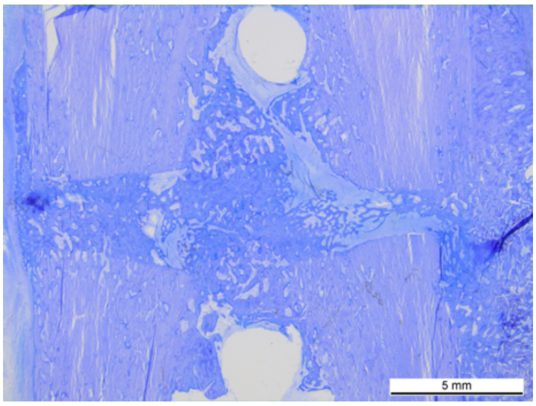

B: Animal 86.08, CI, overview gap, good bone formation at the cis cortex, a lot of callus in the bone marrow cavity, gap not completely healed at the trans cortex, a lot of periosteal callus formation at trans, toluidine blue, mag. 1x7.11

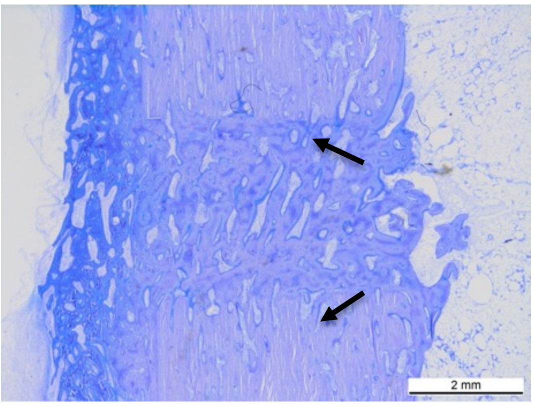

C: Animal 86.11, TI, gap area at cis cortex, new bone highly organized, characterized by dense and regularly oriented structure according to the longitudinal axis at the fracture ends (arrows), toluidine blue, mag. 1x15.5

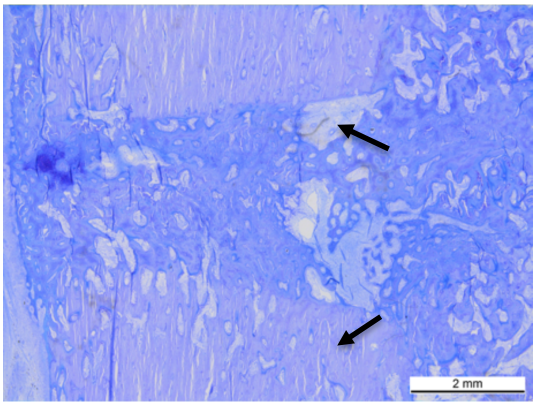

D: Animal 86.08, CI, gap area at cis cortex, new bone formation at the fracture ends (still pronounced and oriented to the transverse axis, black arrows), visible isles of endochondral ossification and mesenchymal tissue, callus formation within bone marrow cavity, toluidine blue, mag. 1x15.5

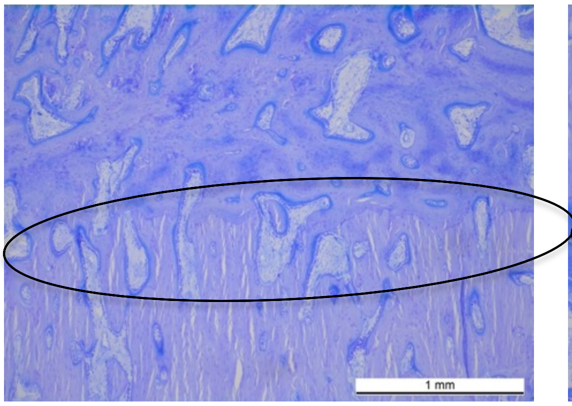

E: Animal 86.11, TI, higher magnification, smooth transition zone fracture end to gap area at cis cortex (black circle), new bone highly organized, characterized by dense and regularly oriented structure, toluidine blue, mag. 1x45

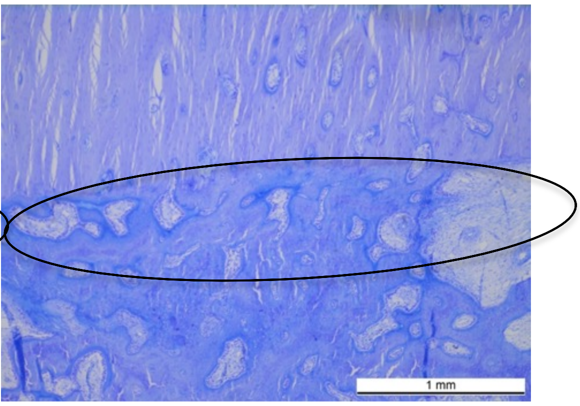

F: Animal 86.08, CI, higher magnification, sharp transition zone fracture end to gap area at cis cortex (black circle), new bone formation, fracture ends still pronounced, callus within gap disorganized, visible isles of mesenchymal tissue, toluidine blue, mag. 1x45

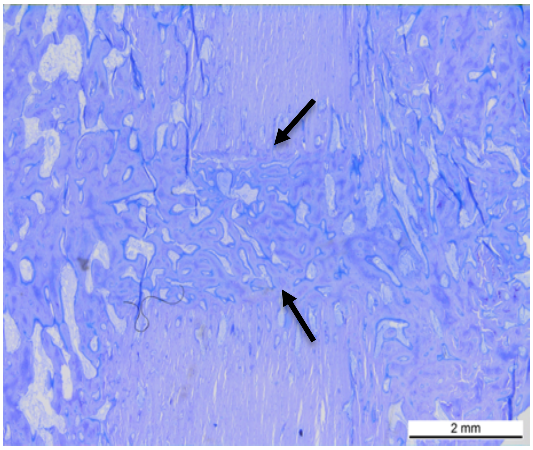

G: Animal 86.11, TI, gap area at trans cortex, gap completely remodeled and united (black arrows), periosteal callus formation, smooth transition zone, new bone highly organized, characterized by dense and regularly oriented structure at the fracture ends, toluidine blue, mag. 1x15.5

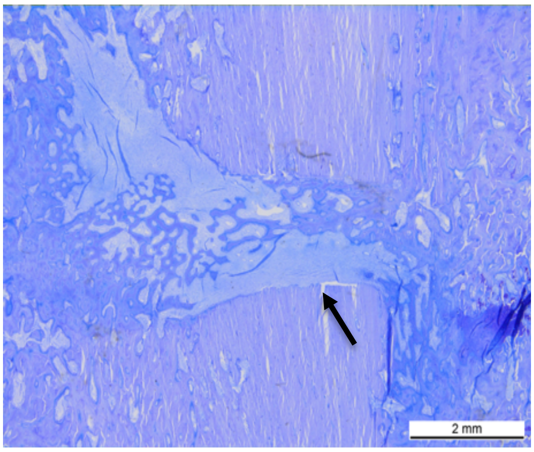

H: Animal 86.08, CI, gap area at trans cortex, gap not completely united (black arrow), large periosteal callus formation, new bone formation at the fracture ends (still pronounced), visible isles of endochondral ossification and mesenchymal tissue, callus within gap disorganized, toluidine blue, mag. 1x15.5

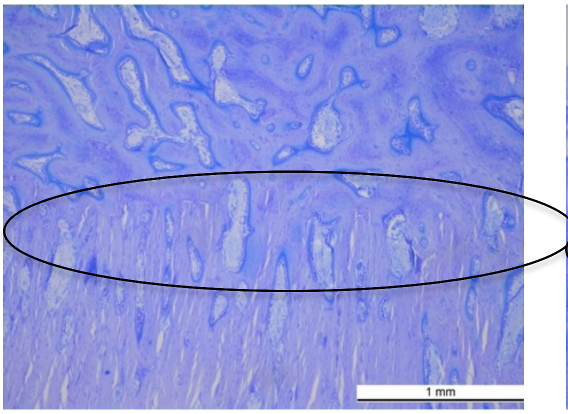

I: Animal 86.11, TI, higher magnification, smooth transition zone between fracture end to gap area at trans cortex (black circle), new bone highly organized, characterized by dense and regularly oriented structure, toluidine blue, mag. 1x45

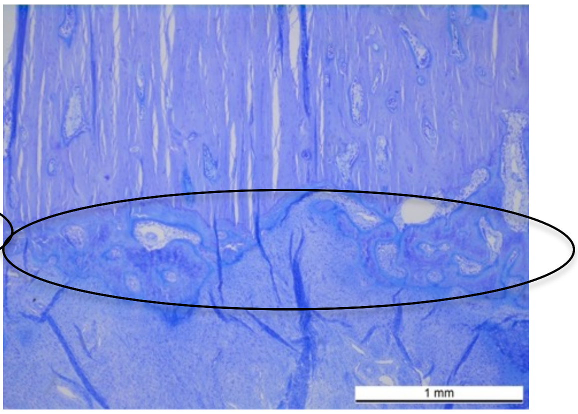

J: Animal 86.09, CI, higher magnification, sharp transition zone between fracture end to gap area at trans cortex (black circle), new bone formation, fracture ends irregular after resorption, less bone formation, abundant mesenchymal tissue, toluidine blue, mag. 1x45

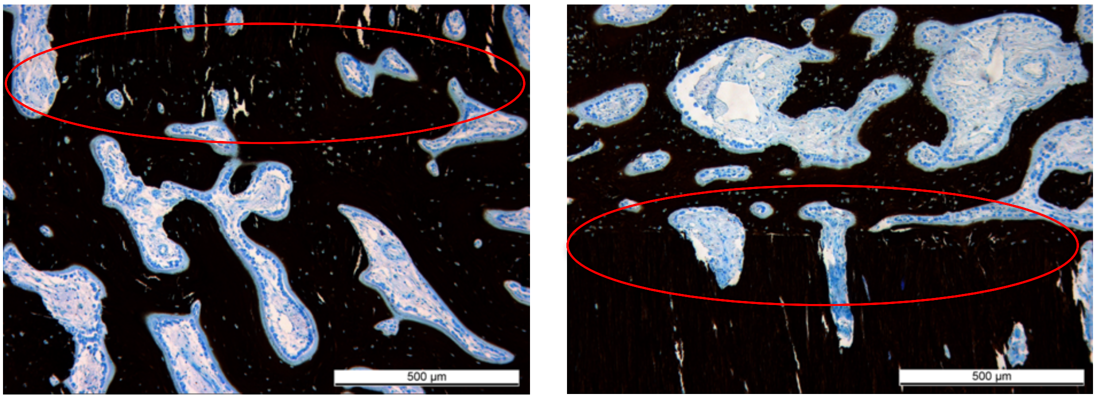

K: Animal 86.11, TI, overview image, smooth transition zone between fracture end to gap area at cis cortex, new bone highly organized, characterized by dense and regularly oriented structure, thick osteoid seam, activated osteoblasts, von Kossa 12.5

L: Animal 86.08, CI, overview image, transition zone between fracture end to gap area at cis cortex, new bone with bigger intertrabecular spaces than in TI, von Kossa 12.5

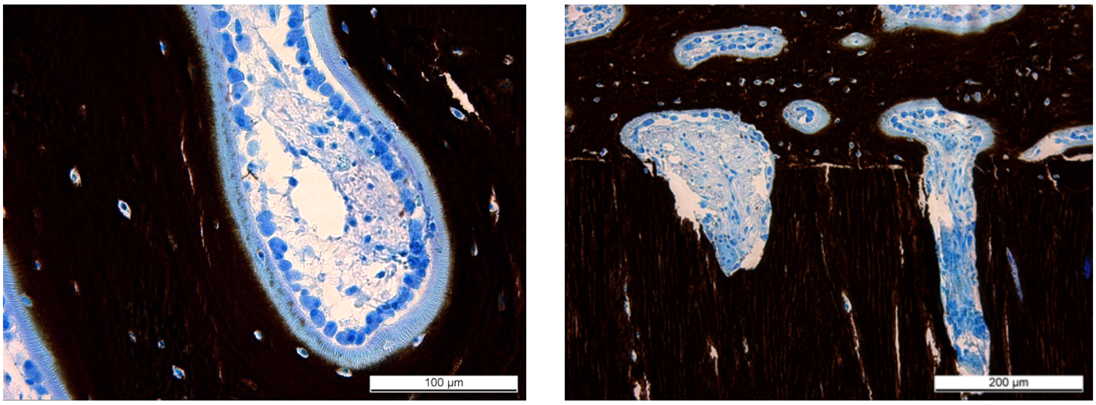

M: Animal 86.11, TI, detail image, thick osteoid seam, highly activated osteoblasts, von Kossa 100x

N: Animal 86.08, CI, transition zone between fracture end to gap area at cis cortex, ativated osteoblast, thinner osteoid seam than in TI, von Kossa 50x

Figure 3.14 A-N: Representative images of histological thin sections for TI and CI.

3.2 17 mm Graft Model

3.2.1 Anesthesia, surgery and post-operative recovery period

In total, 15 animals underwent surgery with a 17mm gap, which was either filled with autograft (12/15) or not filled (3/15 animals). The overall anesthesia time was between 132-236 min (Ø 196 min) and no complications occurred. The surgical procedure lasted between 83-109 min (Ø 99 min).

In 14/15 animals, the tibia osteotomies including internal fixation, as well as the placement of the Marvel screws could be performed without any complications. Only in one sheep of the TI (86.18), the osteotomy cuts were not completely parallel (about 1 mm off) due to a problem with the cutting guide. Nevertheless, the alignment of proximal and distal tibia was good, despite the misalignment of the cut. In all sheep (N=12) with autograft filling of the gap, the harvesting at the iliac crest could be performed without any complications.

For each sheep, the number of the used Universal Transducer SI-ES as well as the measured resistance (Ohm) was noted. The resistance values were within the functional range for all TI (between 90-102 Ohm). In CI, the resistance ranged from 38 to 300 Ohm or some transducers were not working. The detailed measurements for each sheep are attached in Appendix 2.

No complications occurred during the Marvel technology placement (no detached caps, no failures in resistance measurements for TI animals). The Universal Transducer SI-ES was easy to place subcutaneously at the distal part of the tibia and caps were easy to tap to the screw heads. All 15 animals were operated with the re-worked transducer caps, and therefore no detachment occurred.

3.2.2 In-life clinical observations

None of the 15 animals included in the group analysis revealed serious or persistent clinical abnormalities influencing the overall outcome of the study.

After a surgery was completed, each sheep received a full limb cast, which was changed every three weeks during radiographic follow-up examinations and successfully carried until the sacrifice day. Additional cast changes were performed in cases of cast breakage or a cast causing discomfort of an animal. All animals were successfully put in a specially designed suspension system for sheep, thanks to which shear forces put on the operated limb could be minimized. All animals accepted the casts without any issues and majority of them (13/15) tolerated the suspensions systems with no complications. One animal (86.13, CI) developed head and neck edema in the first night after surgery due to positional self-compression of the jugular veins in the suspension system. The animal was treated with furosemide, additional paracetamol & buprenorphine in standard dosages and fully recovered within 2 days and could stay in the suspension system without other complications. The other animal (86.25, NCI) showed repetitive edematous swelling of the left front limb caused by the suspension belt, therefore it needed to be taken out of suspension after 24 days post OP (4 days earlier than planned). The animal fully recovered within the next day.

In the 12 animals, which underwent autograft harvesting at the iliac crest, pain medication was adapted (additional paracetamol for 3-4 days) and consequently the animals did not seem more painful despite the more invasive surgery.

6 weeks post-surgery, one animal (CI: 86.22) developed pressure sores at the udder, caused by irritation and pressure due to the cast. The animal received antibiotics (amoxycillin, 15 mg/kg BW, im) and analgesics (carprofen 4 mg/kg BW sc) for 8 days. After 10 days the animal did fully recover without further complications. Two animals (TI: 86.20, 86.21) lied down more than usual.

All animals tolerated the coils and the therapy could be applied without complications.

3.2.3 Macroscopic findings at sacrifice

In all 15 animals, the sacrifice procedure after 12 weeks could be performed without encountering any problems, according to routine. All samples, including lymph nodes and both tibiae could be harvested as planned.

Overall, the anatomical dissection performed right after sacrifice showed that in both groups, TI and CI, the tissue adjacent to the implants did not show any alteration of the normal structure. No hematoma, edema, encapsulation, and/or other additional gross findings were recorded. The universal transducer and its cables stayed in place and did not interfere with the larger gap. No encapsulation or granuloma were found around the implanted Marvel technology (universal transducer, cables, caps). No cap detachment was detected in any animal from this model.

Resistance of the transducer was measured in order to confirm its connection to the caps. In TI, the resistance values ranged from 0.136 to 91 Ohm, whereas in CI from 0.38 to 88 Ohm or were not functional. Exploration of the gap area and verification of fragment stability showed a macroscopically stable callus in all TI and only 2/6 CI (86.14, 86.15) tibiae. In 5/6 CI samples the gap was unstable, while in 3/3 NCI samples the gap was highly unstable. The gaps of all three NCI samples were collapsed and the plates slightly (86.25, 86.27) and severely bent (86.26).

In addition, no macroscopic abnormalities were found in all harvested lymph nodes.

148/150 locking head screws were found locked and correctly placed in the plate. Only 2/150 locking head screws of one TI animal were found slightly displaced, but firm. No broken screws were observed in all animals.

Metallosis at the screw head - plate junction was found in all sheep of all three groups (TI=6, CI=6, NCI=3) dominantly at the distal screw holes 9 – 12, but also at screw hole 6 (TI=3/6, CI=4/6, NCI=3/3).

All Marvel screws (N=30) were firmly integrated in the bone, no macroscopic loosening was observed.

3.2.4 Micro-CT morphometry and structural analyses

The global morphometric analysis was successfully performed and gave a comprehensive assessment of new bone formation.

Results of the global morphometry showed significantly higher callus volume (p=0.003, mean difference = 4.61 cm^3) and mature callus volume (p=0.002, mean difference = 3.02 cm^3) in TI compared to CI. Even though the callus density difference was not statistically significant, there was a notable trend for a higher value in TI (p=0.055).

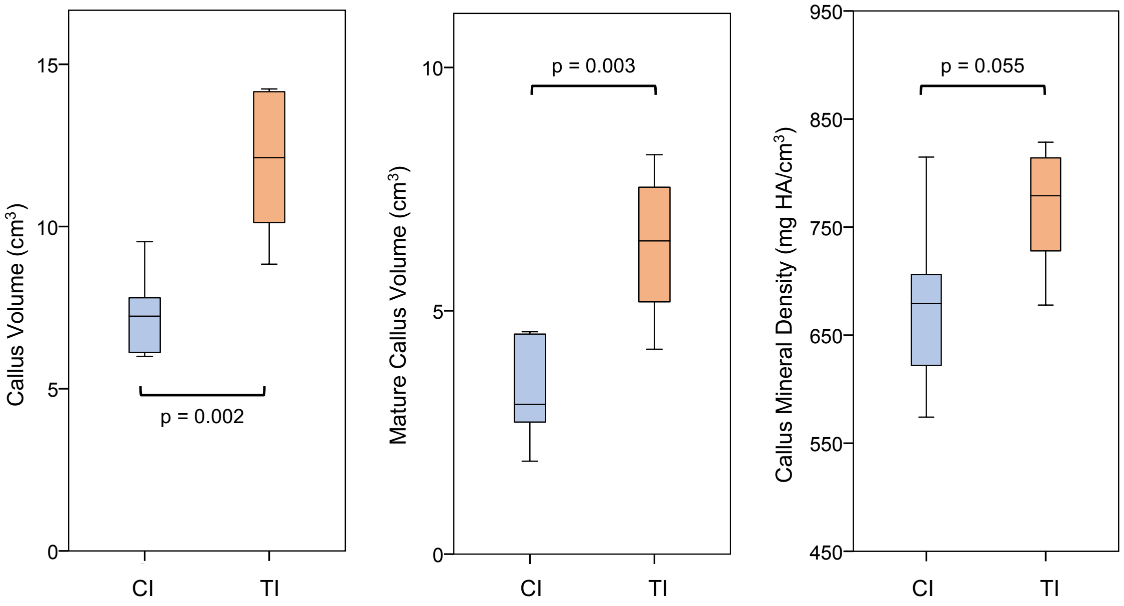

Figure 3.15: Callus volume in cm3, mature callus volume in cm3, callus mineral density in mg HA/cm3 comparing CI and TI (n = 6).

3.2.5 Biomechanics

Biomechanical testing was successfully done in all samples. All results are reported as mean ± SD.

The gauge length was 155 ± 4 mm for non-operated tibiae and 157 ± 2 mm for operated tibiae.

Non-operated tibiae (12 in total) exhibited an overall torsional stiffness of 7.96 ± 1.13 Nm/deg. The non-operated tibiae in the CI group had a torsional stiffness of 7.45 ± 1.15 Nm/deg while the non-operated tibiae in the TI group had a torsional stiffness of 8.46 ± 0.93 Nm/deg. This difference was not statistically significant (p=0.127).

The operated tibiae in the CI group had a torsional stiffness of 2.23 ± 2.19 Nm/deg (98% relative standard deviation) while the operated tibiae in the TI group had a torsional stiffness of 5.81 ± 2.38 Nm/deg (48% relative standard deviation). The difference between CI and TI was statistically significant (p=0.022). Stiffness values for individual animals are shown in Appendix 7: Biomechanics.

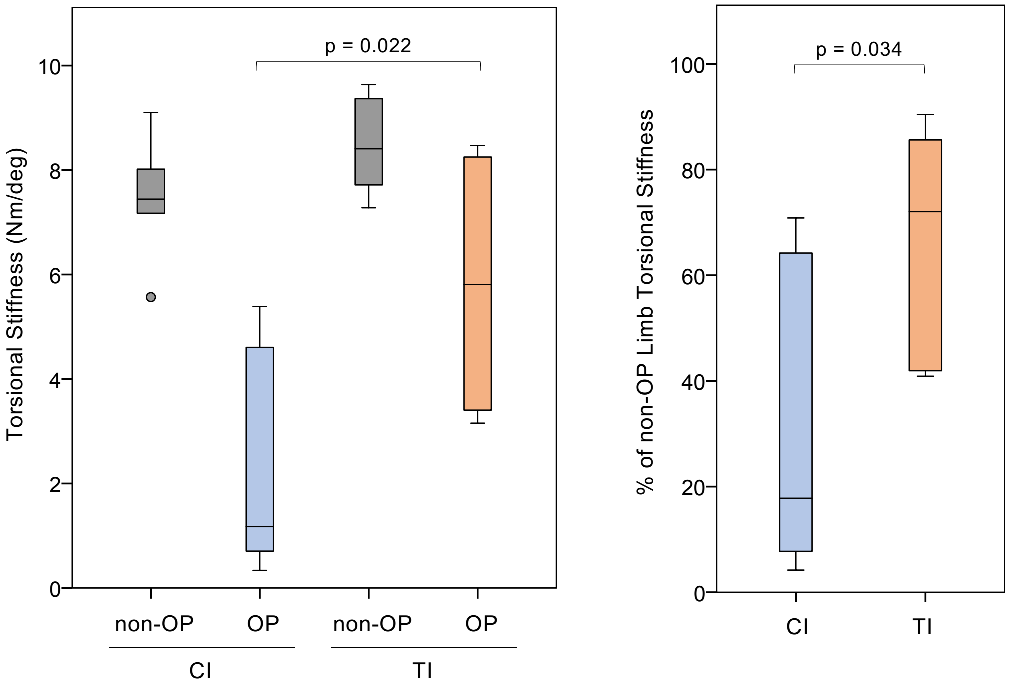

Figure 3.16: Torsional stiffness in Nm/deg of operated and non-operated tibiae and percent (%) torsional stiffness of operated tibiae compared to contralateral non-operated tibiae in CI and TI (n = 6).

Normalizing the operated tibia stiffness to the contralateral non-operated tibia stiffness, the TI group tibiae reached 67 ± 21 % of the contralateral non-operated tibiae stiffness. The CI group tibiae reached 30 ± 29 % of the contralateral non-operated tibiae stiffness. The difference between CI and TI was also statistically significant (p = 0.034). Normalized stiffness values for individual animals are shown in Appendix 7: Biomechanics.

3.2.6 Radiographic evaluation

It was possible to radiographically evaluate all 17mm graft model samples. This was done by the same two independent board-certified reviewers (Prof. Brigitte von Rechenberg and Prof. Mark Flückiger). The same scores were used as for the 3 mm gap group, although with a few modifications. In the TI and CI group gaps were filled with autograft material. Therefore, it was not always possible to clearly distinguish between newly formed periosteal callus and remaining, resp. remodeling autografts. For this reason, cortical callus formation was considered as score 2, when periosteal callus formation over the defect area and autografts were joined and could not be distinguished from each other. Also defect opacity was divided into the opacity of the callus within the defect and periosteal callus bridging the defect. All other variables remained the same as in the 3 mm gap.

For the NCI group, without autografts filling the defect, considerably lower callus opacity was reached. Therefore, scores were different already in the early time points, making it difficult to compare NCI radiographic results with the other groups.

Overall, all radiographs were of excellent quality and positioning, such that assessment of the defect area could be made without problems. In general, the positive results of electromagnetic stimulation could be confirmed as in the 3 mm gap. Note, that the time of sacrifice was longer for this 17mm gap with 12 weeks follow-up compared to the 3mm gap.

None of the defects were completely radiographically healed at 12 weeks. Bridging of the defects with callus was nearly complete in 5/6 TI sheep and apparent only in 1/6 sheep in the CI group. In addition, the overall defect area appeared less evenly filled with bone, with more focally distributed areas in the control group compared to the treated group. In the NCI group, none of the defects was filled with callus and all three plates were bent with a collapse of the trans cortex.

3.2.6.1 Semiquantitative scoring of radiographs

The total score of the 17mm defect was highest for the TI group, followed by the CI and last by the NCI. Generally, new bone formation around the autografts and increased callus formation within the defect was noticed already at 3 weeks in the TI and at 6 weeks in the CI group.

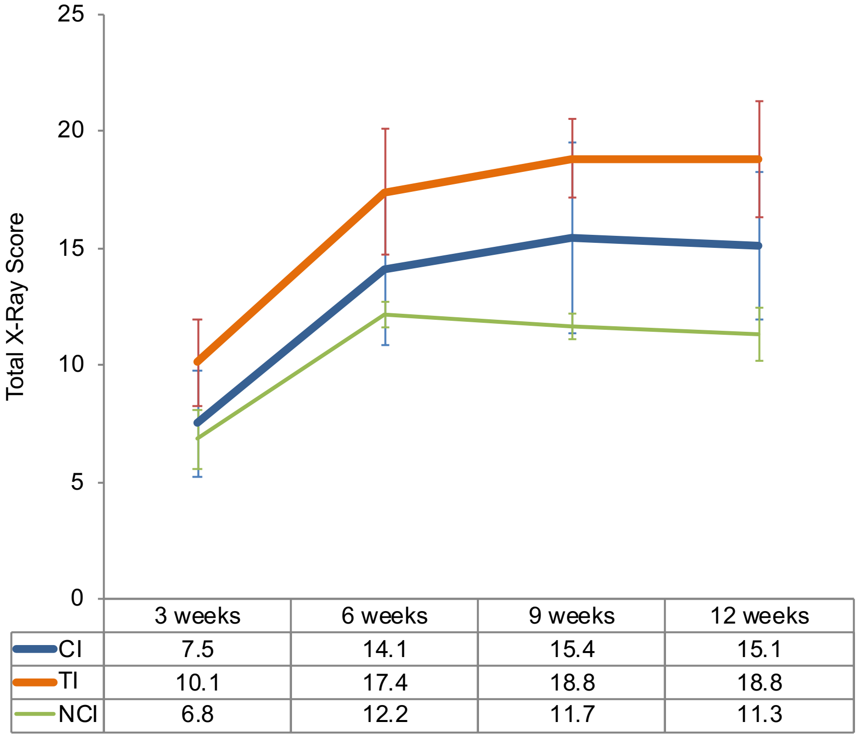

	3 weeks	6 weeks	9 weeks	12 weeks
CI	7.5	14.1	15.4	15.1
TI	10.1	17.4	18.8	18.8
NCI	6.8	12.2	11.7	11.3

Figure 3.17: Mean ± SD total radiographic score (0 – 30) for TI (n=6), CI (n=6) and NCI (n=3) at 3, 6, 9 and 12 weeks post-operatively. The means are also listed in the table.

Cortical callus formation in the anteroposterior view (0° angle) was usually more pronounced at the transcortical area, but new bone formation was also noticed around the autografts laid underneath the cis cortex. Overall, callus bridging almost 80-90% of the gap was noticed at the trans cortex already at 6 weeks in 5/6 sheep of TI, whereas in the CI group this was only the case in 1/6 sheep. At 9 weeks, this was even more pronounced with an overall increase of bone formation within the defect in the TI group, although the cis-cortical area was still clearly less dense. In the CI group, only 1/6 animals showed a bridging callus whereas the others still showed no bridging callus at the trans cortex. Radiographs of 3 sheep in both groups at 10 weeks showed no major advancement. At 12 weeks 2/6 sheep of the TI group showed complete bridging while the others had only a small gap remaining at the trans cortex. The cis cortex was still less dense compared to the trans cortex. In the CI group, only 1/6 sheep showed bridging of the trans cortex, whereas the cis cortex was less dense than the one of the TI group.

The RUST Score confirmed this trend (see Figure 3.18).

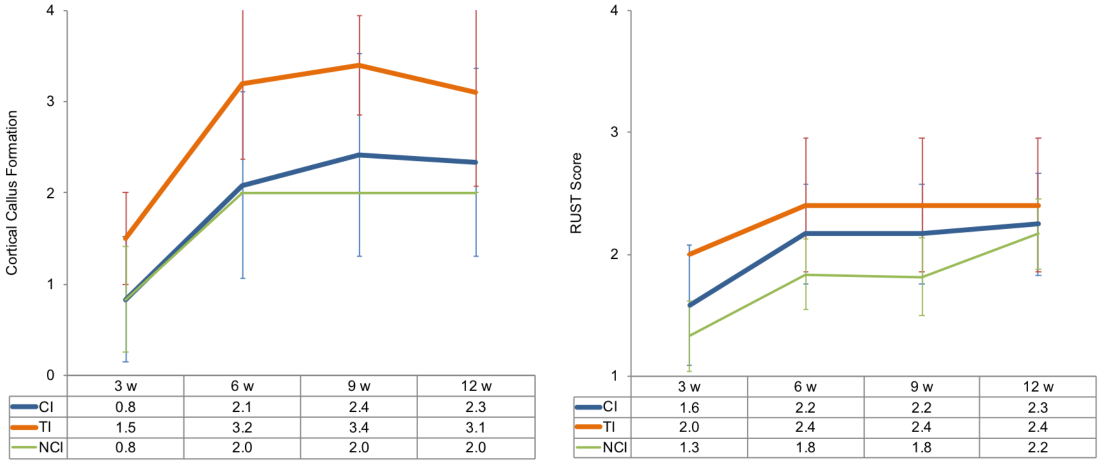

	3 w	6 w	9 w	12 w
CI	0.8	2.1	2.4	2.3
TI	1.5	3.2	3.4	3.1
NCI	0.8	2.0	2.0	2.0

	3 w	6 w	9 w	12 w
CI	1.6	2.2	2.2	2.3
TI	2.0	2.4	2.4	2.4
NCI	1.3	1.8	1.8	2.2

Figure 3.18: Mean ± SD cortical callus formation score (0 – 4) and RUST score (1 – 4) for TI (n=6), CI (n=6) and NCI (n=3) at 3, 6, 9 and 12 weeks post-operatively. The means are also listed in the tables.

<u>The cis cortex</u> at a 0° angle showed a higher score in the TI compared to the CI group, although full bridging with remodeling of the cortical bone was not achieved at 12 weeks. <u>The trans cortex</u> at a 0° angle also showed higher scores in the TI group. In the early time points, the NCI showed more callus formation compared to the CI group. However, this has to be interpreted with caution. The NCI group received no autografts. Therefore, the slightest periosteal reaction could be easily noticed, whereas the autografts may have obscured the view for new callus formation. Nevertheless, scores between the TI and CI group were more pronounced between 3 and 6 weeks and then became gradually less between 9 and 12 weeks.

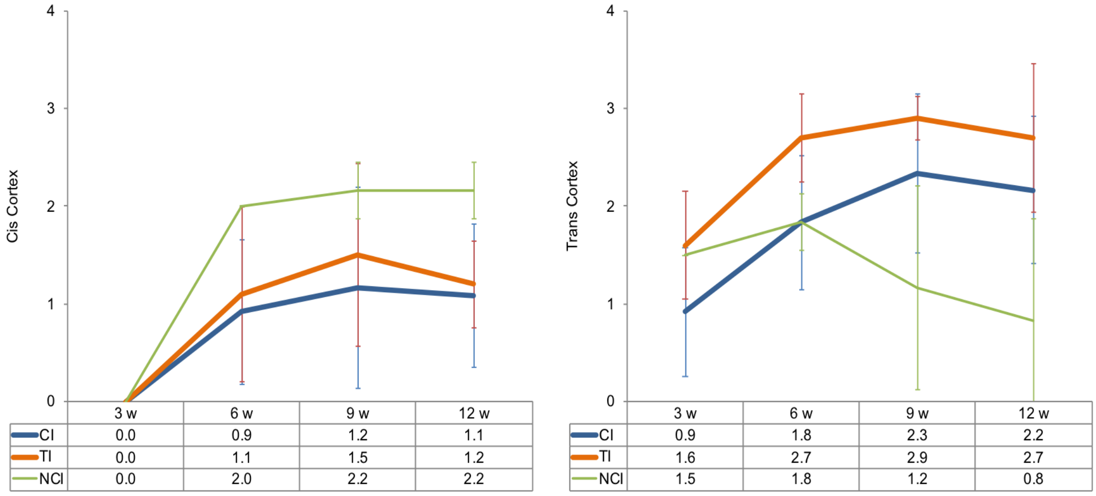

	3 w	6 w	9 w	12 w
CI	0.0	0.9	1.2	1.1
TI	0.0	1.1	1.5	1.2
NCI	0.0	2.0	2.2	2.2

	3 w	6 w	9 w	12 w
CI	0.9	1.8	2.3	2.2
TI	1.6	2.7	2.9	2.7
NCI	1.5	1.8	1.2	0.8

Figure 3.19: Mean ± SD cis cortex score (0 – 4) and trans cortex score (0 – 4) for TI (n=6), CI (n=6) and NCI (n=3) at 3, 6, 9 and 12 weeks post-operatively. The means are also listed in the tables.

The cranial cortical gap (cis cortex) at an 275° angle demonstrated also higher scores for the TI versus the CI group. Differences increased over time starting at 6 weeks for the TI group. In the NCI group, the scores decreased after 9 weeks indicating bone resorption and rounding of the cortical bone fragments.

The caudal cortical gap (trans cortex) at an 265° angle revealed higher scores for the TI group, although not quite as pronounced as in the cranial cortical gap. Especially at 12 weeks, scores of both groups were quite close. Scores of the NCI group were much lower.

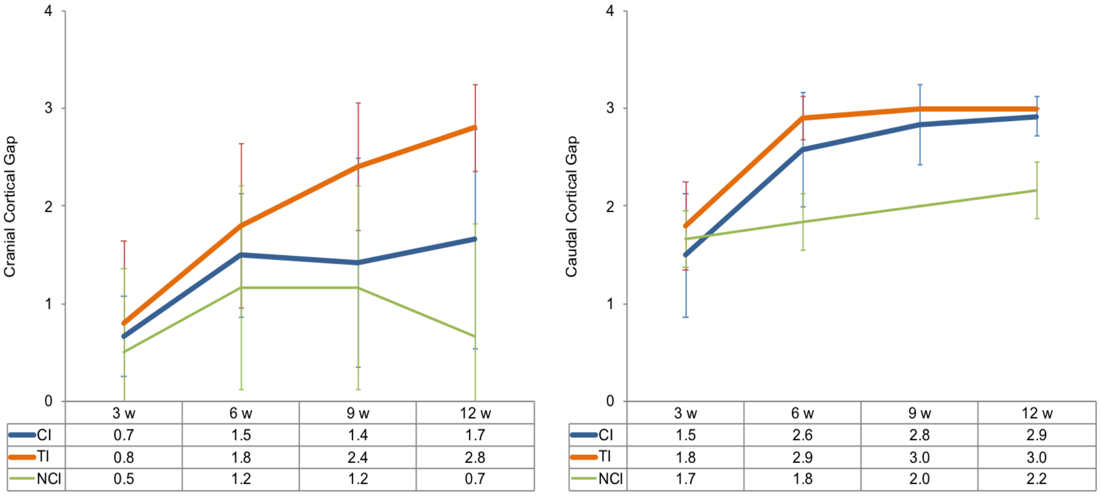

	3 w	6 w	9 w	12 w
CI	0.7	1.5	1.4	1.7
TI	0.8	1.8	2.4	2.8
NCI	0.5	1.2	1.2	0.7

	3 w	6 w	9 w	12 w
CI	1.5	2.6	2.8	2.9
TI	1.8	2.9	3.0	3.0
NCI	1.7	1.8	2.0	2.2

Figure 3.20: Mean ± SD of cranial cortical gap score (0 – 4) and caudal cortical gap score (0 – 4) for TI (n=6), CI (n=6) and NCI (n=3) at 3, 6, 9 and 12 weeks post-operatively. The means are also listed in the tables.

Callus opacity of the bridging callus was similar for both groups in the first 9 weeks for both, the TI and the CI group. The opacity of the NCI group was clearly lower.

Callus opacity within the defects was higher scored in the treated group. However, this result has to be interpreted with some caution, since the opacity of the defect was already given through the autografts alone, which were similar in both groups.

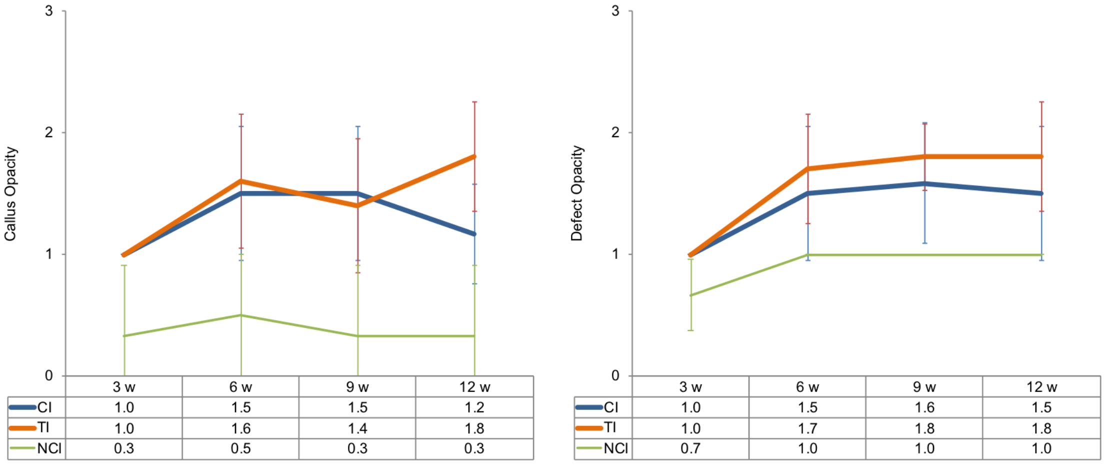

	3 w	6 w	9 w	12 w
CI	1.0	1.5	1.5	1.2
TI	1.0	1.6	1.4	1.8
NCI	0.3	0.5	0.3	0.3

	3 w	6 w	9 w	12 w
CI	1.0	1.5	1.6	1.5
TI	1.0	1.7	1.8	1.8
NCI	0.7	1.0	1.0	1.0

Figure 3.21: Mean ± SD of callus opacity score (0 – 3) and defect opacity score (0 – 3) for TI (n=6), CI (n=6) and NCI (n=3) at 3, 6, 9 and 12 weeks post-operatively. The means are also listed in the tables.

Screw tip callus was also seen on both Marvel screw tips in 5/6 TI sheep already at week 3. This was not seen in most (5/6) CI sheep until week 12. In the NCI group, no sheep developed callus at both Marvel screw tips at any timepoint.

Cortex blurring was clearly observed (score of 1) in 5/6 TI sheep versus 3/6 CI sheep at 6 weeks and in all TI and CI sheep at 9 weeks and 12 weeks. Meanwhile, sheep 86.26 and 86.27 from the NCI group showed slight cortex blurring at 12 weeks, with the cortex blurring appearing more clearly in 86.26 at 9 weeks.

3.2.7 Histomorphometry

12 toluidine blue stained histological ground sections (6 TI and 6 CI) were successfully evaluated histomorphometrically. Microradiographs of the ground sections were used to corroborate the structure of calcified tissue in the toluidine stained samples.

The evaluation was performed using total and sectoral analyses. Concerning total section analysis, for each sample, percentages of old bone, callus (consisting of new bone and autograft material in the gap), non-bone structures and cartilaginous tissue were successfully measured in all samples. Notably, as opposed to the 3 mm gap model, 12 animals in the 17mm graft model received autografts. Both autograft and newly formed bone were indistinguishable (due to enhanced remodeling process) and were, therefore, in this analysis together considered as callus. For the sectoral evaluation, the callus (also including autograft remnants) in the endosteal, cis and trans area could be distinguished in all samples.

Overall, histomorphometrical measurements revealed comparable and good healing of the defect area for both, TI and CI, with the TI showing a more advanced healing.

3.2.7.1 Total section evaluation

Overall, no significant differences were found between TI and CI for any of the values of the total section analysis.

Results for histomorphometric evaluation of the total section are shown in Figure 3.22 and Table 3.6. The percentages of old bone were similar in TI and CI. The trend showing a slightly higher percentage of cartilaginous tissue remnants and non-bone tissue in the CI indicated a more advanced healing process in the TI. The percentage of callus tissue, showed a tendency of higher values for TI compared to CI (mean difference = 6.9%, n=6).

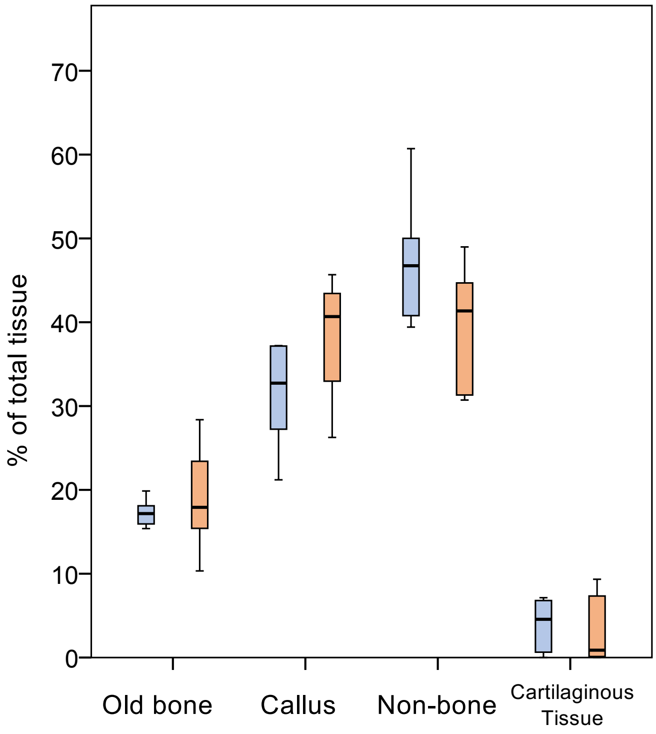

Figure 3.22: Histomorphometric measurements 12 weeks post-surgery of % old bone, % callus, % non-bone structures and % cartilaginous tissue for TI (n=6, marked orange) and CI (n=6, marked blue). Results represent the percentage of the total area measured.

Group	Total Section Analysis			
	Old Bone [%]	Callus [%]	Non-bone [%]	Cartilagineous Tissue [%]
CI	17.27	31.38	47.40	3.95
TI	18.89	38.28	39.73	3.09

Table 3.6: Histomorphometric measurement means 12 weeks post-surgery of % old bone, % callus, % non-bone structures and % cartilaginous tissue for TI (n=6) and CI (n=6). Results represent the percentage of the total area measured.

3.2.7.2 Sectoral evaluation

Overall, no significant differences were found between TI and CI for any of the values of the sectoral analysis.

Results of sectoral histomorphometric evaluation are shown in Figure 3.23 and Table 3.7. Nevertheless, slightly higher callus values were found at the cis-cortex (mean difference = 4.52%) and endosteal (mean difference = 5.85%) in CI, while TI showed higher values at the trans-cortex (mean difference = 10.38%).

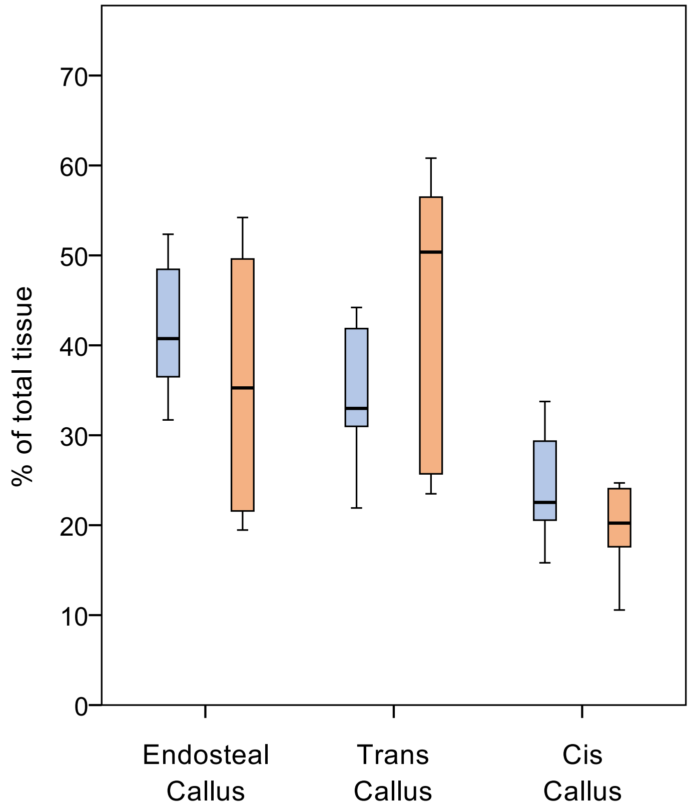

Figure 3.23: Sectoral histomorphometric measurements 12 weeks post-surgery of % endosteal callus, % trans callus and % cis callus for TI (n=6, marked orange) and CI (n=6, marked blue). Results represent percentage of the total area measured.

Group	Sectoral Analysis		
	Cis Callus [%]	Endosteal Callus [%]	Trans Callus [%]
CI	24.09	41.75	34.16
TI	19.57	35.90	44.54

Table 3.7: Sectoral histomorphometric measurement means 12 weeks post-surgery of % endosteal callus, % trans callus and % cis callus for TI (n=6) and CI (n=6). Results represent percentage of the total area measured).

3.2.8 Fluorescence

12 unstained histological fluorescence sections of all TI and CI sheep were successfully evaluated. Fluorescent markers were successfully injected in all animals of the 17 mm graft model at 3 weeks (calcein green), 6 weeks (xylenol orange), and 12 weeks post-surgery (48 hours prior to sacrifice). Fluorescent dyes were well visible in all specimens. Calcium deposition at the various time points could be easily followed with the different colors in all samples.

Overall, both TI and CI revealed similar calcium deposition, which was slightly more pronounced compared to 3mm gap due to autograft remodeling. TI manifested more calcification at the cortices whereas CI more so in the bone marrow. The most active fluorescent signal was present at the 6-week time point.

At 3 weeks, calcein green deposition was only slightly visible in TI and CI mostly within the defect area due to the remodeling process of the implanted autograft material. In comparison to the 3 mm gap model, the calcium deposition was not concentrated at the transcortical periosteum. The transcortical periosteum was removed during surgery of the 17 mm graft model in order to create a non-union defect, when the defect would be left empty. The NCI group presented a very weak fluorescent signal as well. However, it was not accumulated inside the defect but dispersed within the endosteum.

At 6 weeks, xylenol orange was visible in a very similar distribution as calcein green at 3 weeks but was more enhanced within both groups. Intramedullary calcium deposition was almost the same in TI and CI. However, increased deposition at the fracture ends especially at the trans cortex was evident in 5/6 TI samples (see Figure 3.24 - Figure 3.26). The fluorescent signal in the NCI was less pronounced compared to the groups which received autografts, but was still higher at 6 weeks compared to 3 weeks. These samples showed some calcium deposition along the cortices at week 6, which was not apparent at week 3. A particularly active signal was visible at the cis cortex of sheep 86.26, as this was the place where the LCP plate bent and where the gap collapsed.

At 12 weeks, a lower oxytetracycline signal (compared to the xylenol signal at 6 weeks) was seen in the TI and the CI group, indicating a more advanced but still ongoing remodeling process. Notably, some cortical areas in the fracture gap did not exhibit any activity. These areas corresponded with the cartilaginous tissue found in the histomorphometric evaluation of thick sections (see Figure 3.26). Also, NCI exhibited an overall lower signal intensity then the other groups (see Figure 3.27).

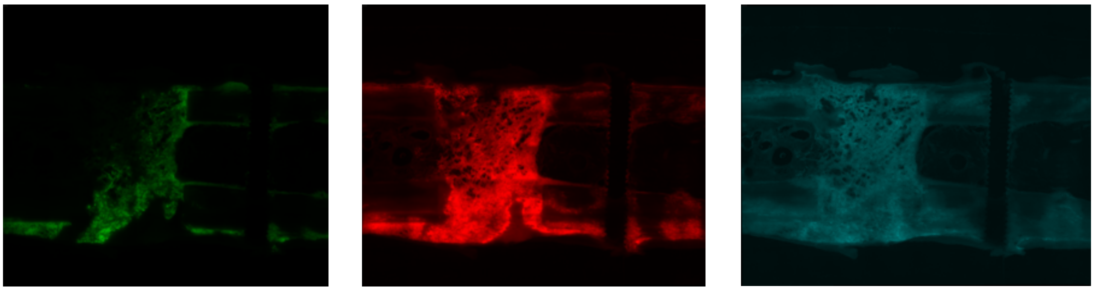

Calcein green at 3 weeks | Xylenol orange at 6 weeks | Oxytetracycline at 12 weeks

Figure 3.24: Fluorescence images of 86.14 CI, at 3 weeks only hardly visible calcium deposition, at 6 and 9 weeks slight deposition, but mainly in the bone marrow cavity and not in the gap area (delayed union).

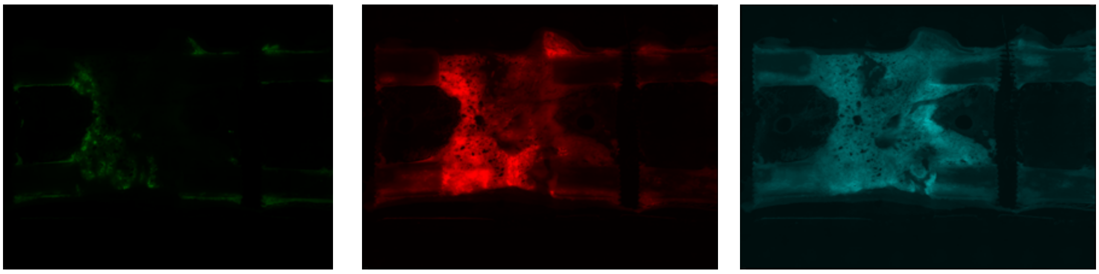

Calcein green at 3 weeks | Xylenol orange at 6 weeks | Oxytetracycline at 12 weeks

Figure 3.25: Representative fluorescence images for TI (86.16), only slight calcium deposition at 3 weeks, pronounced deposition at 6 and 12 weeks in the whole defect area.

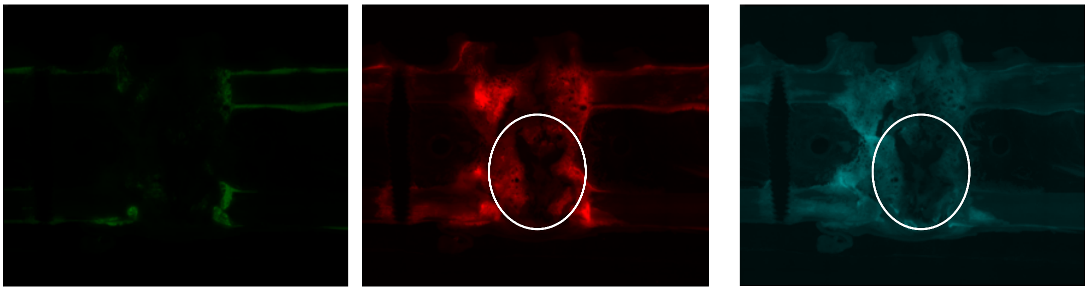

Calcein green at 3 weeks Xylenol orange at 6 weeks Oxytetracycline at 12 weeks

Figure 3.26: Representative fluorescence images for CI (86.13), only slight calcium deposition at 3 weeks, more pronounced at 6 and 12 weeks, with areas where no calcium deposition was detected at the trans cortex and in the bone marrow cavity (cartilaginous tissue detected in stained ground sections at that area).

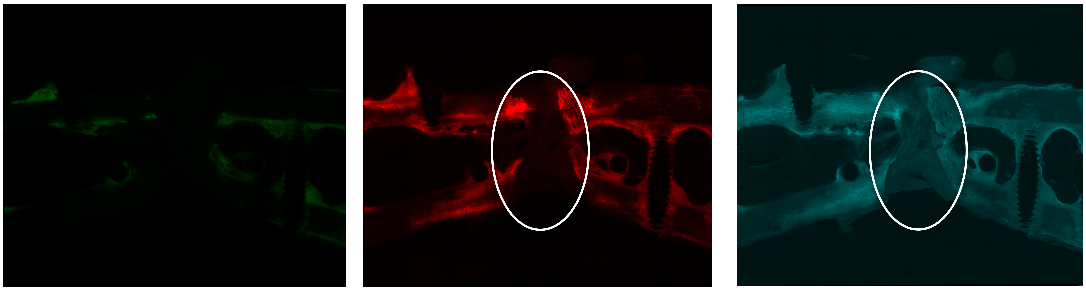

Calcein green at 3 weeks Xylenol orange at 6 weeks Oxytetracycline at 12 weeks

Figure 3.27: Representative fluorescence images for NCI (86.25), very slight calcium deposition in the endosteal area at 3 weeks, more deposition located mostly endosteally but also in the cortical area at 6 and 9 weeks.

3.2.9 Histological evaluation

Assessment of biocompatibility parameters (inflammation and tissue response) and additional observations (traumatic necrosis and foreign debris) of TI and CI were performed at the Marvel screws surrounding tissue of each tibia sample without any problems. Bone activity (resorption and formation), tissue character (cartilage formation, callus maturity) and healing response (defect unity) were scored at the facture ends of cis and trans cortices as well as in the whole gap area.

Due to the size of the gap, each section had to be spread over two slides doubling the total number of thin sections. Therefore, a total of 72 Hematoxylin-Eosin (N=24), toluidine blue (N=24) and von Kossa stained (N=24) histological sections of two groups (TI:6 and CI:6) were evaluated according to ISO-Norm 10993-6:2016(E). The evaluation was performed by two independent observers.

3.2.9.1 Semiquantitative analysis of local tissue effects

Under the conditions of this study, neither TI nor CI demonstrated any abnormal tissue reactions. A physiological number of immune cells within the bone marrow cavity was detected in the surrounding of the Marvel screws in both groups. Individual results are illustrated in Table 3.8.

Overall, no polymorphonuclear cells, eosinophils, lymphocytes, plasma cells, necrosis, osteolysis, fatty infiltrates or foreign debris were noted in the area of the Marvel screws in any of the TI or CI samples.

A low number of macrophages was observed in 1/6 samples of TI (86.16) and 3/6 samples of CI (86.14, 86.23, 86.24). Fibrous tissue in combination with neovascularization was found in 1/6 samples of TI (86.16) and in 3/6 samples of CI (86.13, 86.23, 86.24) in a low amount.

Evaluation zone: Marvel screws and surrounding

Test group: PEMF-treated
Control group: non-treated

	Animal ID	**Test group**						**Control group**					
		86.16	86.17	86.18	86.19	86.20	86.21	86.13	86.14	86.15	86.22	86.23	86.24
Biocompatibility	**1. Inflammation**												
	Polymorphonuclear	0	0	0	0	0	0	0	0	0	0	0	0
	Eosinophils	0	0	0	0	0	0	0	0	0	0	0	0
	Lymphocytes	0	0	0	0	0	0	0	0	0	0	0	0
	Plasma cells	0	0	0	0	0	0	0	0	0	0	0	0
	Macrophages	1	0	0	1	0	0	0	1	0	0	1	1
	Giant cells	0	0	0	0	0	0	0	0	0	0	0	0
	Necrosis/ osteolysis	0	0	0	0	0	0	0	0	0	0	0	0
	SUB-TOTAL	1	0	0	1	0	0	0	1	0	0	1	1
	SUB-TOTAL (x2)	2	0	0	2	0	0	0	2	0	0	2	2
	2. Tissue response												
	Neovascularisation	1	0	0	0	0	0	1	0	0	0	1	1
	Fibrosis/fibrous membrane	1	0	0	1	0	0	1	0	0	0	1	1
	Fatty infiltrate	0	0	0	0	0	0	0	0	0	0	0	0
	F.2 SUB-TOTAL	2	0	0	1	0	0	2	0	0	0	2	2
	TOTAL (1.+2.)	4	0	0	3	0	0	2	2	0	0	4	4
	GROUP TOTAL	7						12					
	Average (Ø)	1.17						2.00					
	Ø TI - Ø CI *	-0.83 = 0											
additional observations	Traumatic necrosis	0	0	0	0	0	0	0	0	0	0	0	0
	Foreign debris	0	0	0	0	0	0	0	0	0	0	0	0

* Used to determine irritant ranking shown below as the conclusion. A negative difference is recorded as zero.

Conclusion: Under the conditions of this study, the Test group was considered to demonstrate the following:
_X_ minimal or no reaction (0.0 up to 2.9);
___ slight reaction (3.0 upt to 8.9);
___ moderate reaction (9.0 upt to 15.0);
___ severe reaction (>15.1)
to the tissue as compared to the non-treaed Control group.

Table 3.8: Results of biocompatibility evaluation at the Marvel screws and surrounding tissue of each tibia sample (light grey labelled animals TI group) of the 17mm graft model.

3.2.9.2 Semiquantitative analysis of bone activity, tissue character and healing response in the gap area

Individual scoring results for semiquantitative analysis of bone activity, tissue character and healing response in the gap area of TI and CI are illustrated in Table 3.9. Representative images of the histological samples can be found in Figure 3.28 A-H.

Overall, for both groups TI and CI, bone activity parameters showed high scores for bone formation (Score 3-4: between 51-100% new bone formation) at the fracture ends and in the gap area with slightly higher bone activity for TI. No bone resorption was observed at the fracture ends and within the bone marrow cavity in both TI and CI. Some scattered osteoclasts could be seen indicating the normal bone remodeling and healing process of a bone defect.

Tissue character was described based on the maturity of the callus and presence of endochondral ossification within the fracture gap and at the fracture ends. The mean total score for callus maturity was slightly higher in TI (3.67) comparing to CI (2.83), representing more mature bone formed within the gap area at this time point.

At the fracture ends (cis and trans), new bone was moderately organized, characterized by dense but still irregularly oriented structure for TI. Moderately organized but less dense new bone was found in CI, with notable cartilaginous tissue isles within the defect area and the fracture ends.

A higher mean total score for endochondral ossification was found in CI (1.50) compared to TI (0.89). In 4/6 samples of CI (86.13, 86.15, 86.22, 86.24), isles of cartilage-like tissue with disorganized fibrous matrix (mixture of collagen fibers and proteoglycans) were visible within the gap (bone marrow and trans cortex area) and in 1/6 samples (86.15) also at one fracture end of the trans cortex (Figure 3.28 f+h). Similar cartilage-like isles were only found in 2/6 samples of TI in the bone marrow cavity of the defect (86.19, 86.21) and in one of these (86.21) also at one fracture end of the trans cortex. The overall healing response was characterized by a defect unity score, which showed slightly higher scores for gap closure in the TI with a mean total score of 3.56 compared to CI with 2.28.

Group	Animal ID	Bone activity						Tissue character						Healing response (thick section)		
		Bone resorption			Bone formation			Endochondral ossification			Maturity of callus/new bone			Defect unity		
		Cis	defect	trans	cis	defect	trans	cis	defect	trans	cis	defect	trans	cis	defect	trans
Test group	86.16	0	0	0	4	4	3	0	2	1	4	4	3	3	3	3
	86.17	0	0	0	4	4	4	1	1	1	4	3	4	2	3	4
	86.18	0	0	0	4	4	4	0	1	0	4	4	4	3	4	4
	86.19	0	0	0	4	4	4	0	2	1	4	4	4	4	4	4
	86.20	0	0	0	3	4	4	0	1	1	3	4	4	3	4	4
	86.21	0	0	0	4	4	4	1	2	1	3	3	3	4	4	4
	Mean	**0.00**	**0.00**	**0.00**	**3.83**	**4.00**	**3.83**	**0.33**	**1.50**	**0.83**	**3.67**	**3.67**	**3.67**	**3.17**	**3.67**	**3.83**
	Mean total gap	**0.00**			**3.89**			**0.89**			**3.67**			**3.56**		
Control group	86.13	0	0	0	4	4	4	1	1	1	3	3	2	4	3	2
	86.14	0	0	0	4	4	4	1	0	1	4	4	4	3	3	4
	86.15	0	0	0	4	3	1	0	2	1	4	3	2	2	2	2
	86.22	0	0	1	3	3	3	2	2	2	3	3	3	2	3	2
	86.23	0	2	3	3	2	2	1	2	3	3	2	1	2	1	0
	86.24	0	0	1	3	3	2	2	3	2	3	2	2	3	2	1
	Mean	**0.00**	**0.33**	**0.83**	**3.50**	**3.17**	**2.67**	**1.17**	**1.67**	**1.67**	**3.33**	**2.83**	**2.33**	**2.67**	**2.33**	**1.83**
	Mean total gap	**0.39**			**3.11**			**1.50**			**2.83**			**2.28**		

Table 3.9: Results for semiquantitative analysis of bone activity, tissue character and healing response in the gap area for TI and CI (range: 0-4) for the 17mm gap model.

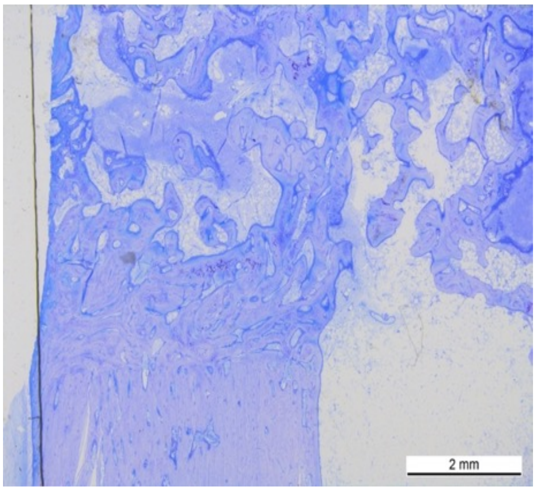

A: Animal 86.17, TI, gap area at cis cortex, overview, toluidine blue, mag. 1x15.5

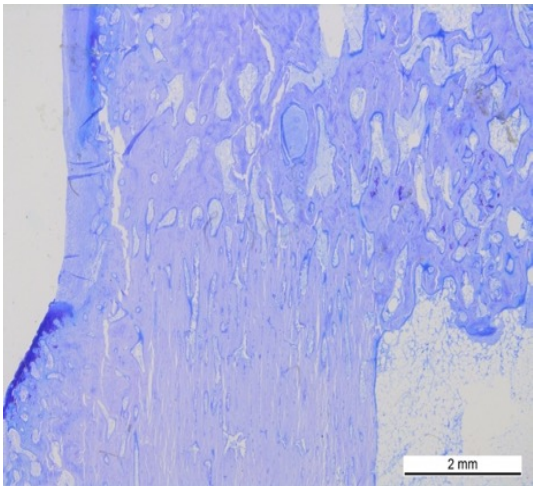

B: Animal 86.15, CI, gap area at cis cortex, overview, toluidine blue, mag. 1x15.5

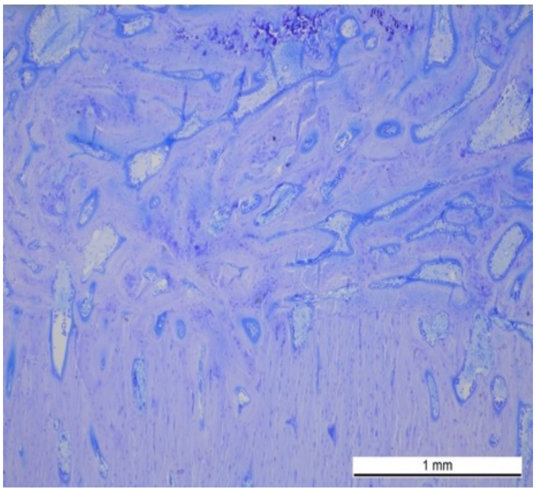

C: Animal 86.17, TI, higher magnification, smooth transition zone fracture end to gap area at cis cortex, new bone moderately organized, characterized by dense but irregularly oriented structure, toluidine blue, mag. 1x45

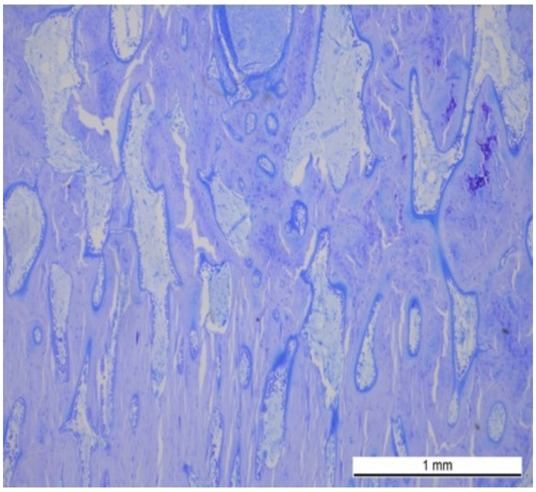

D: Animal 86.15, CI, higher magnification, smooth transition zone fracture end to gap area at cis cortex, new bone moderately organized, characterized by dense but irregularly oriented structure, toluidine blue, mag. 1x45

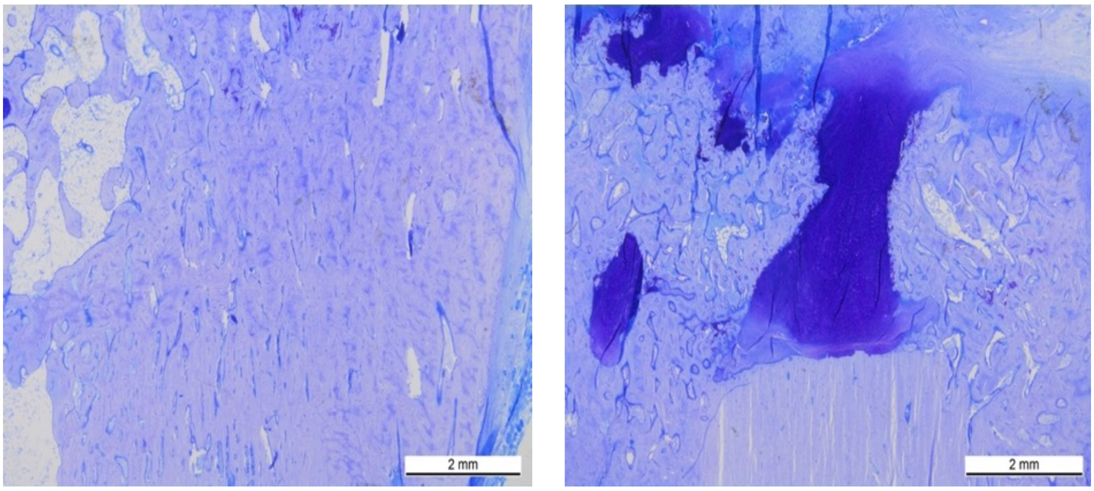

E: Animal 86.17, TI, gap area at trans cortex, fracture end completely remodeled, smooth transition zone, new bone characterized by dense and regularly oriented structure at the fracture ends, toluidine blue, mag. 1x15.5

F: Animal 86.15, CI, gap area at trans cortex, gap not completely united, isles of cartilage-like tissue with disorganized fibrous matrix (mixture of collagen fibers and proteoglycans) reaching to the fracture end, which is still pronounced, callus within gap disorganized, toluidine blue, mag. 1x15.5

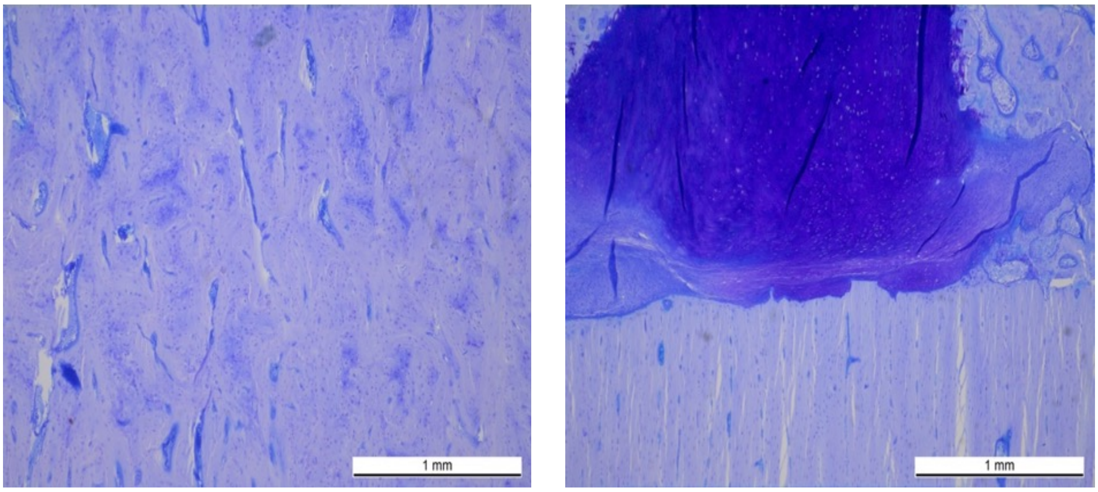

G: Animal 86.11, TI, higher magnification smooth transition zone between fracture end to gap area at trans cortex, new bone highly organized, characterized by dense and regularly oriented structure, toluidine blue, mag. 1x45

H: Animal 86.15, CI, higher magnification, sharp transition zone between fracture end to gap area at trans cortex, isles of cartilage-like tissue with disorganized matrix reaching to the fracture end, toluidine blue, mag. 1x45

Figure 3.28 A-H: Representative images of histological thin sections for TI and CI

4 Discussion

In this study it was shown that internalized Pulsed Electromagnetic Field Stimulation enhances bone formation and callus maturation in both non-critical and critical size defects. In the 3 mm gap model a successful non-critical size defect was achieved with great standardization. Custom designed cutting guides, drill guides and aiming devices made for a very reproducible surgical procedure. This, along with standardized post-operative procedures (cast changes, radiographs, daily observations), contributed to the absence of major complications. A reliable comparison between test item (TI) and control item (CI) was therefore possible. No adverse reactions related to the test item were noticed.

Both groups showed good healing progress and biocompatibility. Radiographic evaluation presented a more advanced callus formation in the test item, which was corroborated with the macroscopic findings during the sacrifice. Fluorescent dye integration indicated more calcium deposition cortically in the TI and endosteally in the CI. Both Micro-CT analysis and histomorphometry proved that new bone of the test item had higher mineral density. Biomechanical testing, although not reaching statistical significance, presented a strong trend towards more advanced healing of the test item, as it reached twice the stiffness of the control item. Higher callus maturity of the TI was also confirmed during the histological evaluation, where it revealed to be qualitatively superior to the control item.

In the 17 mm graft model great standardization was achieved as well, which prevented occurrence of any major complications. Good biocompatibility and no adverse reactions related to the test item were noticed. Radiographically, TI showed both more advanced healing during all timepoints and new bone formation that was focused more in the gap area. The radiographic findings were corroborated macroscopically, with all 6 TI tibiae exhibiting fragment stability compared to only 2/6 CI tibiae. Calcium deposition was focused more at the fracture ends in the TI and more endosteally in the CI. Statistically significant differences were observed regarding total callus volume and mature callus volume, as these values were significantly higher in TI compared to CI. A trend for higher callus density was also noted in the TI. These finding were corroborated with the histomorphometry analysis where higher callus percentage was calculated in the TI. Also, biomechanical testing confirmed the superiority of the test item, reaching statistical significance in torsional stiffness. Test item outperformed control item by a factor of 2.6 times in torsional stiffness. TI also reached 67% of sound limb stiffness compared to only 30% in CI. The same trend was seen during the histological evaluation, where denser new bone structure of TI compared to CI was observed. Overall, TI manifested a more advanced healing of the critical size defect and superior callus quality, showing better callus smoothness, size and opacity, compared to the CI.

As expected in the 17 mm model, all 3 negative control samples that had not received bone graft inside the osteotomy, presented highly unstable and collapsed gaps both macroscopically and radiographically. None of the defects were filled with callus and all three plates were bent with a collapse of the trans cortex. In fact, bone resorption and rounding of the cortical bone fragments started at 9 weeks and was further pronounced at sacrifice, indicating a progression towards a non-union. This result was expected as the NCI group was designed as a negative control, in order to validate the 17mm model as a critical size defect model.

Six sheep per group were used in this study of similar age and weight range. While designing a study, sufficient number of animals is often a crucial point of discussion. On one hand, a higher sample size could decrease variability of results and make it easier to detect smaller differences between groups. In a sample size that equals six, results of each sheep are extremely valuable, leaving no place for outliers. A higher sample size could therefore potentially contribute to more precise results of the researched technology.

On the other hand, there are valid points speaking against increase of sample sizes. Most of all, the question asked in the hypothesis has been answered with only six sheep per group: namely, whether the Marvel technology enhances fracture healing and is safe to use. From the point of view of animal protection, it is very important to aim for the lowest number of animals that is sufficient for answering the main research question. This complies with the principles of the 3Rs (Replace, Reduce and Refine), which support and emphasize ethical use of experimental animals. Reduction in this case was achieved by using the minimal number of sheep, needed to obtain enough data. Concluding, it was proven that amount of sheep used in this research was adequate for detecting differences and proving the efficiency of Marvel technology.

There were several reasons why only female sheep were used. Male animals are difficult to handle and generally less patient and cooperative. A situation when both sexes are kept in the same stables simultaneously would be hard to manage and could cause plenty of complications. Especially in a study like this one, preventing animals from getting nervous or overexcited is of the utmost importance, as any sudden jump or movement could influence healing of the fracture or cause implant breakage. This would be extremely difficult if not impossible while keeping male and female sheep together. Male sheep should also not be put in the suspension systems as belts may put pressure on the urinary tract and cause related to it complications.

Furthermore, females and males have different hormonal levels, which impact such parameters like weight, size, length of the limbs or bone metabolism. Previously conducted studies (Bottlang et al., 2016; Plecko et al., 2013; Plecko et al., 2012; Richter et al., 2015) confirm that female sheep population is representative in regards to whole sheep population and is also sufficiently reflecting the responses seen in human medicine across genders.

It was important to pick sheep with calm characters. As this study required very frequent interactions between people and animals (putting the coils on and off twice a day, changing the casts, taking radiographs), having cooperative sheep was advantageous when it comes to efficient work and injury prevention. Sheep arrived at least two weeks before planned surgeries. This acclimatization time allowed

for exclusion and substitution of anxious ones. Unfortunately, there was one sheep (86.01), which nervous character and constant jumps and moves over the course of the entire in- life duration, partly resulted in broken distal screws, bent plate and completely collapsed gap at the trans cortex, which was an obvious exclusion criterium.

Overall, a good standardization was achieved with surgeries performed in a precise and reproducible manner. This was possible because of custom-designed cutting and drill guides. The whole surgical procedure was also priorly tested during multiple cadaver surgeries. No complications occurred in creating the transverse tibia osteotomy and its internal fixation. Regarding the implantation of the Marvel technology, the Marvel screw positioning and alignment was standardized in all cases by using a customized aiming device. The screws were systematically parallel to each other, which was important to ensure the creation of the local electric field, and positioned at standardized distances from the place and the defect edge. The placement of the transducer was also successful in all animals with no observed displacement or any irritation of the surrounding tissue. While a 12-hole LCP plate was used for the 3 mm gap model without any issues, fixation of 17 mm defects required longer, 13-hole LCP plates, which left less space for manipulations. In these cases, sufficient length of the tibia was critical. To avoid problems, a pre-operative radiologic examination and measuring tibia length could be an option. Nevertheless, from our experience, choosing sheep with longer legs was an optimal strategy, without the need for radiographic check.

The most problematic part of the implanted devices was cap detachment from the Marvel screws, which is a decisive component for this technology to work: all parts have to be tightly connected to each other to ensure PEMF stimulation. Unfortunately, there were several cases of caps detachments, mostly in CI animals but also in two TI animals (86.02 and 86.12). In animal 86.02, cap detachment was detected at the sacrifice, with fibrous tissue growing between the proximal cap and the Marvel screw head, which likely prevented the technology from working properly. This resulted in the exclusion of the animal from the study. One other animal (86.12) had to undergo a re-surgery right after radiographic evidence of cap detachment was found five and a half weeks post osteotomy. Due to these multiple complications, the cap system had to be re-worked. A tighter fit of the transducer caps was provided so that reliable fastening of the cap at the hexagonal screw head was finally achieved. Thanks to this, no case of cap detachment occurred with reworked caps. Nonetheless, a press fit system may not be optimal for assuring perfect placement and contact with the Marvel screws over the course of several months and could be a subject of more design improvements in the future. Another suggestion is the development of a real time verification system or sensor to show that the treatment is being delivered. This could be a great strategic tool in early recognition of any problems related to Marvel technology function.

PEMF treatment was successfully administered throughout the whole study. Coils and belts were tolerated well by animals. The use of positive reinforcement by providing hay during the treatment time, helped sheep acclimatize to the treatment. The belt system could be improved by attaching better closing mechanisms. Indeed, straps had a tendency to loosen with movements and required corrections to ensure optimal coil placement around the fracture area. The straps should also be strengthened to provide more solid support of the coil. Decreasing the weight of the coil could also be a subject of improvement in the future.

Initiating treatment after the inflammatory phase of fracture healing is complete could be another interesting aspect to investigate. This is in contrast to what was performed in this study, by initiating the treatment 3 days post-surgery. Indeed, PEMF has been described to enhance angiogenesis, therefore, a 3-week post trauma treatment initiation time point could provide potential benefits in terms of fracture healing because it would align with the start of angiogenesis. In addition, instead of applying two treatments per day, combining morning and evening treatments into one longer session could be attempted. This would certainly be more convenient for the patients and caregivers. Nevertheless, the treatment regimen applied in our studies was successful and, therefore, it makes it questionable to repeat animal studies to clarify these questions. Possibly, this could be verified in future clinical trials in humans.

Regarding the choice of the 9-week end point in the 3 mm group, the in- life length was decided based on radiographic healing kinetics. A 9-week time point may not have been optimal for detection of huge differences, as the callus was already starting to consolidate. As known, non-critical size defects heal with time and distinguishing bigger differences in results could be better possible earlier, for example on the 7th or 8th week. This was clearly seen on the radiographs at week 6 and 7, where TI showed more callus focus inside the gap compared to the CI. This was also corroborated by the pattern of fluorescent calcium deposition at week 6, appearing more cortical in TI and more endosteal in CI. These findings support the potential idea of earlier sacrifice time point in order to detect bigger differences of healing.

In the 17mm graft model, none of the defects were radiographically completely healed after 12 weeks. The sacrifice time point was chosen based on radiographic evidence of new bone formation and was aimed at detecting the largest difference in remodelling kinetics. In this case, the 12 week in-life duration was optimal for distinguishing these differences between the TI and CI.

The other aspect is optimizing radiographic examination intervals to reduce the need of sheep handling and cast changes. The 4th and 5th week timepoints did not provide any additional value in assessing healing kinetics. That being said, the weekly radiographic follow-up was necessary in this case, because a new technology was being tested. Intermediate radiological timepoints could be skipped if a similar technology is tested in the future. Therefore, if future studies are planned, performing radiographs would be suggested in non-critical size defect animals at the following intervals: post OP, 3rd week, 6th week and weekly thereafter until sacrifice.

During the application of fluorescent dyes, pre- surgical weight was always used, therefore potentially under- or overestimating the weight of the animal at the injections time. All animals were weighed only once throughout the course of the entire study as there was no clinical reason to weigh them post-operatively. In addition, transporting them to another building in order to weight them would cause too much stress, uncontrolled movement and increased the danger of re-fracture. This added risk would not compensate the benefits of administering a more accurate dose of fluorescent dyes as the variation in weight was deemed small. Therefore, dosages of injected fluorescent dyes could be slightly higher for the sheep that lost weight and slightly lower for the ones that put weight on. Nevertheless, minor discrepancies in dosage was acceptable for the qualitative assessment of the fluorescent sections.

Evaluating these sections mostly relies on their thickness as more dye is accumulated in the thicker sections. Thickness of the slides depended on the manual adjustment of the saw during the process of cutting and was therefore not always the same. Measuring slide thickness was done in order to choose the ones with the most similar values, however, differences were often encountered. For future evaluations, a calibration method for normalizing signal intensity would be useful. Alternatively, one could still reliably assess the localization of calcium integration, rather than the signal intensity. In this case, slide thickness variation would not be a problem.

Various methods of callus size measurement were performed. A quantitative radiographic analysis was attempted for all timepoints and all animals but it did not provide accurate data. In the cranial (275°) projection, the measurements were not possible, as often wires, caps and Marvel screws covered the areas of interest. Also, because the endosteal callus could not be measured by those means, only callus at the trans cortex in the anteroposterior (0°) projection and callus at the caudal cortex in the caudal (265°) projection were measured, delivering a very limited set of data. Also, measurements of callus size were done during macroscopic evaluation. This method proved to be very inaccurate and difficult to standardize because the macroscopic detection of callus boundaries was not always clear, especially in very smooth calluses.

Morphometric measurements were performed using Micro-CT scans. This examination was definitely a very reliable and helpful method in assessing healing progress objectively. Using calibration protocols, callus density could be converted from Hounsfield Units to mineralization (in mg hydroxyapatite per cm^3). The most challenging part of the 3D segmentation was that new bone often happened to be as dense as the old bone, which made it difficult to distinguish using automated density thresholding (see Figure 4.1). In some cases, the amount of this unidentified, mature, rigid callus would make the majority of the whole new bone formation. For that reason, in order to accurately segment new bone from old bone, manual slice by slice tissue selection had to be accomplished at the University of Lehigh.

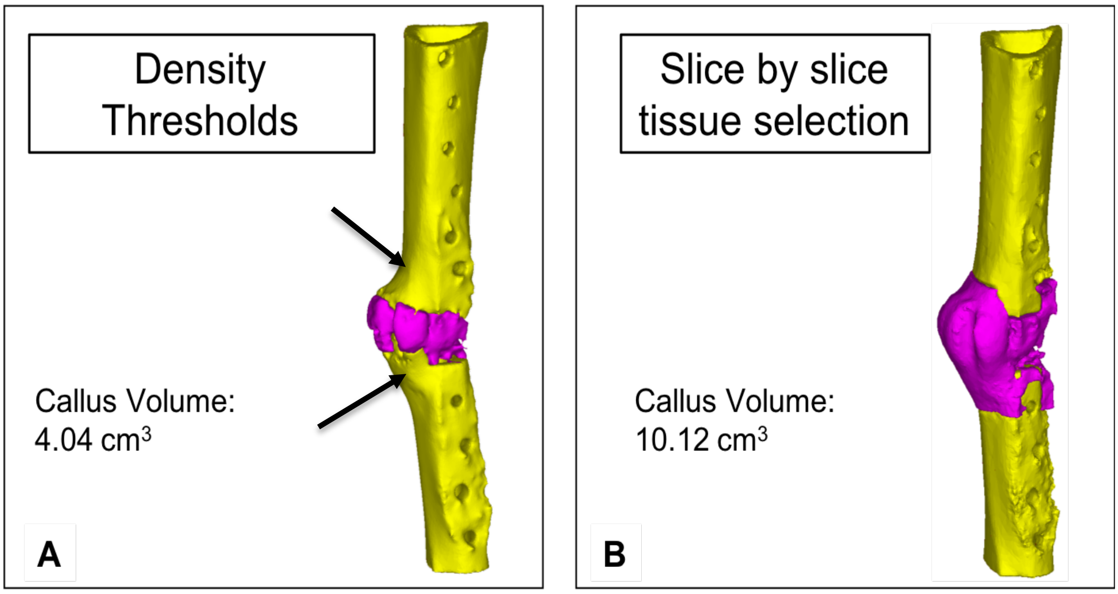

Figure 4.1: Callus volume calculation of the same sample using automated density thresholding (A) versus slice by slice tissue segmentation (B). Density thresholding resulted in falsely recognizing mature callus (see arrows in Figure A) as cortical bone due to its high mineral density. Slice by slice selection, however, successfully distinguished old bone from the new bone formation, thereby providing a more accurate callus volume.

Non- destructive mechanical test was the chosen evaluation method, as it was essential to keep the osteotomy area intact for the histology processing. If there were any abnormalities related to the testing procedure, a test could be repeated, as the tissue would not be damaged. This was not often a case, however, would be impossible after performing destructive testing. Destructive tests would certainly be very interesting and could provide more complete information regarding bone properties. Nevertheless, the principle of the 3Rs speaks against it as in the case of destructive mechanical testing, different samples would have to be used for histological examination, thereby requiring twice the number of samples and therefore twice the number of animals. A non-destructive mechanical test was therefore a good compromise.

The slope of the linear part of the loading curves was generated automatically to calculate torsional stiffness. The loading curves had to be checked to ensure the slope was correctly evaluated. In several cases the curve profiles looked abnormal or did not reach the targeted 10 Nm. It was essential that the higher part of the curve that was linear was selected as it was more representative of bone stiffness. Analysing every single loading curve was also important to ensure the mechanical testing was performed successfully. Even though most of these calculations were automated, it was nevertheless necessary to verify them.

Overall, looking at intact tibiae, biomechanical testing exhibited an inherent 21% relative standard deviation, likely coming from both interanimal differences and potting technique. Whether increase in the number of sheep could influence this high variability stays an open question. Non-operated tibiae were very similar in torsional stiffness. There are no major differences in bone stiffness variability between TI and CI. The 3mm gap model sheep showed a 26% relative standard deviation compared to only 14% in the 17mm model. This difference was a contributing factor in the ability to detect statistical significance in the 17 mm model study but not in the 3 mm. A more detailed group distribution is presented in the Table 4.1. This proves that interanimal differences, in this case related to torsional bone stiffness, inevitably influence the results of a study despite animal randomization.

Experiment	Group	Sample size (n)	Intact Tibiae Torsional Stiffness (Nm/deg)	Relative Standard Deviation (%)
3 mm gap model	Test Item (TI)	6	7.51 ± 1.81	24.1
	Control Item (CI)	6	6.04 ± 1.51	25.0
	TI + CI	12	6.77 ± 1.76	26.0
17 mm graft model	Test Item (TI)	6	8.47 ± 0.93	11.0
	Control item (CI)	6	7.46 ± 1.15	15.4
	TI + CI	12	7.96 ± 1.13	14.2
Both	All	24	7.37 ± 1.57	21.3

Table 4.1: Torsional stiffness of intact tibia across groups reported as mean ± SD. The relative standard deviation is also reported to indicate interanimal variability within groups.

Another potentially interesting analysis would be testing the biomechanics of the callus area specifically, and not the tibia as a whole, which was the case in this study. This would require placing some markers on the callus and tracking the displacement of the callus in real time during a mechanical test.

Histological evaluations relied in part on analysing ground sections. It needs to be emphasized, however, that one slide does not represent bone as a whole and this must be taken into account during the evaluation. Indeed, in some samples (for instance, sheep 86.20 and 21), although full defect closure was not detected on one ground section (Figure 4.2 A), evident progress in new bone formation and even callus bridging was nevertheless seen in the consecutive ground section (Figure 4.2 B). Thin sections could be used to corroborate ground section observations.

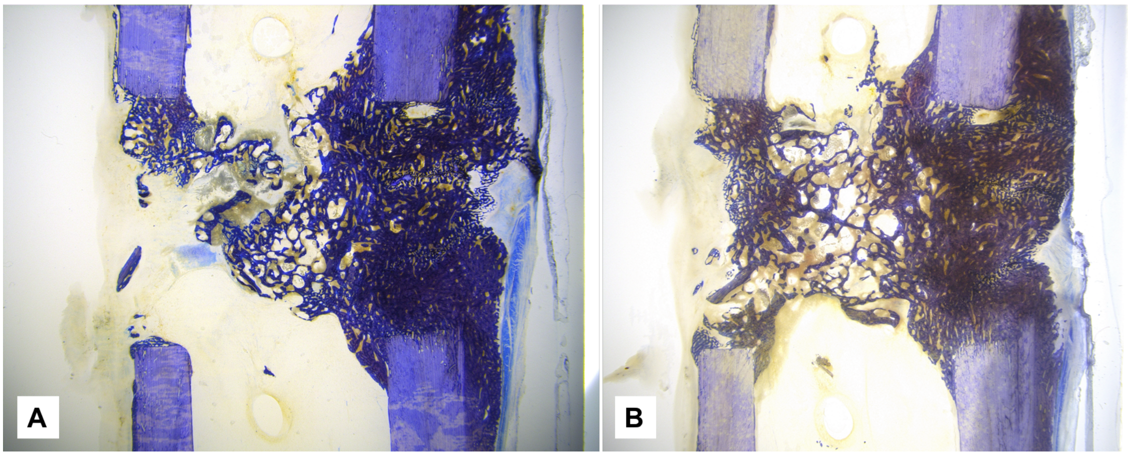

Figure 4.2 (A, B): Comparison of two consecutive ground section slides of animal 86.20, showing no bridging callus at the cis cortex area on the first section (A) and bridging callus on the consecutive section(B).

Tissue loss due to sample processing, like cutting or polishing is another problem. Most of the evaluated histology slides corresponded well to radiographic, Micro-CT or biomechanical findings. Bone formation seen under the microscope usually reflected well if bridging callus was apparent and if fragment stability was achieved. Nevertheless, in some cases, histology showed inferior bone healing compared to other methods. Because of these reasons, multiple histological slides should be examined and histology should always be evaluated together with other methods and never alone.

This study definitely shed some new light on electromagnetic influence on bone healing. Electromagnetism is not a new concept, however, the majority of so far conducted studies showed little standardization or compared very different forms of PEMF. It is not uncommon to find different treatment lengths (from 10 minutes to 12 or even 24 hours a day) (Fredericks et al., 2000; Sharrard, 1990), durations (days, weeks, months)(Dallari et al., 2009; Ding et al., 2011; Midura et al., 2005; Sharrard, 1990), various start points (delayed unions of 16 weeks to 6 months within the same study) (Shi et al., 2013), usage of other types of stimulating devices (Midura et al., 2005) and different parameters (different PEMF signal configuration, repetition frequency, pulse duration and shape amongst others) (Dhawan et al., 2004; Mammi et al., 1993).

Moreover, most of human studies show large variations regarding age, affected bones, environmental influence, presence of predisposing factors (smoking, diabetes).

These heterogeneous treatment regime and sample groups exerted a tremendous influence on the outcome of each study and were reflected in dramatically varied results:

PEMF success rate ranging from 15.4 to 93.9 % (Shi et al., 2013). Moreover, there were no optimal device parameters established by now and none of the studies used direct electric stimulation and provided detailed systematic analysis, which was a case in this research thanks to the implementation of the transducer and the Marvel screws, acting as electrodes, on both sides of the defect. The majority of already conducted studies also reported beginning of the treatment only after non-union establishment, delivering little information about early stage application. In these few reports on both fresh human fractures and animal osteotomies, bones responded better to PEMF when treatment began soon after trauma.

From our experience, earlier treatment implementation is essential not only in non- union prevention but also in healing time shortening.
It would be suggested that standard PEMF treatment is implemented in all patients at risk: diabetic, elderly, smokers or with fractures that could potentially evolve in delayed or non- unions: displaced, infected and with big gaps. This would decrease healing time and lower complications risks.

Conclusion

The chosen animal models were appropriate to evaluate the effect of the Marvel technology on bone healing in both, a non-critical and a critical size bone defect augmented with autograft. There were no abnormalities or healing complications related to the Marvel technology which proved to be both safe and effective. Furthermore, the Marvel therapy accelerated and enhanced the healing process in both models, resulting in better new bone structure, better callus morphology and superior biomechanical properties.

5 Bibliography

Bibiography:

Aaron, R.K., Boyan, B.D., Ciombor, D.M., Schwartz, Z., Simon, B.J., 2004. Stimulation of growth factor synthesis by electric and electromagnetic fields. Clin Orthop Relat Res, 30-37.

Aaron, R.K., Ciombor, D.M., 1993. Therapeutic effects of electromagnetic fields in the stimulation of connective tissue repair. J Cell Biochem 52, 42-46.

Alkhiary, Y.M., Gerstenfeld, L.C., Krall, E., Westmore, M., Sato, M., Mitlak, B.H., Einhorn, T.A., 2005. Enhancement of experimental fracture-healing by systemic administration of recombinant human parathyroid hormone (PTH 1-34). J Bone Joint Surg Am 87, 731-741.

Balmer, T.W., Vesztergom, S., Broekmann, P., Stahel, A., Buchler, P., 2018. Characterization of the electrical conductivity of bone and its correlation to osseous structure. Sci Rep 8, 8601.

Bassett, C.A., 1993. Beneficial effects of electromagnetic fields. J Cell Biochem 51, 387-393.

Bassett, C.A., Pawluk, R.J., Becker, R.O., 1964. Effects of Electric Currents on Bone in Vivo. Nature 204, 652-654.

Bassett, C.A., Pawluk, R.J., Pilla, A.A., 1974. Augmentation of bone repair by inductively coupled electromagnetic fields. Science 184, 575-577.

Benazzo, F., Cadossi, M., Cavani, F., Fini, M., Giavaresi, G., Setti, S., Cadossi, R., Giardino, R., 2008. Cartilage repair with osteochondral autografts in sheep: effect of biophysical stimulation with pulsed electromagnetic fields. J Orthop Res 26, 631-642.

Betti, E.M., S.; Cadossi, R.; Faldini, C.; Faldini, A., 1999. Effect of Stimulation by Low-Frequency Pulsed Electromagnetic Fields in Subjects with Fracture of the Femoral Neck, In: Electricity and Magnetism in Biology and Medicine. Springer, Boston, MA, pp. pp 853-855.

Biggane, P., Jackson, X., Nazarian, A., 2016. Bone composition and healing: open electromagnetic and biomechanical problems. Conf Proc IEEE Eng Med Biol Soc 2016, 6026-6029.

Borsalino, G., Bagnacani, M., Bettati, E., Fornaciari, F., Rocchi, R., Uluhogian, S., Ceccherelli, G., Cadossi, R., Traina, G.C., 1988. Electrical stimulation of human femoral intertrochanteric osteotomies. Double-blind study. Clin Orthop Relat Res, 256-263.

Bottlang, M., Tsai, S., Bliven, E.K., von Rechenberg, B., Klein, K., Augat, P., Henschel, J., Fitzpatrick, D.C., Madey, S.M., 2016. Dynamic Stabilization with Active Locking Plates Delivers Faster, Stronger, and More Symmetric Fracture-Healing. J Bone Joint Surg Am 98, 466-474.

Brighton, C.T., Wang, W., Seldes, R., Zhang, G., Pollack, S.R., 2001. Signal transduction in electrically stimulated bone cells. J Bone Joint Surg Am 83-A, 1514-1523.

Cane, V., Botti, P., Soana, S., 1993. Pulsed magnetic fields improve osteoblast activity during the repair of an experimental osseous defect. J Orthop Res 11, 664-670.

Capanna, R., Donati, D., Masetti, C., Manfrini, M., Panozzo, A., Cadossi, R., Campanacci, M., 1994. Effect of electromagnetic fields on patients undergoing massive bone graft following bone tumor resection. A double blind study. Clin Orthop Relat Res, 213-221.

Chalidis, B., Sachinis, N., Assiotis, A., Maccauro, G., 2011. Stimulation of bone formation and fracture healing with pulsed electromagnetic fields: biologic responses and clinical implications. Int J Immunopathol Pharmacol 24, 17-20.

Charan, J., Kantharia, N.D., 2013. How to calculate sample size in animal studies? J Pharmacol Pharmacother 4, 303-306.

Dallari, D., Fini, M., Giavaresi, G., Del Piccolo, N., Stagni, C., Amendola, L., Rani, N., Gnudi, S., Giardino, R., 2009. Effects of pulsed electromagnetic stimulation on patients undergoing hip revision prostheses: a randomized prospective double-blind study. Bioelectromagnetics 30, 423-430.

Dhawan, S.K., Conti, S.F., Towers, J., Abidi, N.A., Vogt, M., 2004. The effect of pulsed electromagnetic fields on hindfoot arthrodesis: a prospective study. J Foot Ankle Surg 43, 93-96.

Ding, S., Peng, H., Fang, H.S., Zhou, J.L., Wang, Z., 2011. Pulsed electromagnetic fields stimulation prevents steroid-induced osteonecrosis in rats. BMC Musculoskelet Disord 12, 215.

Einhorn, T.A., 1995. Enhancement of fracture-healing. J Bone Joint Surg Am 77, 940-956.

Einhorn, T.A., Gerstenfeld, L.C., 2015. Fracture healing: mechanisms and interventions. Nat Rev Rheumatol 11, 45-54.

Fredericks, D.C., Nepola, J.V., Baker, J.T., Abbott, J., Simon, B., 2000. Effects of pulsed electromagnetic fields on bone healing in a rabbit tibial osteotomy model. J Orthop Trauma 14, 93-100.

Funk, R.H., Monsees, T.K., 2006. Effects of electromagnetic fields on cells: physiological and therapeutical approaches and molecular mechanisms of interaction. A review. Cells Tissues Organs 182, 59-78.

Garrison, K.R., Shemilt, I., Donell, S., Ryder, J.J., Mugford, M., Harvey, I., Song, F., Alt, V., 2010. Bone morphogenetic protein (BMP) for fracture healing in adults. Cochrane Database Syst Rev, CD006950.

Ghiasi, M.S., Chen, J., Vaziri, A., Rodriguez, E.K., Nazarian, A., 2017. Bone fracture healing in mechanobiological modeling: A review of principles and methods. Bone Rep 6, 87-100.

Glass, G.E., Jain, A., 2013. Cochrane corner: bone morphogenetic protein (BMP) for fracture healing in adults. J Hand Surg Eur Vol 38, 447-449.

Gossling, H.R., Bernstein, R.A., Abbott, J., 1992. Treatment of ununited tibial fractures: a comparison of surgery and pulsed electromagnetic fields (PEMF). Orthopedics 15, 711-719.

Griffin, X.L., Costa, M.L., Parsons, N., Smith, N., 2011. Electromagnetic field stimulation for treating delayed union or non-union of long bone fractures in adults. Cochrane Database Syst Rev, CD008471.

Griffin, X.L., Warner, F., Costa, M., 2008. The role of electromagnetic stimulation in the management of established non-union of long bone fractures: what is the evidence? Injury 39, 419-429.

Hannemann, P., Gottgens, K.W., van Wely, B.J., Kolkman, K.A., Werre, A.J., Poeze, M., Brink, P.R., 2011. Pulsed Electromagnetic Fields in the treatment of fresh scaphoid fractures. A multicenter, prospective, double blind, placebo controlled, randomized trial. BMC Musculoskelet Disord 12, 90.

Heckman, J.D., Ryaby, J.P., McCabe, J., Frey, J.J., Kilcoyne, R.F., 1994. Acceleration of tibial fracture-healing by non-invasive, low-intensity pulsed ultrasound. J Bone Joint Surg Am 76, 26-34.

Holmes, G.B., Jr., 1994. Treatment of delayed unions and nonunions of the proximal fifth metatarsal with pulsed electromagnetic fields. Foot Ankle Int 15, 552-556.

Ikegami, A., Ueshima, K., Saito, M., Ikoma, K., Fujioka, M., Hayashi, S., Ishida, M., Fujiwara, H., Mazda, O., Kubo, T., 2015. Femoral perfusion after pulsed electromagnetic field stimulation in a steroid-induced osteonecrosis model. Bioelectromagnetics 36, 349-357.

Kraus, W., Lechner, F., 1972. [Healing of pseudoarthrosis and spontaneous fractures with structure-forming electrodynamic potentials]. Munch Med Wochenschr 114, 1814-1819.

Kubo, T., 2012. Piezoelectricity of bone and electrical callus. J Orthop Sci 17, 105-106.

Ledda, M., D'Emilia, E., Giuliani, L., Marchese, R., Foletti, A., Grimaldi, S., Lisi, A., 2015. Nonpulsed sinusoidal electromagnetic fields as a noninvasive strategy in bone repair: the effect on human mesenchymal stem cell osteogenic differentiation. Tissue Eng Part C Methods 21, 207-217.

Leisner, S., Shahar, R., Aizenberg, I., Lichovsky, D., Levin-Harrus, T., 2002. The effect of short-duration, high-intensity electromagnetic pulses on fresh ulnar fractures in rats. J Vet Med A Physiol Pathol Clin Med 49, 33-37.

Mammi, G.I., Rocchi, R., Cadossi, R., Massari, L., Traina, G.C., 1993. The electrical stimulation of tibial osteotomies. Double-blind study. Clin Orthop Relat Res, 246-253.

Marks, R.A., 2000. Spine fusion for discogenic low back pain: outcomes in patients treated with or without pulsed electromagnetic field stimulation. Adv Ther 17, 57-67.

Marsell, R., Einhorn, T.A., 2011. The biology of fracture healing. Injury 42, 551-555.

Martini, L., Fini, M., Giavaresi, G., Giardino, R., 2001. Sheep model in orthopedic research: a literature review. Comp Med 51, 292-299.

McAllister, B.S., Haghighat, K., 2007. Bone augmentation techniques. J Periodontol 78, 377-396.

Midura, R.J., Ibiwoye, M.O., Powell, K.A., Sakai, Y., Doehring, T., Grabiner, M.D., Patterson, T.E., Zborowski, M., Wolfman, A., 2005. Pulsed electromagnetic field treatments enhance the healing of fibular osteotomies. J Orthop Res 23, 1035-1046.

Mooney, V., 1990. A randomized double-blind prospective study of the efficacy of pulsed electromagnetic fields for interbody lumbar fusions. Spine (Phila Pa 1976) 15, 708-712.

Morshed, S., 2014. Current Options for Determining Fracture Union. Adv Med 2014, 708574.

Nakase, T., Yoshikawa, H., 2006. [Fracture repair and bone morphogenetic protein (BMP)]. Clin Calcium 16, 755-765.

Nolte, P.A., van der Krans, A., Patka, P., Janssen, I.M., Ryaby, J.P., Albers, G.H., 2001. Low-intensity pulsed ultrasound in the treatment of nonunions. J Trauma 51, 693-702; discussion 702-693.

Noris-Suarez, K., Lira-Olivares, J., Ferreira, A.M., Feijoo, J.L., Suarez, N., Hernandez, M.C., Barrios, E., 2007. In vitro deposition of hydroxyapatite on cortical bone collagen stimulated by deformation-induced piezoelectricity. Biomacromolecules 8, 941-948.

Otter, M.W., McLeod, K.J., Rubin, C.T., 1998. Effects of electromagnetic fields in experimental fracture repair. Clin Orthop Relat Res, S90-104.

Pearce, A.I., Richards, R.G., Milz, S., Schneider, E., Pearce, S.G., 2007. Animal models for implant biomaterial research in bone: a review. Eur Cell Mater 13, 1-10.

Pivonka, P., Dunstan, C.R., 2012. Role of mathematical modeling in bone fracture healing. Bonekey Rep 1, 221.

Pivonka, P., Komarova, S.V., 2010. Mathematical modeling in bone biology: from intracellular signaling to tissue mechanics. Bone 47, 181-189.

Plecko, M., Lagerpusch, N., Andermatt, D., Frigg, R., Koch, R., Sidler, M., Kronen, P., Klein, K., Nuss, K., Burki, A., Ferguson, S.J., Stoeckle, U., Auer, J.A., von Rechenberg, B., 2013. The dynamisation of locking plate osteosynthesis by means of dynamic locking screws (DLS)-an experimental study in sheep. Injury 44, 1346-1357.

Plecko, M., Lagerpusch, N., Pegel, B., Andermatt, D., Frigg, R., Koch, R., Sidler, M., Kronen, P., Klein, K., Nuss, K., Gedet, P., Burki, A., Ferguson, S.J., Stoeckle, U., Auer, J.A., von Rechenberg, B., 2012. The influence of different osteosynthesis configurations with locking compression plates (LCP) on stability and fracture healing after an oblique 45 degrees angle osteotomy. Injury 43, 1041-1051.

Randau, T.M., Kabir, K., Gravius, S., Wimmer, M.D., Friedrich, M.J., Burger, C., Goost, H., 2014. [Low-intensity pulsed ultrasound for treatment of fractures and nonunions - current evidence and insights from basic research and clinical application]. Z Orthop Unfall 152, 328-333.

Richter, H., Plecko, M., Andermatt, D., Frigg, R., Kronen, P.W., Klein, K., Nuss, K., Ferguson, S.J., Stockle, U., von Rechenberg, B., 2015. Dynamization at the near cortex in locking plate osteosynthesis by means of dynamic locking screws: an experimental study of transverse tibial osteotomies in sheep. J Bone Joint Surg Am 97, 208-215.

Ryaby, J.T., 1998. Clinical effects of electromagnetic and electric fields on fracture healing. Clin Orthop Relat Res, S205-215.

Ryang We, S., Koog, Y.H., Jeong, K.I., Wi, H., 2013. Effects of pulsed electromagnetic field on knee osteoarthritis: a systematic review. Rheumatology (Oxford) 52, 815-824.

Saliev, T., Baiskhanova, D.M., Akhmetova, A., Begimbetova, D.A., Akishev, M., Kulsharova, G., Molkenov, A., Nurgozhin, T., Alekseyeva, T., Mikhalovsky, S., 2019. Impact of electromagnetic fields on in vitro toxicity of silver and graphene nanoparticles. Electromagn Biol Med 38, 21-31.

Sharrard, W.J., 1990. A double-blind trial of pulsed electromagnetic fields for delayed union of tibial fractures. J Bone Joint Surg Br 72, 347-355.

Shi, H.F., Xiong, J., Chen, Y.X., Wang, J.F., Qiu, X.S., Wang, Y.H., Qiu, Y., 2013. Early application of pulsed electromagnetic field in the treatment of postoperative delayed union of long-bone fractures: a prospective randomized controlled study. BMC Musculoskelet Disord 14, 35.

Simonis, R.B., Parnell, E.J., Ray, P.S., Peacock, J.L., 2003. Electrical treatment of tibial non-union: a prospective, randomised, double-blind trial. Injury 34, 357-362.

Streit, A., Watson, B.C., Granata, J.D., Philbin, T.M., Lin, H.N., O'Connor, J.P., Lin, S., 2016. Effect on Clinical Outcome and Growth Factor Synthesis With Adjunctive Use of Pulsed Electromagnetic Fields for Fifth Metatarsal Nonunion Fracture: A Double-Blind Randomized Study. Foot Ankle Int 37, 919-923.

Stroe, M.C., Crolet, J.M., Racila, M., 2013. Mechanotransduction in cortical bone and the role of piezoelectricity: a numerical approach. Comput Methods Biomech Biomed Engin 16, 119-129.

Trock, D.H., 2000. Electromagnetic fields and magnets. Investigational treatment for musculoskeletal disorders. Rheum Dis Clin North Am 26, 51-62, viii.

Trock, D.H., Bollet, A.J., Dyer, R.H., Jr., Fielding, L.P., Miner, W.K., Markoll, R., 1993. A double-blind trial of the clinical effects of pulsed electromagnetic fields in osteoarthritis. J Rheumatol 20, 456-460.

Turner, M.D., Nedjai, B., Hurst, T., Pennington, D.J., 2014. Cytokines and chemokines: At the crossroads of cell signalling and inflammatory disease. Biochim Biophys Acta 1843, 2563-2582.

Vavken, P., Arrich, F., Schuhfried, O., Dorotka, R., 2009. Effectiveness of pulsed electromagnetic field therapy in the management of osteoarthritis of the knee: a meta-analysis of randomized controlled trials. J Rehabil Med 41, 406-411.

Wang, T., Zhang, X., Bikle, D.D., 2017. Osteogenic Differentiation of Periosteal Cells During Fracture Healing. J Cell Physiol 232, 913-921.

Wang, W., Yeung, K.W.K., 2017. Bone grafts and biomaterials substitutes for bone defect repair: A review. Bioact Mater 2, 224-247.

Yuan, J., Xin, F., Jiang, W., 2018. Underlying Signaling Pathways and Therapeutic Applications of Pulsed Electromagnetic Fields in Bone Repair. Cell Physiol Biochem 46, 1581-1594.

6 Abbreviation list

BID	Two times per day
BW	Body Weight
CI	Control Item
HU	Hounsfield Units
im	intramuscularly
iv	intravenously
MSRU	Musculoskeletal Research Unit
n/a, N/A	not applicable
NaCl	Sodium Chloride
NCI	Negative Control Item
Nm	Newton meter
OA	Osteoarthritis
PEMF	Pulsed Electromagnetic Field Therapy
ROI	Region of interest
sc	subcutaneously
SID	Once per day
SOP	Standard Operating Procedure
TI	Test Item
TID	Three times per day

7 Appendices

7.1 Appendix 1

	Group	Animal	Transducer [ID nr]	Resistance [Ohm]	Intra-OP Notes	Recovery Abnormalities
3 mm gap model	Test Item	86.01	427	91.4	-	-
		86.02	433	92.2	-	-
		86.03	434	90.5	The transducer was replaced because of the too high resistance value measured (140 Ohm).	-
		86.10	420	92.6; after handling 102	The cauter was not available during the first part of the surgery (cut, access to the bone), therefore, more bleeding occured. Post surgical radiographs revealed that the distal transducer cap+G14 was loose. The sheep underwent the next surgery right after, the cap was placed on the screw head again. Resistance measurement was higher in comparison to the one measured during the first surgery.	-
		86.11	416	92	-	-
		86.12	436	96	Due to the cap loosening 5 weeks after the surgery, the sheep underwent a second surgery. A single 5 cm long cut was made cranio- medially from the plate, proximal cap was re- attached.	-
		86.28	601	93.6	-	-
		86.29	529	93.5	-	-
	Control Item	86.04	418	91.5	-	-
		86.05	428	90.8	-	-
		86.06	417	92.4	-	-
		86.07	431	92	-	Stopped breathing after the extubation, intubated again, mechanically ventilated, received oxygen, stabilized after about an hour, extubated.
		86.08	423	91.7	-	-
		86.09	432	91.4	First inserted transducer had to be replaced because the cap would not hold on the screw	-

Table 7.1: Individual surgical notes in the 3 mm gap model.

7.2 Appendix 2

	Group	Animal	Transducer [ID nr]	Resistance [Ohm]	Intra-OP Notes	Recovery Abnormalities
17 mm Defect	Test Item	86.16	505	94.1	-	-
		86.17	498	92.6	-	-
		86.18	474	101.5	There was a problem with the aiming device and the cuts were therefore not parallel (about 1mm off). The alignment of the distal and proximal tibia, however, seemed good, despite that cut misalignment.	-
		86.19	505	91.6	-	
		86.20	516	91.1	-	-
		86.21	487	94.8	-	-
	Control Item	86.13	482	-	Implanted transducer does not work, but it is a sham sheep so it will have no impact.	-
		86.14	477	92.2	-	
		86.15	493	107.7	Not much bleeding from bone marrow (unlike sheep 86.13 and 86.14)	-
		86.22	426	different values between 200-300	-	-
		86.23	600	38	-	-
		86.24	480	99.8	-	-
	Negative Control Item	86.25	419	-	-	-
		86.26	486	-	-	-
		86.27	496	92		-

Table 7.2: Individual surgical notes for the 17 mm gap model.

7.3 Appendix 3: Radiographs

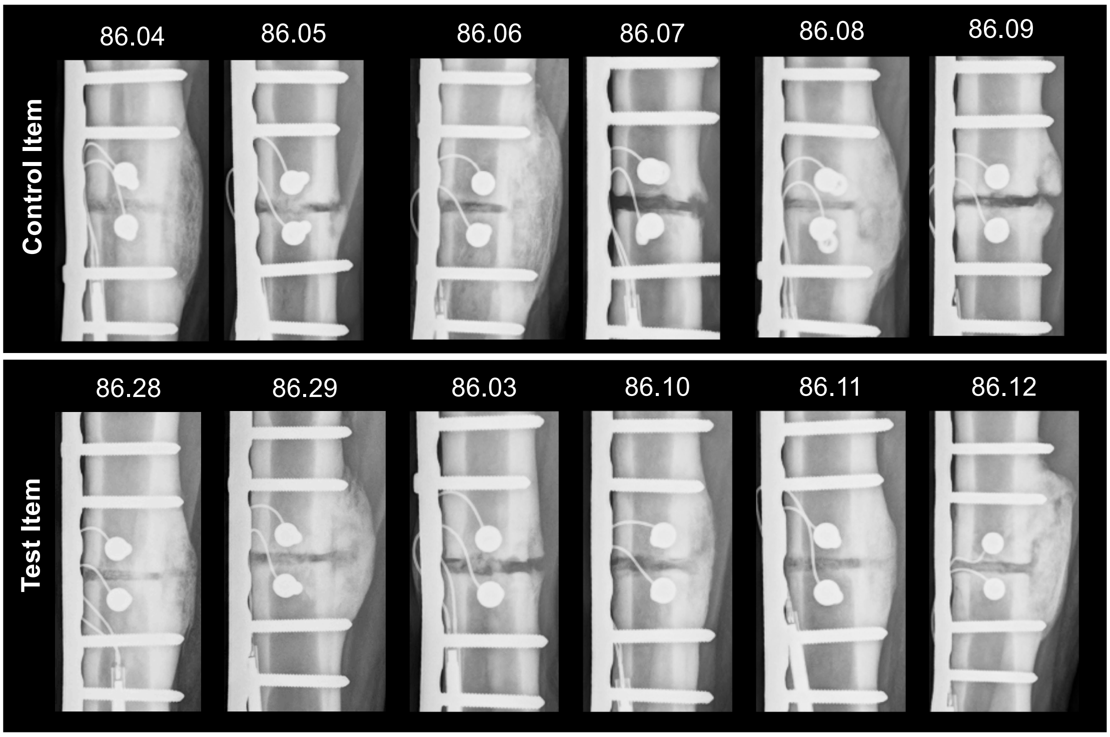

Figure 7.1: Radiographic summary at 9 weeks post-operatively for all animals in 3mm gap model.

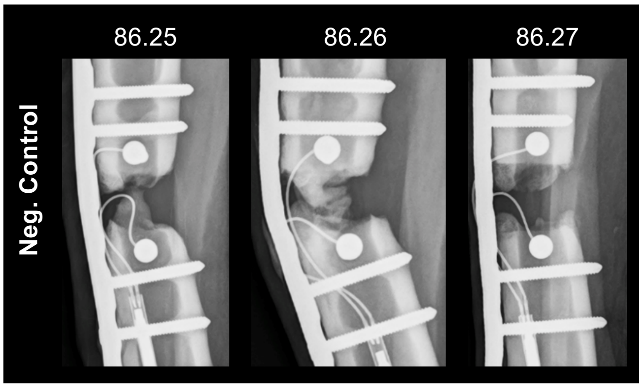

Figure 7.2: Radiographic summary at 12 weeks post-operatively for all NCI animals in 17mm graft model.

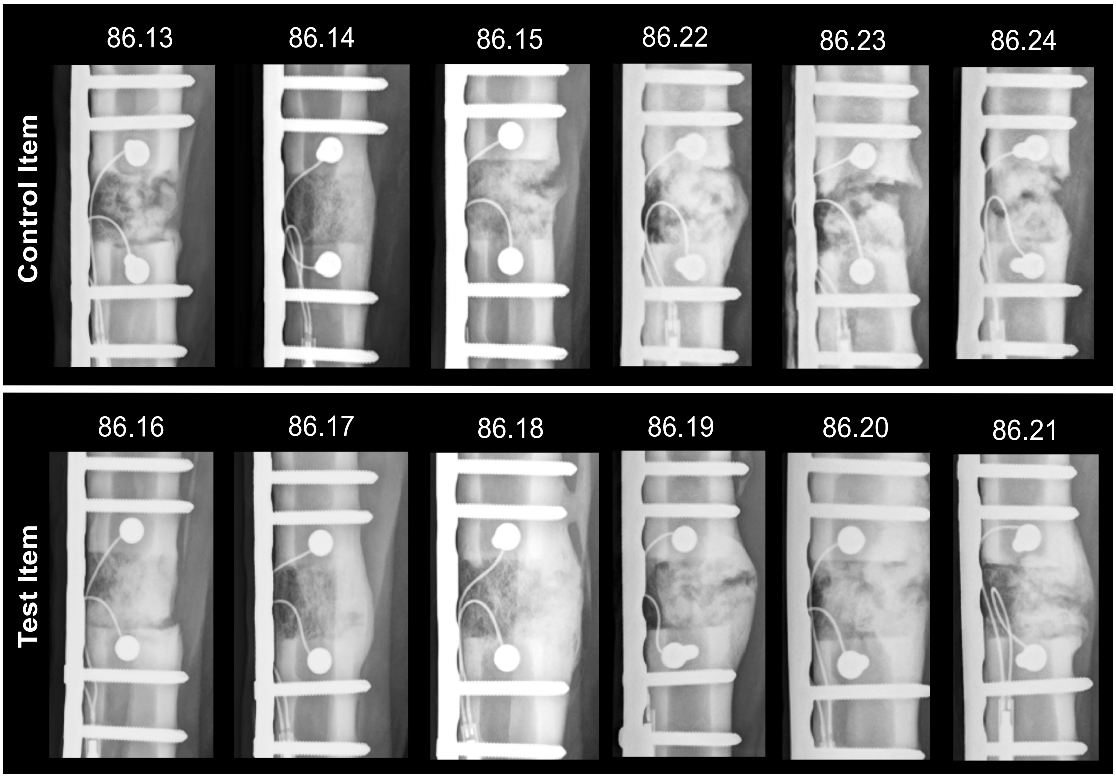

Figure 7.3: Radiographic summary at 12 weeks post-operatively for all animals treated with TI or CI in 17mm graft model.

7.4 Appendix 4: Macroscopic evaluation pictures

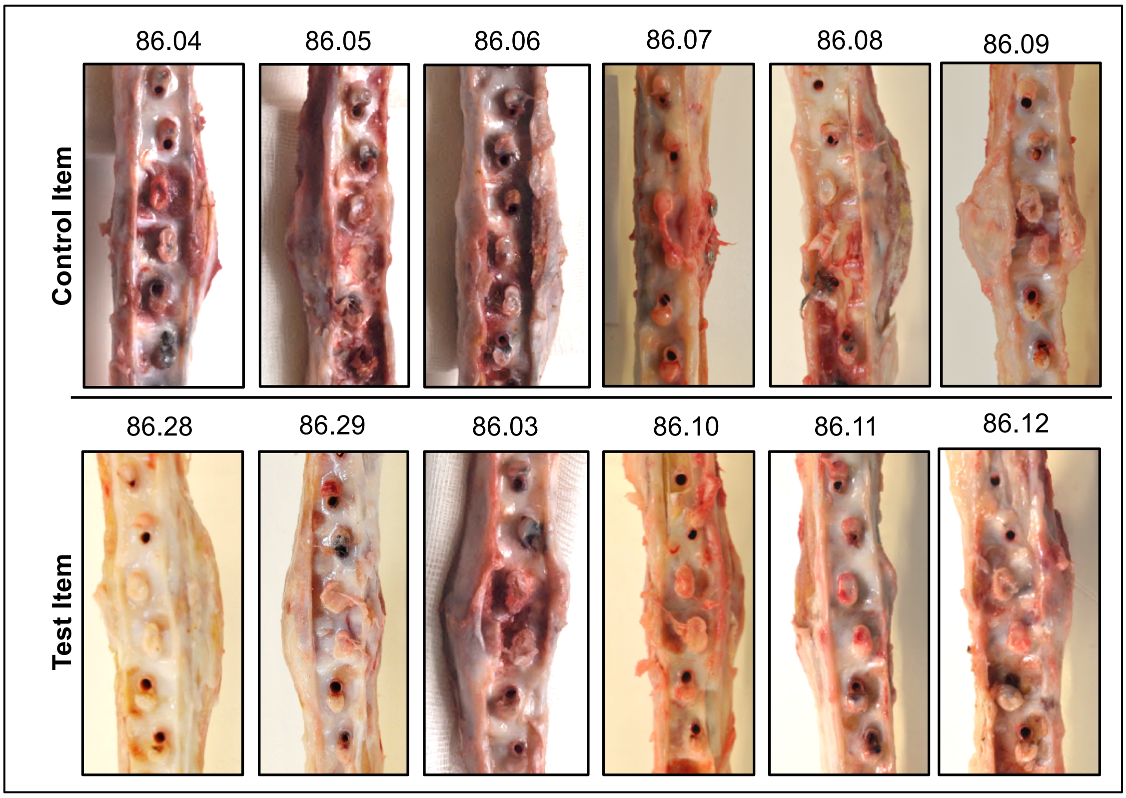

Figure 7.4: Macroscopic images (medial view) of all animals in 3mm gap model.

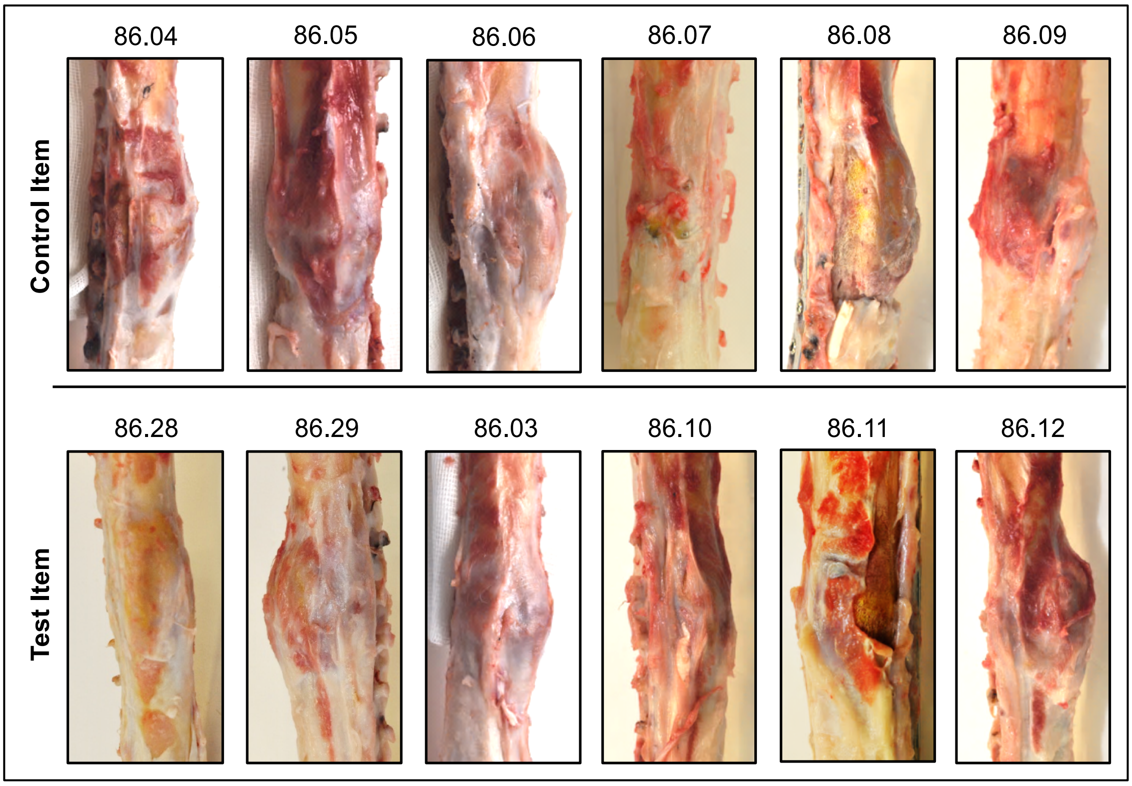

Figure 7.5: Macroscopic images (caudal view) of all animals in 3mm gap model.

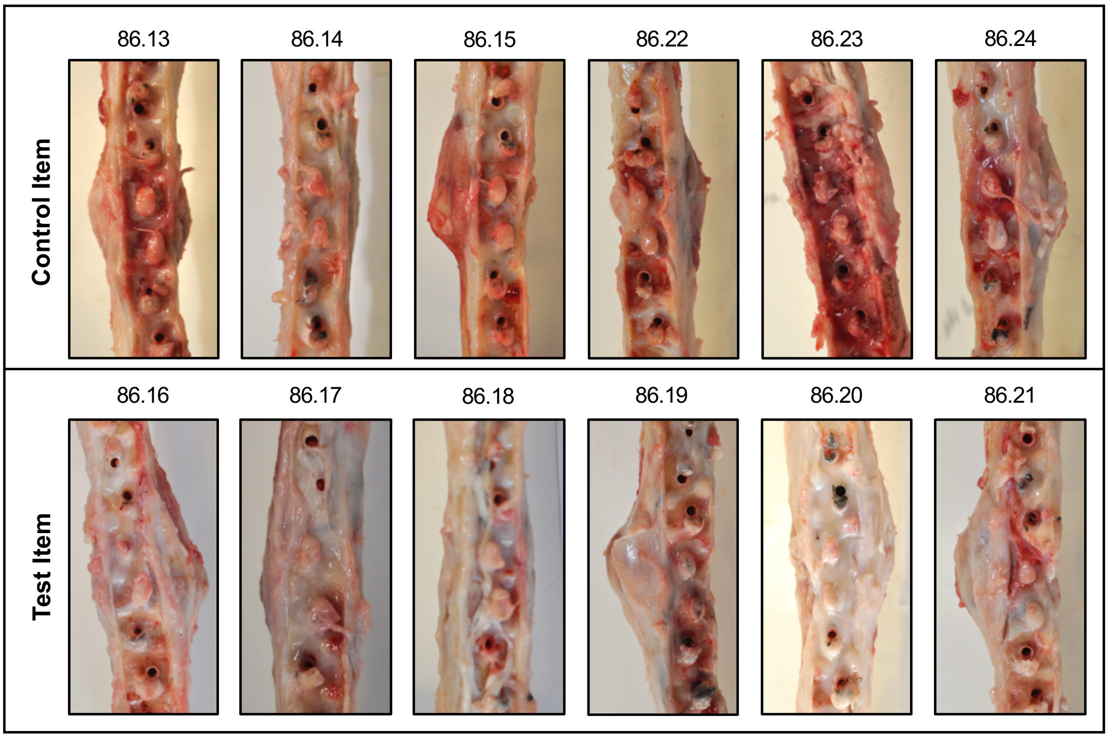

Figure 7.6: Macroscopic images (medial view) of TI and CI animals in 17mm graft model.

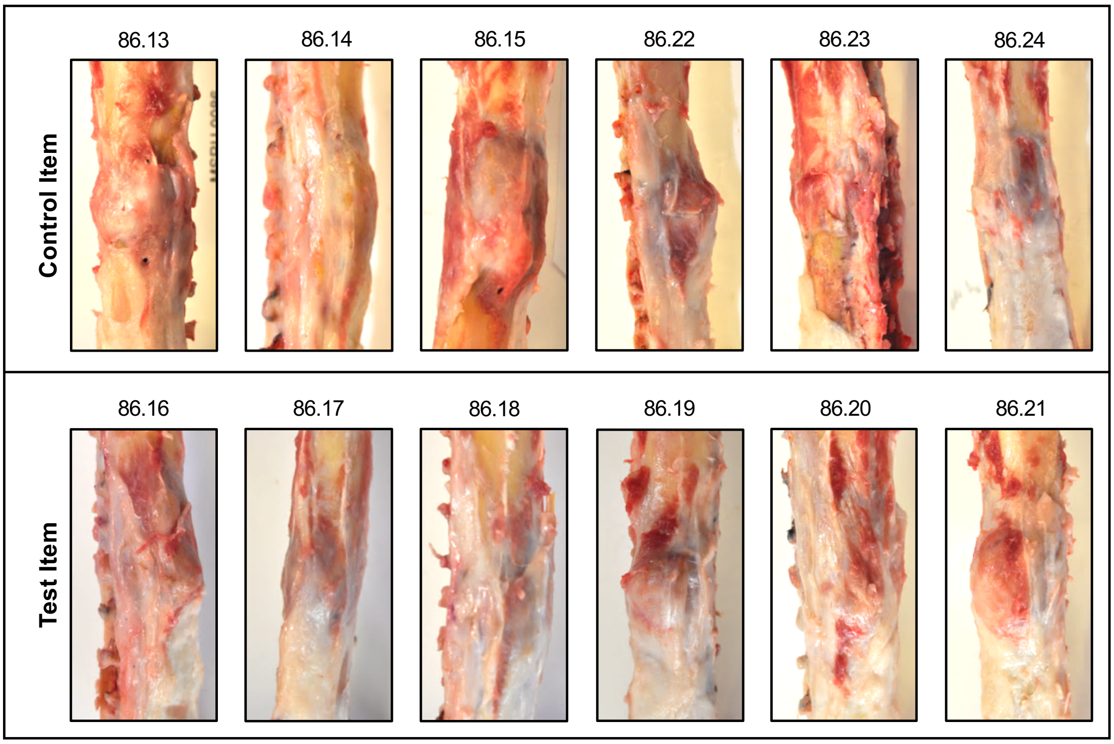

Figure 7.7: Macroscopic images (caudal view) of TI and CI animals in 17mm graft model.

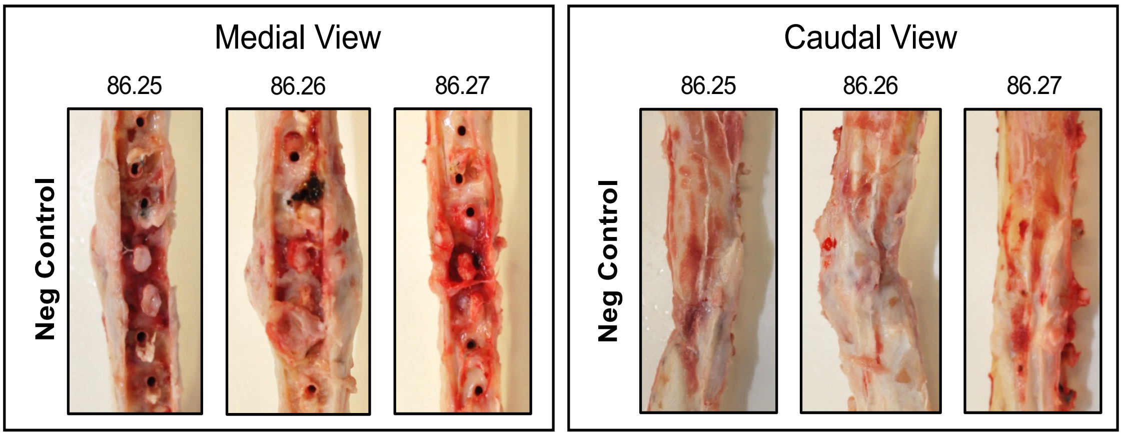

Figure 7.8: Macroscopic images of all NCI animals in 17mm graft model.

7.5 Appendix 5: Histology

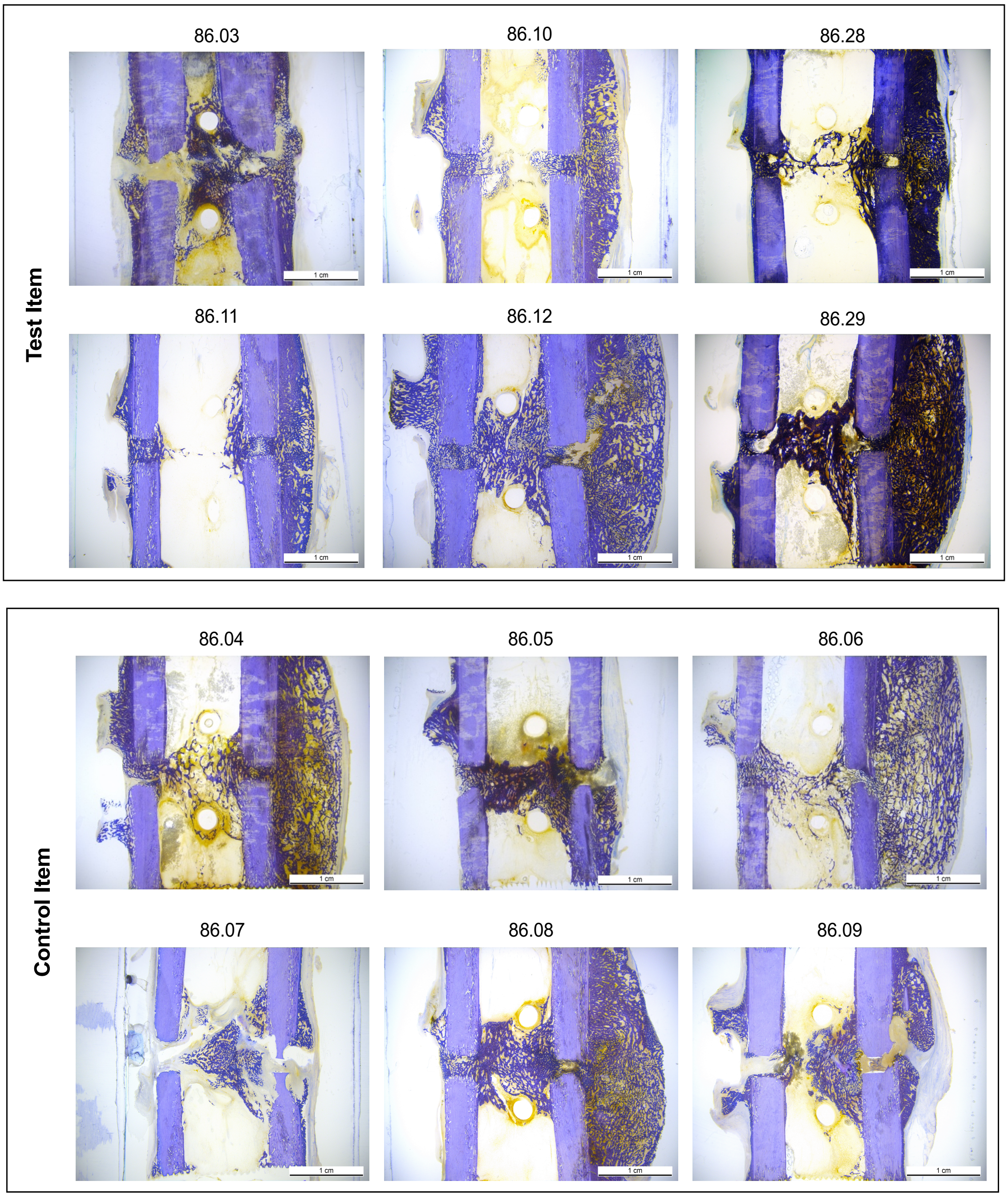

Figure 7.9: Ground sections, surface stained with Toluidine Blue of all processed 3mm gap model samples.

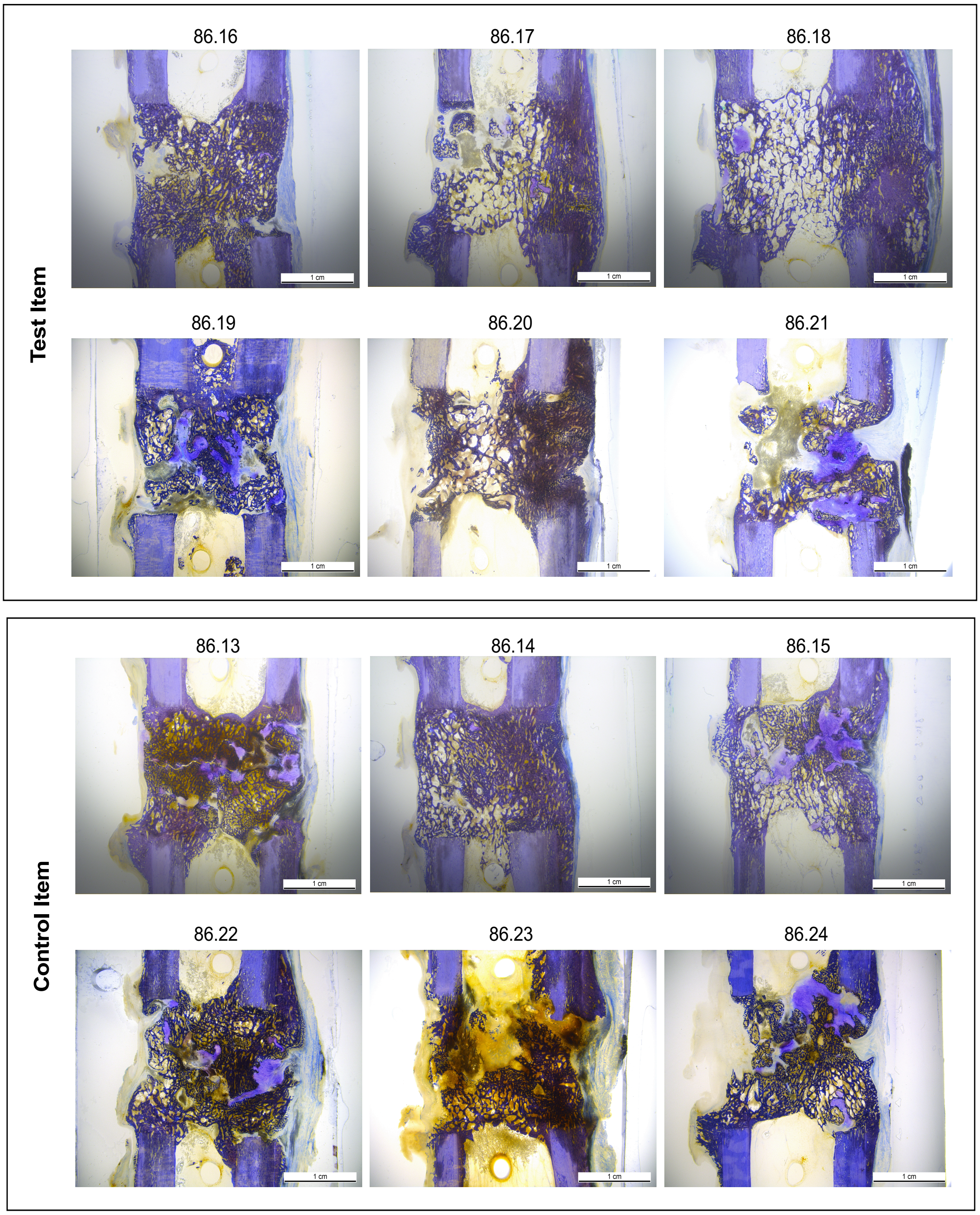

Figure 7.10: Ground sections surface stained with Toluidine Blue of all processed 17mm graft model samples.

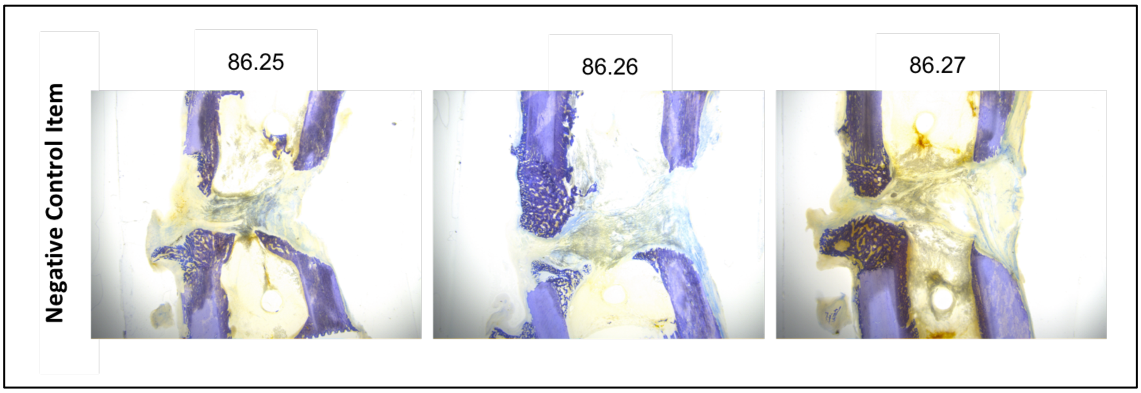

Figure 7.11: Ground sections surface stained with Toluidine Blue of all processed negative control 17mm model samples.

7.6 Appendix 6: Micro-CT scans

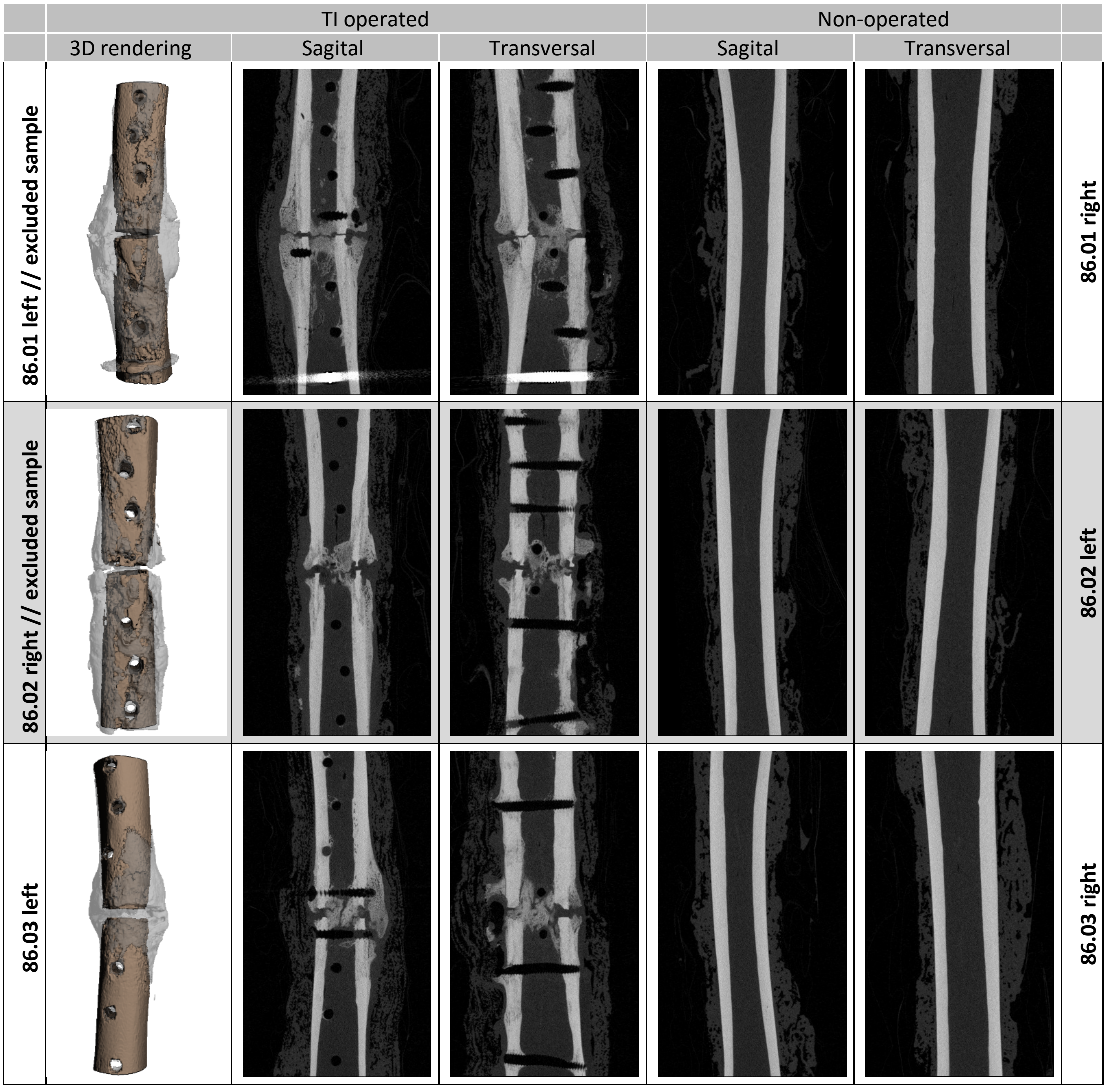

	TI operated			Non-operated		
	3D rendering	Sagital	Transversal	Sagital	Transversal	
86.10 right		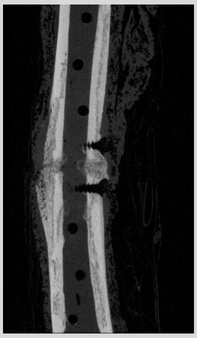	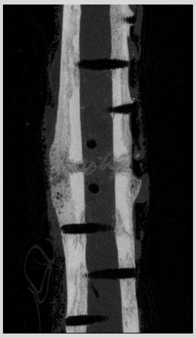		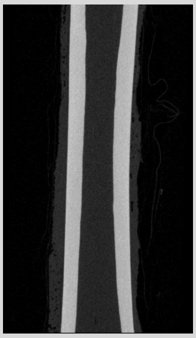	**86.10 left**
86.11 left		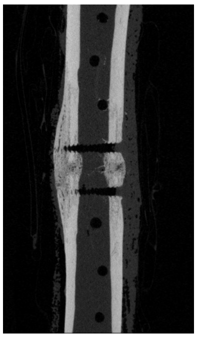	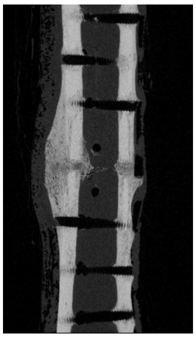	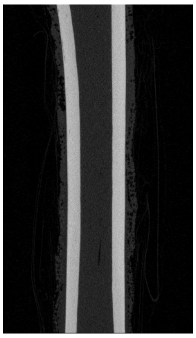	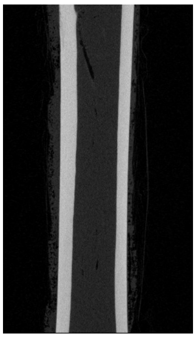	**86.11 right**
86.12 right		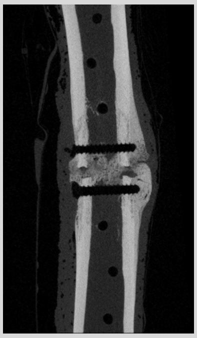	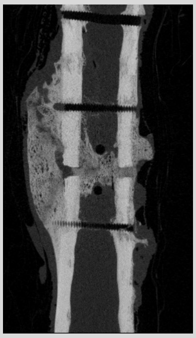	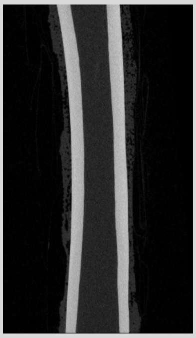	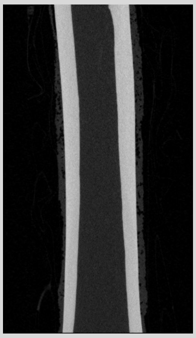	**86.12 left**
86.16 right			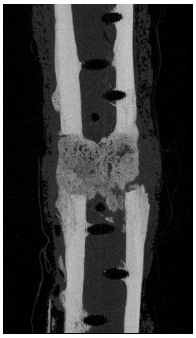	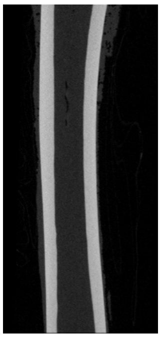	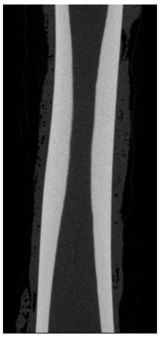	**86.16 left**

	TI operated			Non-operated		
	3D rendering	Sagital	Transversal	Sagital	Transversal	
86.17 left		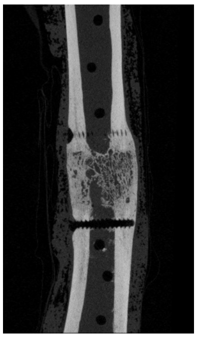	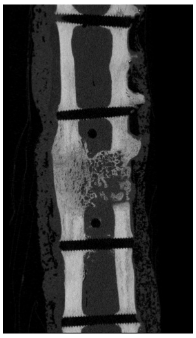		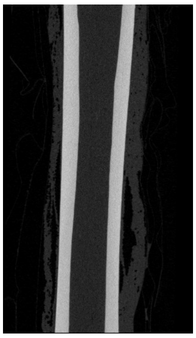	**86.17 right**
86.18 right		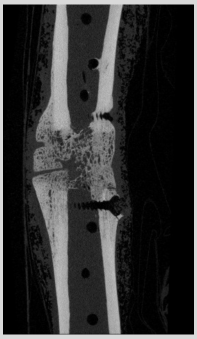		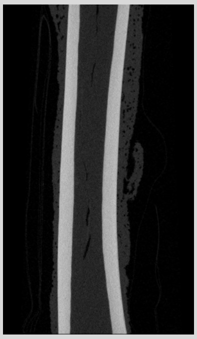	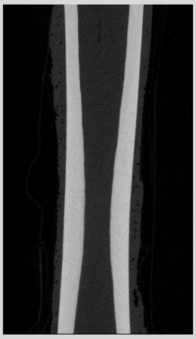	**86.18 left**
86.19 left	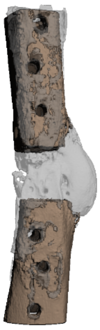	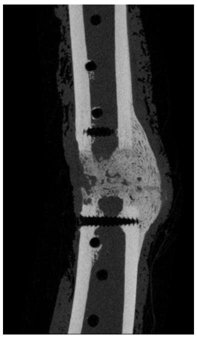	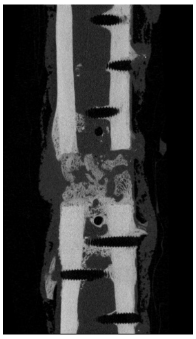	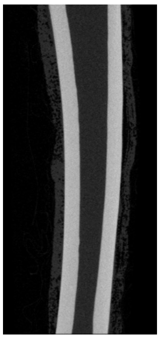	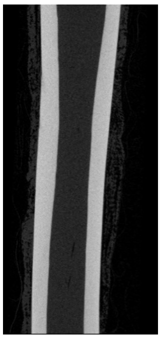	**86.19 right**
86.20 right		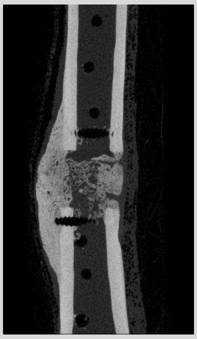		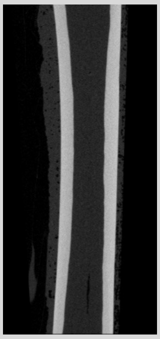	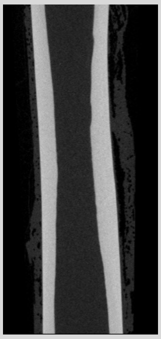	**86.20 left**

	TI operated			Non-operated		
	3D rendering	Sagital	Transversal	Sagital	Transversal	
86.21 left		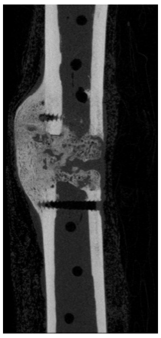	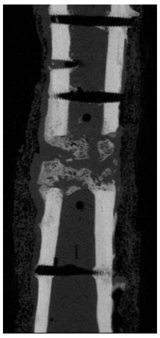	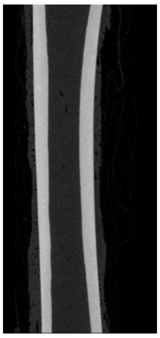	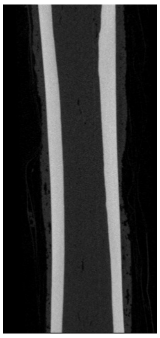	**86.21 right**
86.28 right	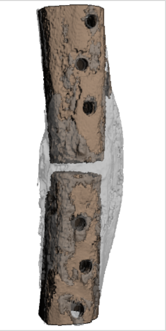	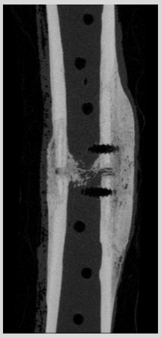	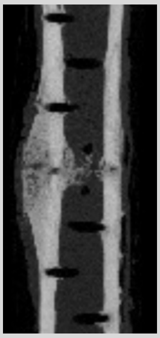	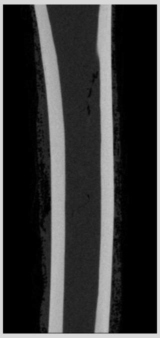	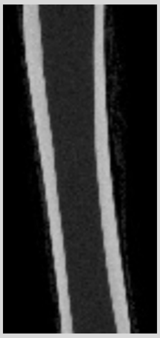	**86.28 left**
86.29 left			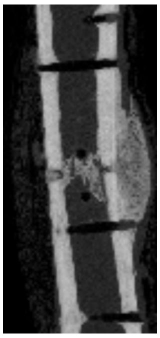	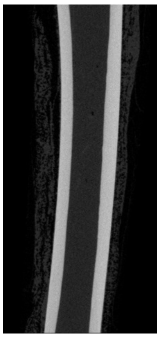	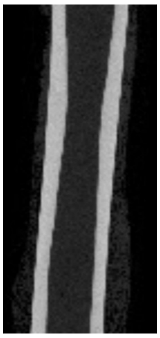	**86.29 right**

	CI operated			Non-operated		
	3D rendering	Sagital	Transversal	Sagital	Transversal	
86.04 right	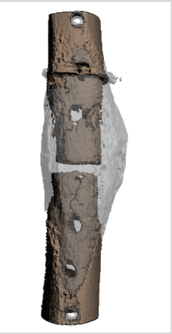		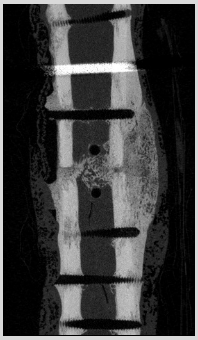	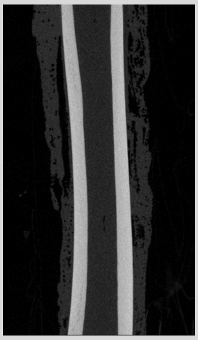	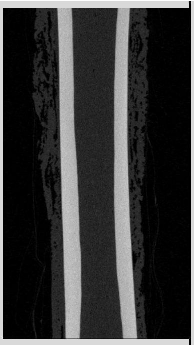	**86.04 left**
86.05 left		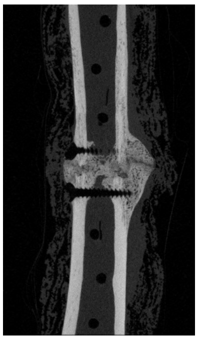	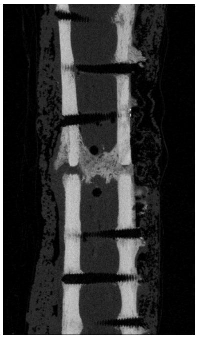	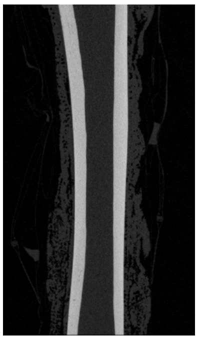	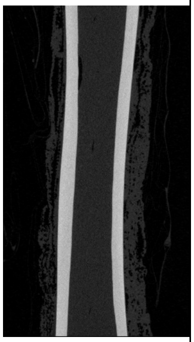	**86.05 right**
86.06 right				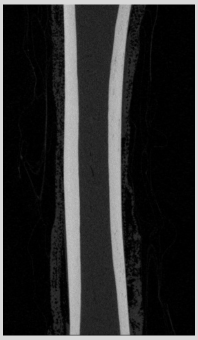	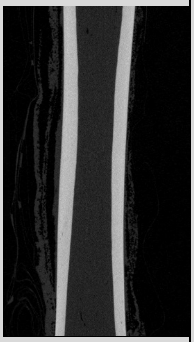	**86.06 left**
86.07 left		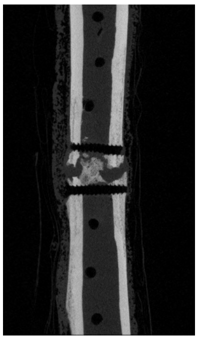	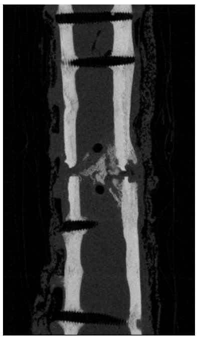	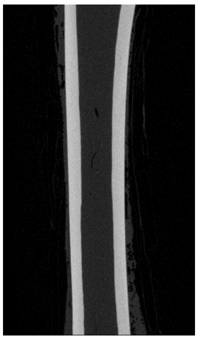	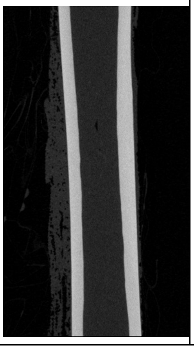	**86.07 right**

	CI operated			Non-operated		
	3D rendering	Sagital	Transversal	Sagital	Transversal	
86.08 right	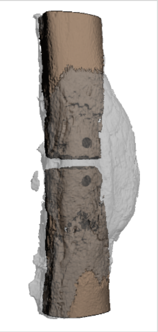	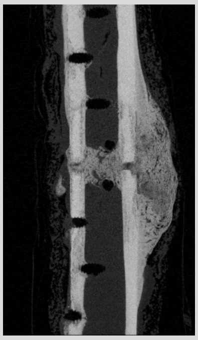	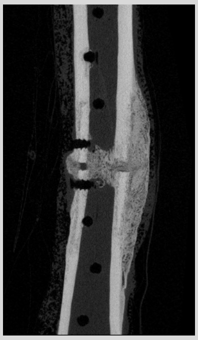	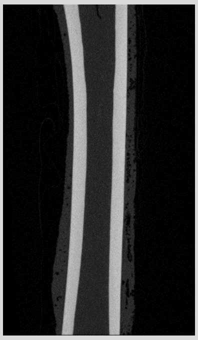		**86.08 left**
86.09 left		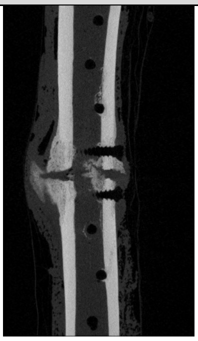		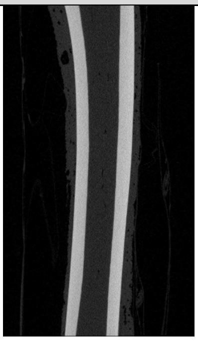	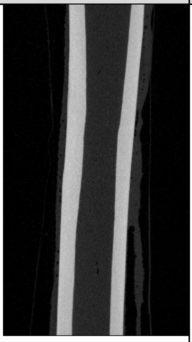	**86.09 right**
86.13 left		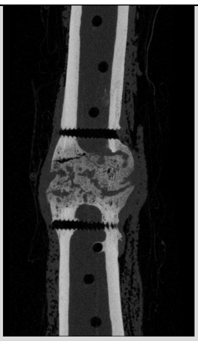	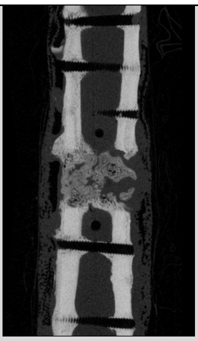	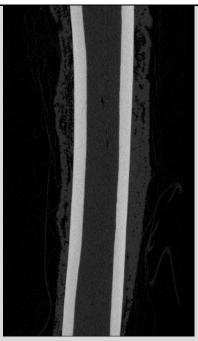	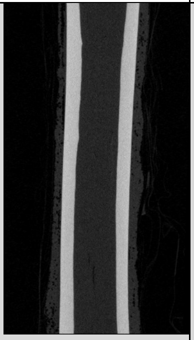	**86.13 right**
86.14 right		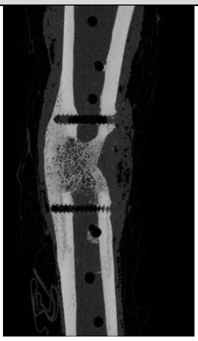			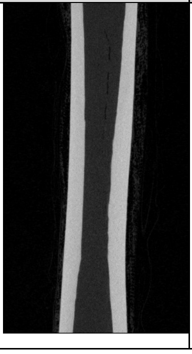	**86.14 left**

	CI operated			Non-operated		
	3D rendering	Sagital	Transversal	Sagital	Transversal	
86.15 left		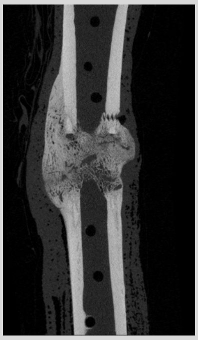	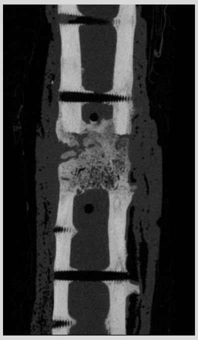	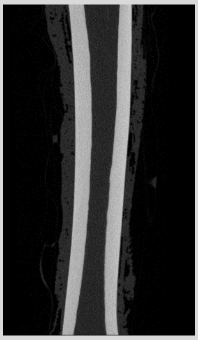	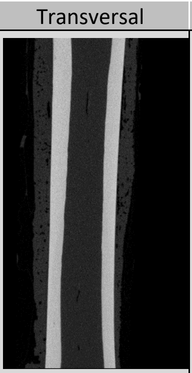	**86.15 right**
86.22 right			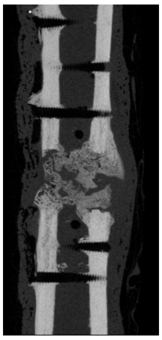		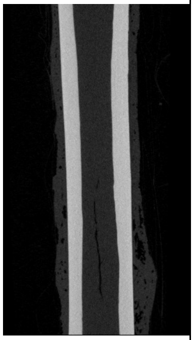	**86.22 left**
86.23 left	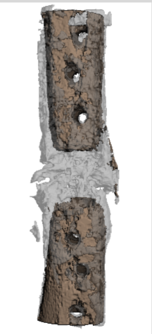	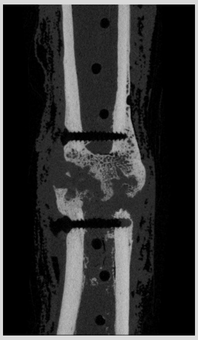	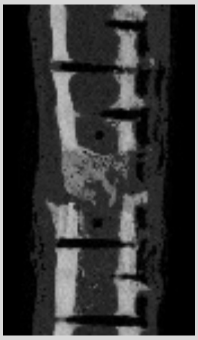	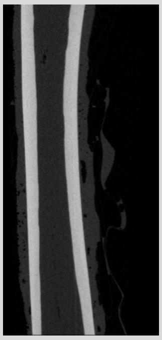	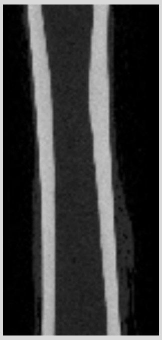	**86.23 right**
86.24 right		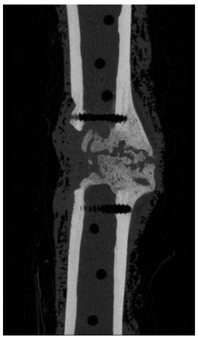	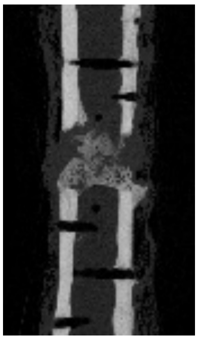	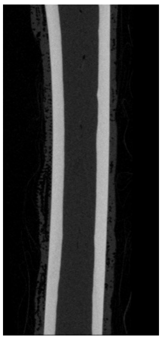	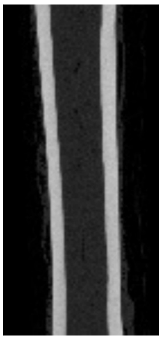	**86.24 left**

NCI operated		
3D rendering	Sagital	Transversal
	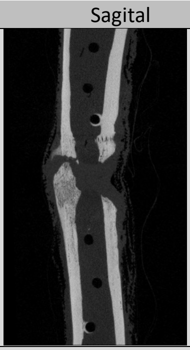	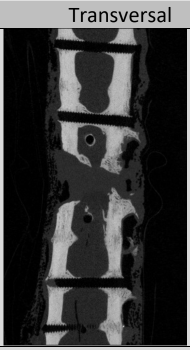
86.25 left		
	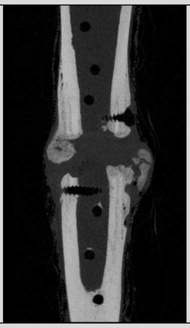	
86.26 right		
	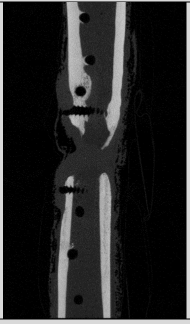	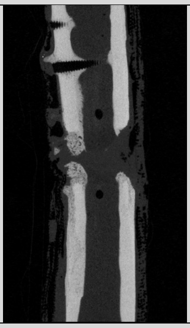
86.27 left		

Figure 7.12 Micro-CT scans of both operated and non-operated tibiae of all sheep.

7.7 Appendix 7: Biomechanics

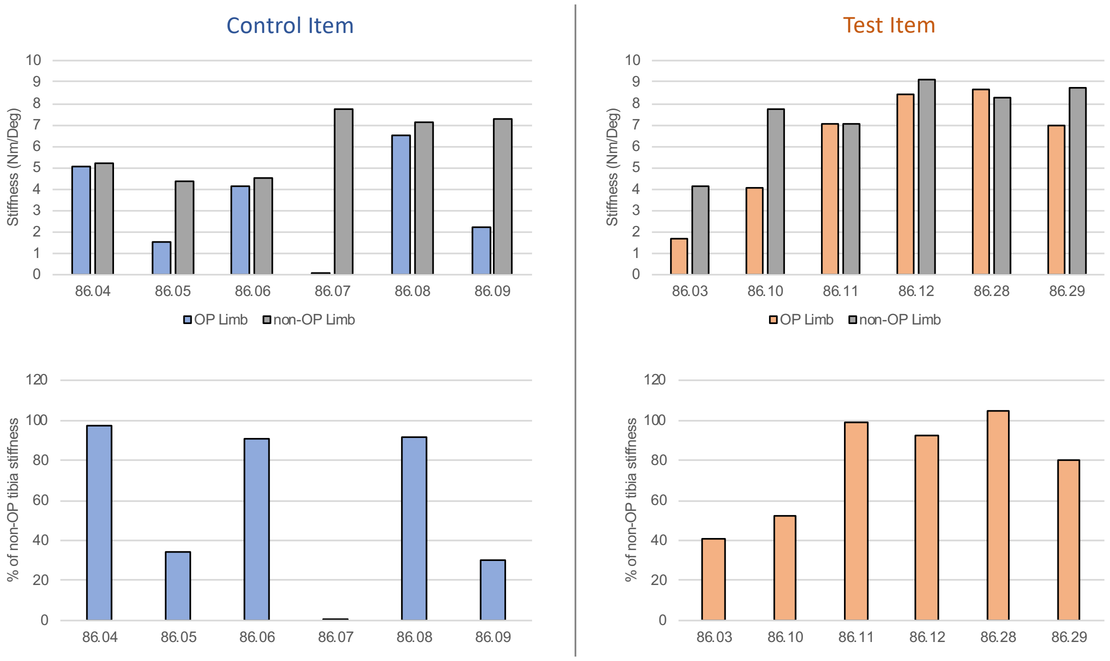

Figure 7.13: Torsional stiffness in Nm/deg and torsional stiffness of operated tibiae normalized to contralateral tibiae, shown per animal treated with CI or TI in the 3 mm gap model.

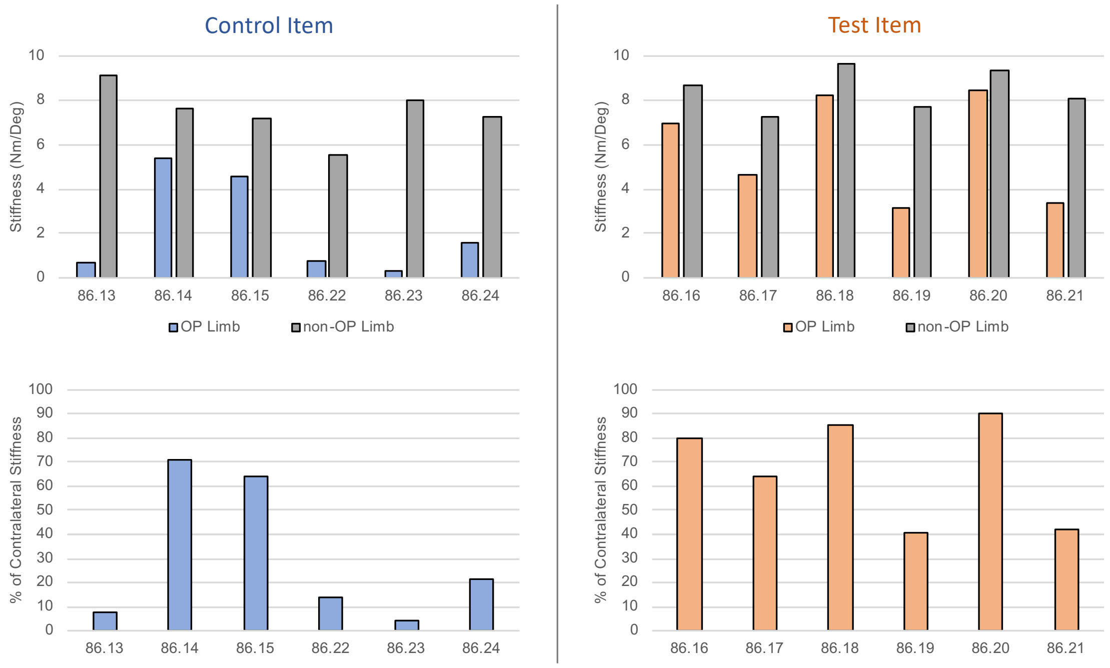

Figure 7.14: Torsional stiffness in Nm/deg and torsional stiffness of operated tibiae normalized to contralateral tibiae, shown per animal treated with CI or TI in the 17 mm graft model.

Acknowledgements

I would like to express my deepest gratitude to **Prof. Dr. Brigitte von Rechenberg**, for making me part of her Research Group and assigning me to this particular project. She was extremely supportive and generous with her time, always willing to share her thoughts and experiences.

I would also like to thank my study director, **Dr. Salim Darwiche, PhD**, for his patient guidance, endless enthusiasm and long hours of work spent on this project. I learned a lot from him and he made this journey really enjoyable for me.

My special thanks go to **Dr. med. vet. Karina Klein, PhD**, who performed all surgeries and guided me in the clinical work. She was always extremely helpful and provided invaluable support during all phases of the study.

I was particularly grateful for having **Beat Lechmann** from DePuy Synthes as part of the team. His positive attitude, outstanding organisation, close cooperation and help were invaluable and I am extremely glad I had a chance to work with him.

Thank you to **Dr. med. vet. Myrna Gunning**, whose work during this project was irreplaceable. She was always there to help with the clinical work and her positivity made working at MSRU a real pleasure.

I wish to express my gratitude to **Dr. med. vet. Dagmar Verdino** for her flawless anesthesia and to **Dr. Katja Nuss** for her assistance during surgeries.

I especially want to thank all MSRU doctoral candidates: **med. vet. Katrin Planzer, med. vet. Raphael Arz, med. vet. Konrad Finck, med. vet. Isabel Heckel, med. vet. Alina Steigerwald, med. vet. David Michalik, med. vet. Anna Geks, med. vet. Christina Wiezorek, med. vet. Katharina Siwy, med. vet. Martina Heygen, med. vet. Claudia Michaelis, med. vet. Milena Tegelkamp** and to **Manuel Koch** and **Barbara Kollar** for their hard work during this entire project. Without their help it wouldn’t have been possible.

I wish to acknowledge the help provided by the rest of the MSRU Team, **Dr. med. vet. Peter Kronen, Dr. Flurina Clement Frey, Dr. Sabine Koch, Prof. Dr. Thomas Steffen**, as well as **Ljubica Dimbrek, Rikke Grundtvig** and **Gabriella Kaelin-Hanselmann**. Particularly grateful am I for the help provided by **Rosita Walther** with the fluorescent sections.

My grateful thanks are also extended to **Prof. Dr. Stephen Ferguson** and his team, **Dominique Neuhaus** and **Pascal Behm**, for performing all biomechanical tests and analyses and the teams of **Magnetodyn** and **Scanco AG** for their cooperation.

I would like to thank **Prof. Dr. Mark Flückiger** for the expertise during the radiographic evaluation and to **Rainer Egle** for the IT support.

I would also like to extend my thanks to all people that performed the laboratory word, **Käthi Kämpf, Dr. Sabina Wunderlin**, **Dr. Andrea Laimbacher, Aymone Lenisa** and particularly **Dr. med. vet. Agnieszka Karol** for her invaluable opinions and expertise during the histological evaluations.

Help from the animal takers, especially **Silvana Ressegatti** and the whole team of the Ruminant Clinic was greatly appreciated. I also want to thank the **Knüsel Family** for the kind cooperation.

Last but not least, with my whole heart I want to thank my family, friends and my partner, **Matteo Cortonesi**, for their support, encouragement and being there for me.

Curriculum Vitae

Name	Anna Kaczmarek
Date of birth	02.08.1991
Place of birth	Lodz, Poland
Nationality	Polish

09/1998 - 06/2004	Primary School, Lodz, Poland
09/2004 – 06/2007	Secondary School, Lodz, Poland
09/2007 – 06/2010	XXI Highschool, Lodz, Poland
10/2010 – 01/2016	Master's Degree in Veterinary Medicine, University of Environmental and Life Sciences, Wroclaw, Poland
10/2016 – 09/2017	Rotating Internship in Equine Medicine, University of Veterinary Medicine in Vienna, Austria
10/2017 – 12/2019	Preparation of the thesis under the direction of Prof. Dr. med. vet. Brigitte von Rechenberg at the Musculoskeletal Research Unit (MSRU), Department of Molecular Mechanisms of Disease of the Vetsuisse Faculty, University of Zürich. Director: Prof. Dr. med. vet. et phil. Michael Hottiger